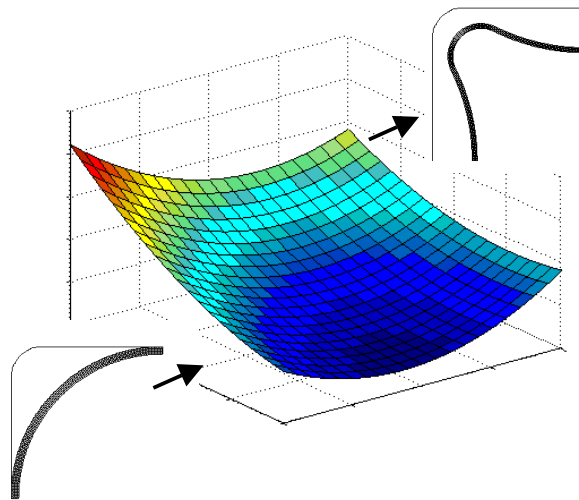




University of Twente
The Netherlands

Optimisation of the Initial Tube Geometry for Tube Hydroforming

A mathematical approach



P. Kömmelt

December 2004

CTW.04/TM.5490



CORUS

Optimisation of the Initial Tube Geometry for Tube Hydroforming

A mathematical approach

Master Thesis Report

P. Kömmelt
December 2004

University of Twente

Faculty of Engineering Technology
Department of Applied Mechanics

Committee members:

Prof. dr. ir. J. Huétink (chairman)
ir. M.H. Kelder (Corus, mentor)
Dr. ir. A.H. van den Boogaard (mentor)
ir. Martijn Bonte (mentor)
Dr. ir. L. Warnet (external committee member)

Summary

Tube hydroforming uses a combination of internal pressure and axial feeding to form complex parts, like exhausts, engine cradles and roof rails. Tubes used for hydroforming are mostly round of shape and are subjected to several forming steps prior to hydroforming. These steps are necessary to fit the tube in the die cavity and successfully produce the hydroformed part.

To reduce the number of production steps prior to hydroforming, the initial tube geometry should be improved. To find this geometry a research study is conducted using an optimisation strategy. The optimisation described in this report is based on Response Surface Methodology. This technique uses a number of finite element simulations, executed according to an experimental design. An objective function is used to evaluate the results of the finite element simulations and is a function of the design variables describing the initial tube geometry. From the collected data a response surface (metamodel) is build with linear regression analysis, which is an approximation of the objective function. The optimum of the metamodel is found using a line search technique in Matlab.

In this report the optimisation of a tube to a square die is described. To find the optimum the initial tube geometry is described with design variables, which are altered according to an experimental design and subsequently simulated using the finite element package DiekA. The simulated hydroform products are evaluated by determining the wall thickness distribution. The optimisation searches for the tube with a uniform distribution.

From the optimisation it is found that the largest influence on the wall thickness distribution is not so much a single design variable, but the perimeter of the initial tube. The larger the perimeter of the initial tube, the more uniform the wall thickness distribution. A further study by altering the constraint concerning the maximum allowable perimeter resulted in a preference for square tubes with a small radius and a small dent in the sides of the box.

Table of Contents

1	Introduction	1
2	Hydroforming	3
2.1	Tube Hydroforming	3
2.2	Production Steps Prior to Tube Hydroforming	4
2.2.1	Tube Forming	4
2.2.2	Pre-forming	5
2.3	Influence of Process Parameters	6
2.4	Influence of Tube Geometry on the Hydroform Process	8
3	Theory: Mathematical Optimisation	9
3.1	Parameters	9
3.2	Objective Function	10
3.3	Constraints	10
3.4	Optimisation	11
3.4.1	Iterative and Approximation Methods	12
3.5	Response Surface Methodology	14
3.5.1	Design of Experiments	14
3.5.2	Function Order	15
3.5.3	Lack-Of-Fit	16
3.5.4	Optimisation Algorithms	18
4	Experimental Simulations	21
4.1	Choice of Design Parameters	21
4.1.1	Design Variables	21
4.1.2	Design Parameters and Constants	23
4.2	Objective Function	24
4.2.1	Wall Thickness Distribution	24
4.2.2	Absolute Difference	24
4.2.3	Relative Difference	27
4.2.4	Quotient	27
4.2.5	Objective Function Selection	28
4.3	Constraints	29
4.4	Interpretation of the Design of Experiments	31
5	Two-Dimensional Experiments	33
5.1	Finite Element Model	33
5.1.1	Extracting Simulation Data	34
5.1.2	Results of the Simulation	35
5.2	Response Surface Methodology	36
5.2.1	Metamodel	37
5.2.2	Optimisation	40
5.3	Validation of the Optimisation	43

5.3.1	Comparison with the Results of the Simulations.....	43
5.3.2	Finite Element Model Validation.....	44
5.3.3	Fractional Factorial Design.....	48
6	3D Simulations.....	51
6.1	Finite Element Model.....	51
6.1.1	Results of the Simulation.....	52
6.2	Response Surface Methodology.....	52
6.2.1	Metamodel.....	52
6.2.2	Optimisation.....	53
6.3	Data Comparison with 2D Simulations.....	54
7	Discussion.....	57
7.1	Screening Design.....	57
7.1.1	Results of the Screening.....	58
7.2	Constant Mass of the Tube.....	58
7.3	Decrease of Acceptable Maximum Perimeter.....	59
7.4	Data Point not satisfying an Implicit Constraint.....	61
7.5	Combination of the Feasible Domain and the Experimental Design.....	61
8	Conclusions and Recommendations.....	63
8.1	Conclusions.....	63
8.2	Recommendations.....	64
	Acknowledgement.....	65
	References.....	66
	Appendix A. Design of Experiments.....	70
	Appendix B. Design Variables.....	77
	Appendix C. Necking.....	82
	Appendix D. Finite Element Models for the Two-Dimensional Simulations.....	84
	Appendix E. Wall Thickness as Function of the Perimeter.....	89
	Appendix F. Confidence Intervals of the Metamodel.....	91
	Appendix G. Bending of Sheet.....	95
	Appendix H. Screening Designs.....	98

1 Introduction

Manufacturers are continuously searching for improvement of their processes to gain better quality products for lower costs (make more profit). This applies to all kinds of industry, including the metal forming industry. In the past customer demands were met by using experimental trial-and-error methods, which is a time-consuming and expensive process. With the rise of the computer era the experiments could be simulated using computer models. This allowed for the trial-and-error process to be conducted on the computer, thereby reducing the stress on production resources. Nowadays the manufacturers are interested in maximum efficiency for a minimum expense, leading to the search for optimal processes. This demands for a more systematic approach of the problem and led to the development of mathematical tools. The coupling between mathematical optimisation algorithms and finite element simulations is an important step for industrial optimisation.

The Aim of the Thesis

The aim of an optimisation is to find a set of parameters that minimise the objective function subjected to a set of constraints. To implement this for the industry the Netherlands Institute for Metal Research (NIMR) started the project “optimisation of forming processes”, which aims at developing an optimisation strategy for metal forming processes. The PhD student Martijn Bonte at the University of Twente conducts this project using mathematical tools in combination with the finite element method.

Together with Corus a graduation project was formed to gain a better understanding in the utilisation of optimisation for forming processes. The project is concentrated on one forming process, namely hydroforming. This technique uses a water emulsion to form metal sheets or tubes into the shape of a die. In this case tube hydroforming to a prismatic die shape is investigated.

The project is a case study for optimisation of a hydroformed product. The problem is formulated as the optimisation of the initial tube geometry for hydroforming. The investigation aims at the reduction of forming steps prior to the hydroform step by selecting a better tube geometry. The input parameters are formed by the geometrical description of the initial tube. As an objective for the problem the distribution of the wall thickness is used. A better distribution implies a more uniform thinning of the wall across the perimeter and additionally a more uniform strain distribution in the entire tube.

Report Structure

An introduction into the hydroforming technique is given in chapter two. Here the different stages of hydroforming are discussed to get a feeling for the work hardening of the material. The strain introduced into the material influences the forming capability during the hydroform process and must be prevented if possible.

The third chapter discusses the theory used for optimisation of the hydroform process. The focus is on the preparation and evaluation of the optimisation rather than on the used algorithms. For the optimisation itself use is made of a Matlab tool.

The use of the theory for the optimisation of the initial tube geometry for hydroforming is discussed in the chapters four to six. At first the preparation of the optimisation problem is described, where the choice of variables, objective functions (criterion) and constraints is discussed. Furthermore the experiments (runs) are presented, which are used to gain as

much information as possible. The experiments consist of two- and three-dimensional finite element simulations. The two-dimensional simulations are validated by mesh refinement and comparison with a model taking in account the work hardening of the tube forming process. In chapter seven the results and procedure of the optimisation are discussed. The report finishes with the conclusions and recommendations in chapter eight.

2 Hydroforming

Hydroforming is a general term to denote sheet or tube forming using a pressurized medium. Initial hydroforming started in 1940, when J.E. Grey et al. [16] investigated the possibility for making seamless copper sockets. In the early days, the technique was mostly used by the sanitary industry fabricating sockets. Since then a lot of theoretical studies and experiments have been carried out to investigate the technique of hydroforming in general.

The automobile industry started their investigations of the techniques usability in the 70s followed by a decline of interest and in the last decade large-scale production of both tube- and sheet-hydroforming became more common. Nevertheless the theoretical and practical knowledge of hydroforming is less extensive and detailed compared to deep drawing due to large investment costs needed for research [14, 20].

The advantage of hydroforming compared to deep drawing is the ability to produce complex hollow parts without the need of an assembly step. The absent of flanges needed for assembly reduces the weight and the continuous weld in longitudinal direction of the tube increases the stiffness. Replacing traditional deep drawing designs by a hydroformed part is only economical when the traditional design consists of multiple deep drawing components, due to the high production cost of hydroformed parts.

This report focuses on tube hydroforming, explained in more detail in the following sections. In section 2.2 the production cycle is described to indicate several pre-forming steps, followed by a section about the process parameters and possible failure modes of the hydroform process. The last sections describe the influence of the tube geometry on the ability to produce hydroform parts.

2.1 Tube Hydroforming

Tube hydroforming, depicted in Figure 2.1 uses a combination of internal pressure and axial feeding to form complex parts, like exhausts, engine cradles, roof rails, longitudinal beams and pillars as shown in Figure 2.2. A hydroform cycle can be divided into four steps; Placing the tube in the die cavity (1), filling the tube with a water emulsion (2), increasing the internal pressure and applying axial feeding (3) and ejecting the hydroformed product (4). The axial feeding can be stroke- or force controlled, while the pressurized medium can be pressure or volume controlled.

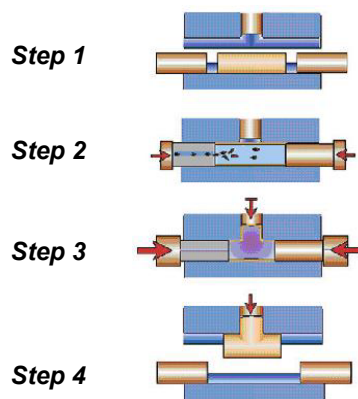


Figure 2.1. A typical hydroform process for a T-piece

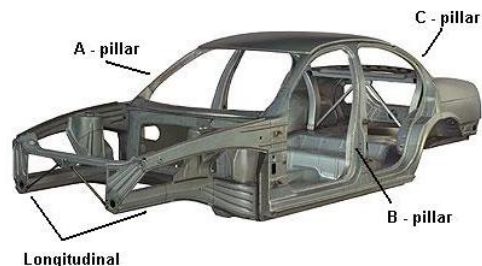


Figure 2.2. A Body-in-White structure

Hydroforming can be divided into Pressure Sequence Hydroforming (PSH) and High Pressure Hydroforming (HPH). With the former technique the tube is deformed in a bending mode, while the latter technique uses elongation of the tube wall. Tubes used in HPH have a 5 to 10 percent smaller perimeter compared to the die perimeter. When the die is closed, an internal pressure is applied forcing the tube to adopt the shape of the die. Hereby the tube is inflated, increasing its perimeter and causing the wall thickness to decrease. The difference in the perimeter between the tube and the die, forces the tube to expand along the entire perimeter. Variation of the wall thickness around the perimeter is caused by partial contact of the tube wall with the die during expansion, see Figure 2.3. Contact between the tube and the die restricts free forming, where material flow becomes dependent on the amount of friction. To overcome this, the internal pressure is increased causing an increase of friction, which is proportional to the internal pressure. The minimum corner radius of the die (corner filling) determines the ultimate internal pressure, also called calibration pressure. With PSH the perimeter is equal to the perimeter of the die and deformation of the low-pressurised tube takes place during the closure of the die. For further reference on PSH is referred to [21...24].

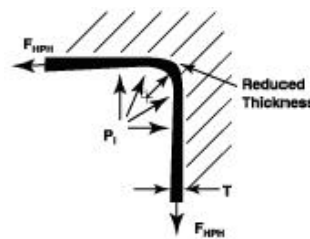


Figure 2.3. Wall thinning due to friction

2.2 Production Steps Prior to Tube Hydroforming

Prior to hydroforming the material is subjected to a number of forming steps. At first a metal sheet is bent to form a tube. Dependent on the final product, the tube is bent and pre-formed to fit into the die cavity. These forming steps introduce plastic deformation to the material, resulting in a decreased formability of the material for the subsequent forming step. In this section a few pre-forming steps applied for hydroforming are briefly discussed.

2.2.1 Tube Forming

In the next sections two tube making techniques are shortly explained, roll-forming and tubular blank [26]. Another technique for producing tubes is extrusion, which is mostly used for making seamless aluminium tubes. This report is focused on steel tubes used for hydroforming and therefore extrusion is not discussed.

Roll-forming

A continuous process to produce tubes out of strip, sheet or coiled stock is called roll-forming. The sheet metal is guided through a row of roll stations, see Figure 2.4, forming a tube with uniform cross-section. The production line consists of up to 25 stations including two or more rolls per station.

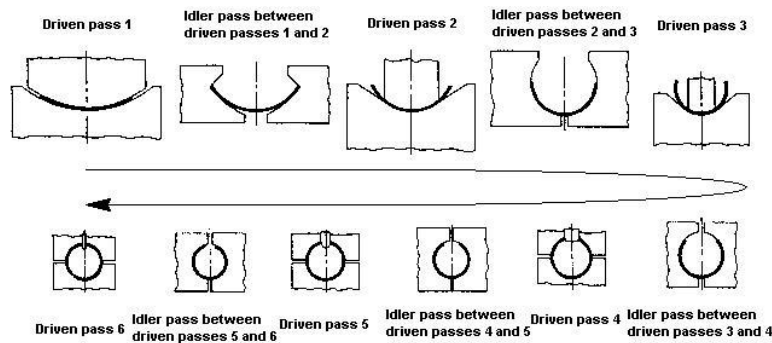


Figure 2.4. Roll-forming

The rolls can be divided into forming rolls and sizing rolls, the former one is subdivided into breakdown and finishing rolls.

When the sheet is bent in the right shape and calibrated, the sheet is welded to form a closed cross-section, forming a so-called mother tube. This mother tube is cut into predefined lengths. The process takes place with a speed of ± 75 meter per minute, depending on the cut and weld speed in the line.

The roll forming process not only introduces stress in the circumferential direction but also in the longitudinal direction caused by the non-simultaneous bending of the sheet (in the entire production line). Most of the stresses though are caused by the calibration step, the last step in the roll forming process. In this step the tube not only obtains its final shape, it also acts as a power drive for the production line. To pull the tube through the line, the tube is slightly squeezed for grip, with that introducing extra strain in circumferential direction. The strains have a non-uniform distribution of approximately 6 percent.

Tubular Blank

The tubular blank process is a discontinuous process, forming a pre-cut metal sheet in several steps on a press brake by bending, see Figure 2.5. In approximately 5 to 7 steps the sheet is bent to a round shape after which the tube is laser welded. This principle lends itself for making normal, tailored or conical tubes. Tailored tubes consist of multiple sheets made from different materials and/or various thicknesses. The tubular blank is formed by bending only, introducing uniform strains in the circumferential direction of approximately 2 percent.



Figure 2.5. Tubular blank process: press forming
(source: Corus: The tubular blank)

2.2.2 Pre-forming

Pre-form operations, like bending or crushing, often are necessary before hydroforming to prevent material trapping during closure of the die, see Figure 2.6.

Strains and stresses are introduced during pre-forming, influencing the formability of the tube. During pre-forming wall thinning occurs at several places of the tube wall. To prevent further thinning, elongation of these spots should be avoided by introducing contact between the die

and tube wall. Due to friction the elongation of the tube wall in contact with the die is blocked, which is called wall locking [4].

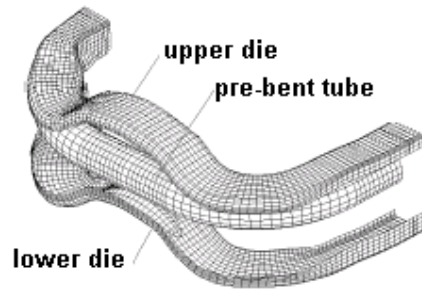


Figure 2.6. Bent tube within die

When only pure expansion occurs due to limited material flow, crushing and pre-forming processes become important steps prior to hydroforming of circular tubes into various cross-sections. Many hydroform operations require pre-forming in order to fit the tubes into the hydroforming die cavity and close the tool without chance on die trapping.

For some hydroform operations the pre-forming step is conducted by the closing of the die, which leads to higher demands on the hydroforming tools, although saving an extra process step with corresponding tools. When die trapping can occur a separate step is needed.

Crushing is used to decrease the contact area between the tube and die before hydroforming, thereby decreasing the hydraulic pressure and clamping force needed, and leads to a more uniform wall thickness distribution. After a pre-forming step annealing may be necessary to remove residual stresses, although it is an expensive and unwanted production step [15].

2.3 Influence of Process Parameters

Process parameters like internal pressure, axial force and friction have a large influence on the formability of the hydroformed tube. Two parameters are directly controlled, namely the internal pressure and axial feeding, and the interaction between them on the formability is shown in Figure 2.7. The chart forms a process window in which the process has to take place to form a correct part. When the load path, the relation between the internal pressure and axial force, is located outside the process window, failure occurs.

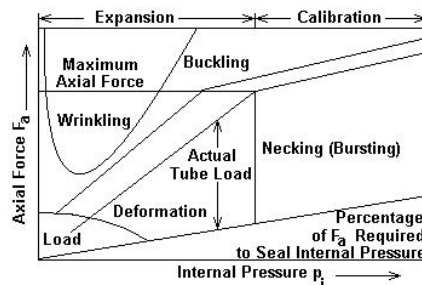


Figure 2.7. Process window

Excessive axial feeding at the beginning of the forming process, in combination with low pressure, while the tube has no contact with the die wall, leads to buckling depicted in Figure

2.8b. Wrinkling, local buckling, occurs both in the beginning and further along in the process and is caused, like buckling, due to high compressive stresses in the tube wall. Buckling generally occurs for relatively long, thick-walled tubes, while wrinkling occurs for tubes with a relatively small wall-thickness for both long and short tubes.

Excessive internal pressure leads to necking. This is a local instability of the tube wall caused by high internal pressure in combination with lack of axial feeding and is mostly followed by bursting.

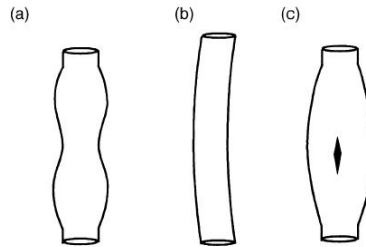


Figure 2.8. Common failure modes, which limit the THF process. (a) Wrinkling; (b) buckling, (c) bursting.

Axial feeding or axial force is applied for multiple reasons dependent on the type of process. For all process types the axial force is used to seal off the tube to make internal pressure build up possible and is therefore dependent on the internal pressure in combination with the surface area on which the pressure is working. In the process window shown in Figure 2.7 it results in a straight line as a lower limit.

Axial feeding is only efficient in the area near the end of the tube. Figure 2.9 shows characteristic areas of the tube and the effect on material feeding possibilities. Feeding material to areas further along the tube needs much higher axial forces to overcome the friction between the tube and the die, increasing the possibility to exceed the material strength. Regardless of the tube length, no axial feeding is possible to areas after a bend due to wrinkles occurring in the inside of the bend.

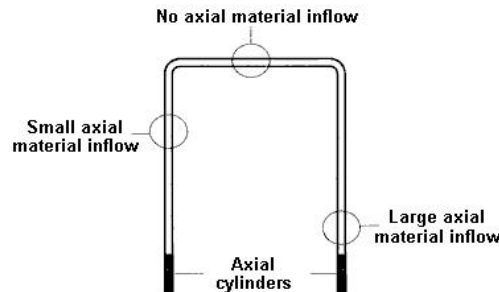


Figure 2.9. Different zones of axial feeding in a hydroform product

Many studies are conducted to optimise the process parameters involving hydroforming. Particularly the relation between the internal pressure and axial feeding is investigated using experimental and theoretical studies, where the latter imply both analytical studies and optimisation routines.

2.4 Influence of Tube Geometry on the Hydroform Process

The most used initial tube geometry is circular. The choice of tube diameter and wall thickness depends on the final hydroform part shape and application, pursuing an optimal mass to strength and mass to stiffness ratio. Stiffness is determined by the part geometry, thus for a given die geometry fully dependent on the wall thickness and wall thickness distribution. Strength of the hydroformed part is besides on the geometry also dependent on the material characteristics, where work hardening is of great importance.

HPH uses tubes with a perimeter approximately 5 to 10% smaller than the die perimeter. This leads to a high elongation in the tube wall. High pressure needed for complete expansion of the tube causes high normal stresses between the tube wall and die, with that increasing friction leading to locking of the tube wall areas in contact with the die. This locking leads to a reduced material flow in the contact areas, leading to increased expansion in the rest of the tube.

Tubes described above all have a circular perimeter and are uniform along the length of the tube. A new development of hydroform tubes is a conical tube suited for hydroform parts with a largely varying perimeter along the length of the tube. For instance a B-pillar of a body-in-white, as shown in Figure 2.2, with a large perimeter at the bottom and small perimeter at the top. A big advantage of conical tubes is the reduced expansion compared to a normal tube with a perimeter equal to the smallest perimeter of the hydroformed part, moreover optimising the wall thickness distribution over the length of the tube. Both advantages mentioned are important for increasing strength and rigidity with decreasing the mass, using high strength steels.

J.Spörer et. al. [30] show a development of a tube with a non-circular perimeter suited for manufacturing an aluminium rear cross member for the rear axle mounting using hydroform technique. The use of these kind of new tubes can lead to a reduction of the cycle time by reducing the number of production steps. In this case the pre-forming step and the heat treatment became redundant, as shown in Figure 2.10.

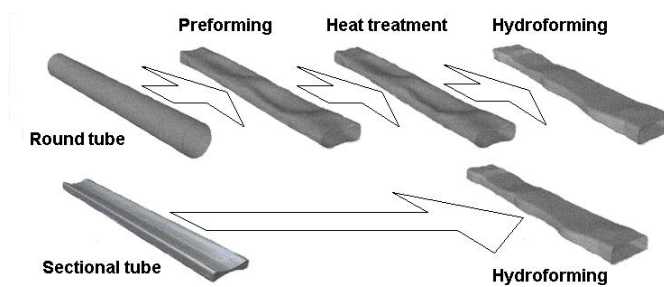


Figure 2.10. Optimisation of initial tube by BMW [30]

Tubes with non-circular cross-sections have, as described above, the potential advantages to produce more complex parts or to achieve a more cost efficient production. The engineer finds himself for a new task finding the optimal, or at least better, cross-section. In the next chapter a mathematical approach is presented for finding these kinds of optima.

3 Theory: Mathematical Optimisation

To optimise industrial problems a systematic approach is necessary to increase the chance of reaching the desired goal in a reasonable amount of time. Mathematical tools form the basis for this approach. The optimisation problem is first evaluated before experiments are conducted to minimize the use of resources without affecting the outcome of the optimisation problem. The approach divides the optimisation problem into four steps:

1. Selecting variables
2. Defining objective function / criterion
3. Defining a set of constraints
4. Determining the optimum with the corresponding set of variables

The input of the optimisation problem is selected in the first step, taking into account the most important and interesting parameters. A distinction is made between variable and constant parameters; see section 3.1.

The second and third item of the approach is the definition of the desired goal and restrictions of the optimisation problem in a mathematical form. The objective function is the mathematical formulation of the aim of an optimisation problem (section 3.2). A badly defined objective function can lead to an outcome of the optimisation problem, which is of no or less interest to the engineer. Therefore the objective function must be formulated with care.

Restrictions of the optimisation problem are formed by the constraints of the parameters, but can also depend on the outcome of the experiments. This is discussed in section 3.3.

After these three steps the problem is well defined and can be solved. The mathematical algorithm needed for this step depends not only on the optimisation problem, but also on the approach of the solving step itself. This is explained in section 3.4 followed by the description of *Response Surface Methodology* (RSM) (section 3.5). RSM is an optimisation strategy using regression analysis to approximate a response surface of the objective function.

3.1 Parameters

The design parameters are the input or conditions of the optimisation problem. The parameters can be both continuous (the pressure inside the hydroform tube) and discrete (the number of tubes). The design parameters can be divided into variables, parameters and constants. All three groups are explained below in separate sections. The type of variable influences the choice of optimisation algorithm suited for the problem solving. Optimisation problems consisting of continuous variables can be solved using classical algorithms, while discrete variables need special kind of algorithms. In this report only continuous variables are used, therefore discrete variables are not discussed any further.

Design Variables

The design variables or factors are altered to obtain the different settings of the experiments. The number of design variables determines the kind of algorithm needed. Problems with a few variables need a different kind of algorithm than problems containing several hundreds of variables to ensure an effective way of finding a solution. The complexity of the problem depends on the number of variables present in the optimisation problem. Therefore if possible only the most significant and important parameters need to be considered.

Design Parameters

The variables of less interest are the parameters, which are constant for the current optimisation problem. They can however be altered by the engineer. Design variables and design parameters are interchangeable, resulting in a new optimisation problem.

Design Constants

The last group of parameters are the design constants. These parameters cannot be controlled by the engineer but are of influence on the outcome of the optimisation problem; for instance gravity.

3.2 Objective Function

With the determination of the design variables, parameters and constants, the input of the optimisation problem is known. The outcome of the problem is formed by the objective function, a mathematical description of the optimisation goal. The true optimum of the objective function is called the global optimum and can either be a maximum or a minimum. In the case of this report, minimisation problems are considered. However, a maximisation problem can be transformed to a minimisation problem by $\max(f) = \min(-f)$, with f the objective function.

It is possible to optimise more than one objective function at the same time. This requires another type of algorithms to solve the optimisation problem and is the field of multi-objective optimisation. The optimum points are called "Pareto" points (see [5].) Before conducting the optimisation problem with multiple objective functions, the possibility to concentrate on one objective function must be considered. The remaining objective functions can be transformed in criteria for the experiments and thereby forming implicit constraints. This is further explained in section 3.3.

3.3 Constraints

The type of algorithm needed for finding a solution for the objective function, depends on the restrictions of the optimisation problem. When no restrictions are present the problem is unconstrained. Most industrial optimisation problems however are restricted in some sort of way, thereby forming a constrained problem. The constraints form a boundary of the solution space, with it forming a feasible domain. The optimum can be located within the feasible domain or on its border. The former one is called an interior optimum and can be treated as an unconstrained problem.



Figure 3.1. Schematic representation of the input and output of an experiment

In Figure 3.1 the input and the output of an experiment is represented. Here a division is shown between constraints known prior to the experiment and formed by the response of the experiment. The constraints are called explicit and implicit constraints respectively. Both types of constraints can be either equality or inequality and are either linear or non-linear. The optimum for an equality constraint is located on a boundary for at least one of the design

variables. For an inequality constraint a boundary is formed to which a relation must be larger or smaller. The total optimisation problem can now be formulated as follows:

$$\begin{aligned} \min \quad & f(\mathbf{x}) \\ \text{s.t.} \quad & h(\mathbf{x}) = 0 \\ & g(\mathbf{x}) \leq 0 \end{aligned} \tag{Eq. 3.1}$$

Where \mathbf{x} denotes the design variables.

As mentioned in the previous section, objective functions can be transformed into implicit constraints. Like the objective functions these constraints depend on the outcome of the experiment. The transformation from objective function to implicit constraint is not complicated. For each objective function, for example $f_2(\mathbf{x})$ a maximum value (in case of a minimisation problem) for which the outcome is still acceptable must be determined, say f_2^* . The implicit constraint becomes:

$$f_2(\mathbf{x}) \leq f_2^* \tag{Eq. 3.2}$$

Which is rewritten to:

$$\begin{aligned} f_2(\mathbf{x}) - f_2^* &\leq 0 \\ \Rightarrow g_{impl}(\mathbf{x}) &\leq 0 \end{aligned} \tag{Eq. 3.3}$$

The shape of an implicit constraint is not known and dependent on the used optimisation algorithm; only the direction of the constraint for an experimental run can be determined. With Response Surface Methodology, discussed in section 3.5, an approximation of the constraint can be made.

Together all the constraints form the boundary of the feasible domain. Within this domain the optimum is solved. Experiments can only be run if the values of the design variables are located within or on the border of the feasible domain. Before the first experiment is executed the feasible domain is formed by the explicit constraints only. The actual boundary of the domain is not known until sufficient experiments are executed to determine the exact location of the remaining implicit constraints.

The feasible domain is the maximum domain usable for conclusions about the optimisation problem, i.e. the shape of the objective function. However, the actual domain suitable for optimisation is determined by the location and number of experimental data within the feasible domain. Extrapolation of experimental data is not allowed, to prevent a meaningless conclusion.

3.4 Optimisation

With the above, the first three points of the optimisation procedure stated at the beginning of this chapter are completed. The last step is the actual optimisation of the problem. For this a good algorithm is needed to find the optimum in an efficient way. In this section the optimisation algorithms are briefly discussed. The optimisation method used for this thesis is Response Surface Methodology (RSM). Interested readers are referred to literature (L.F. Alvarez [2] and M Bonte [5])

3.4.1 Iterative and Approximation Methods

The optimisation in this thesis is based on finite element simulations, which are computational expensive operations. Therefore an optimisation method with a low number of simulations is best to be used. Most classical optimisation algorithms are iterative techniques. For each iteration a new finite element simulation is needed. The iteration tends to be slow in the neighbourhood of an optimum, which can lead to a large number of iteration steps thus a large number of finite element simulation.

Another disadvantage of iterative techniques is the validity of the optimum. The optimum is always a local optimum and no statement can be made whether the optimum is the global optimum. In Figure 3.2 a function is depicted, where point A is a local and point B the global optimum. The optimum reached depends on the starting point of the iteration.

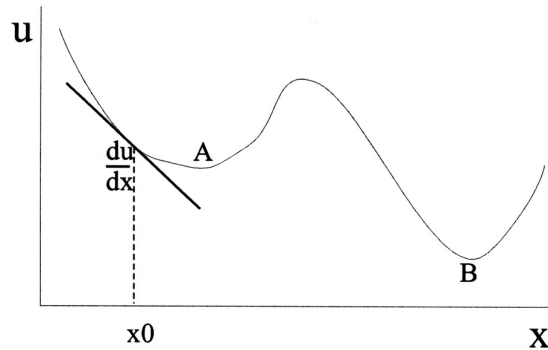


Figure 3.2. Derivative of a function in point x_0 , with A and B local optima

Furthermore the iterative technique is often based on the derivative of the objective function. The code of the finite element program needs to be adjusted to obtain the derivative of the objective function, which is dependent on the optimisation problem. Most finite element packages are not suited for adjustments by the user. A few iterative algorithms obtain the derivatives independent of the finite element (FE) code or do not use derivatives at all. However, these algorithms are highly inefficient.

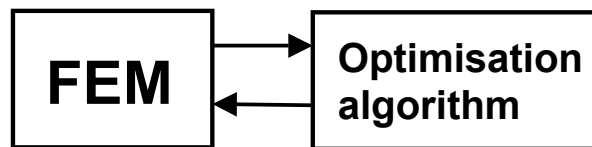


Figure 3.3. Schematic representation of iterative optimisation

To reduce the number of needed FEM simulations another technique for optimisation was developed, called approximation optimisation methods. The solution of this method is not the true optimum, but an approximation. The lack of accuracy is compensated by the relatively small computational costs.

For approximation methods both local and global algorithms exist. A well known global approximation strategy is response surface methodology (RSM). The technique combined with FEM is schematically depicted in Figure 3.4.

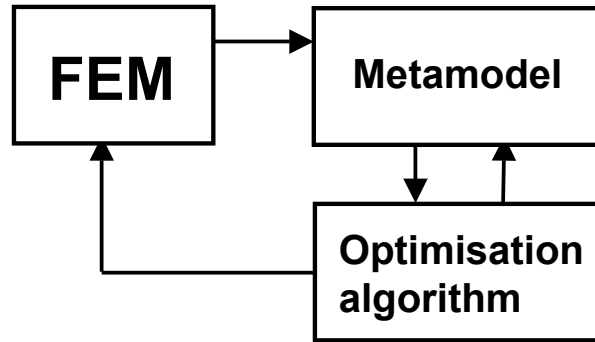


Figure 3.4. Schematic representation of approximate optimisation

RSM uses a metamodel constructed from a number of data points, formed by the FE simulations in combination with the objective function. To obtain as much information from a small number of simulations as possible, an experimental design is used. In this case a Design of Experiments (DOE) strategy. This design forms a scheme with the variations of the design variables. The model is built using linear regression analysis like least square method and is solved with classical algorithms.

RSM was originally developed for responses obtained from physical experiments, which involve random errors due to noise. Later it is used for computer experiments, which have a deterministic character. In recent years Design and Analysis of Computer Experiments (DACE) is developed. This is an optimisation strategy, using experimental design, to adapt to the more local behaviour of the response. An example of this technique is Kriging. The difference between a deterministic and non-deterministic (stochastic) approach is depicted in Figure 3.5.

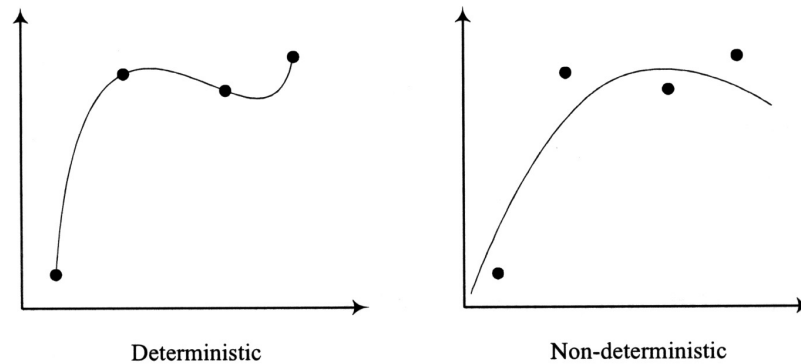


Figure 3.5. Deterministic and stochastic metamodel

The solution obtained from the metamodel can be quite coarse. Further investigation of the approximated optimum can be conducted by using sequential approximate optimisation. Around the approximated optimum an area of the original domain is selected, where a new optimisation is performed. This can be done using both iterative as approximate optimisation methods. For this thesis RSM is used and further discussed in the next section.

3.5 Response Surface Methodology

Response surface methodology (RSM) is as described in the previous section an approximating technique for optimisation of objective functions. RSM is subdivided into several steps to obtain a metamodel for optimisation. The first step is the selection of the experiments. For this a Design of Experiment strategy is used, which is described in section 3.5.1.

In the second and most time consuming step the experiments are conducted according to the experimental design. The results of the experiments are used to form a metamodel with linear regression analysis. The model is subsequently optimised with a standard Matlab function for constrained optimisation based on Quasi-Newton line search. The underlying algorithms for the tool are explained briefly in section 3.5.4.

3.5.1 Design of Experiments

Design Of Experiments (DOE) is the deliberately changing of one or more variables in order to investigate the effect of the changes on one or more response variables. The number of experiments and the spreading of the results in the feasible domain influence the forming of the metamodel. A DOE places the experiments in the feasible domain to obtain a model, which beholds as much information as possible with as low as possible number of experiments [20,25].

The most common Designs of Experiments are the classical designs. These designs form either a hyper cube or a hyper sphere in the design space. Advanced designs use computer software to place the points in the design space using several criteria, thereby obtaining the ability to fill the feasible domain more efficiently compared to classical design space.

For this project the use is made of a Box-Wilson Face Centred Central Composite design (CCD). For the terminology and background of the classical designs the reader is referred to Appendix A. In this section only a few global characteristics of the CCD design are denoted.

The basis of a CCD design is a two-level full factorial design, capable of determining linear and two-factor interaction behaviour of the response. To determine quadratic behaviour also, extra points are added. A centre run, located in the exact middle of the design, is suited for better prediction of interaction effects and indicates the presence of quadratic effects. The centre run alone cannot estimate the quadratic effects and therefore the star points are added. The star points, two times the number of design variables, are located at a distance α of the centre of the design. In Figure 3.6 the three variants of Central Composite Design for two design variables are depicted.

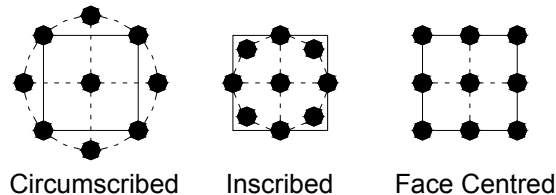


Figure 3.6. Central Composite Designs

For n design variables the number of runs of the designs is equal to $2^n + 2n + 1$ (two-level design plus the star points plus the centre run). The Face Centred CCD is the only CCD design forming a hyper cube in the design space. The star points for the Face Centred design are located at $|\alpha| = 1$. This means that in contrast of the two central composite designs mentioned above, the design has three levels per factor. The design is less suited for estimating the quadratic effects due to the number of levels. The advantage however is the

better spreading of points in the design space compared to the inscribed design and the smaller range compared to the circumscribed design. This last argument is important due to potential impossible combinations of levels of the design variables.

To reduce the number of experiments a fraction of the design can be used to determine the metamodel. The reduction of experiments leads to confounding of effects, which is minimised by following multiplications rules. Confounding means effects are paired (for instance linear with interaction effects), which makes it impossible to estimate individual effects. The degree of confounding is further explained in Appendix A.

3.5.2 Function Order

Linear regression analysis is used to determine the values of parameters of the metamodel based on the results of the experiments. The analysis is performed using a least-square-error method to find the values of parameters resulting in the best fit. The regression analysis however is not capable of determining the type of function needed, but use an on forehand stated function.

The experimental design used (Face Centred CCD) is capable of determining linear, quadratic and interaction terms. To see what kind of model best represents the experimental data several models are fitted. The first model fitted with linear regression analysis is a simple linear model of the form.

$$f = \alpha_0 + \alpha_i x_i \tag{Eq. 3.4}$$

The fit of the model is checked using lack-of-fit tools (discussed in the next section). If the model has a sufficient fit to the experimental data, the optimisation is performed. Otherwise the model is altered by adding terms to Eq. 3.4. This is repeated until a good model is found. The models used are:

$$\begin{aligned} f &= \alpha_0 + \alpha_i x_i + \alpha_{jk} x_{jk} && \text{Linear model with interactions if } j < k \\ f &= \alpha_0 + \alpha_{ii} x_{ii} && \text{Quadratic model} \\ f &= \alpha_0 + \alpha_i x_i + \alpha_{jk} x_{jk} && \text{Quadratic model with interactions if } j \leq k \end{aligned} \tag{Eq. 3.5}$$

It is known that adding terms to the model will always lead to a better description of the experimental data. Therefore the regression analysis starts with the simplest model. The last model of Eq. 3.5 is not expanded further due to the property of the Face Centred CCD, which is only capable of determining quadratic effects at its maximum. Furthermore, a higher order model consists out of a must larger number of terms. Fitting these models becomes numerically expensive. Remark must be made to the design. The number of levels is only three, which is the minimal number of points needed to fit a quadratic function. Due to the absence of control points the model will always find a good fit for the quadratic terms.

3.5.3 Lack-Of-Fit

The response surface formed with the linear regression analysis of the previous section is an approximation of the data points formed by the experimental design of section 3.5.1. This means the data points are not located on the response surface. The regression analysis selected the values of the parameters for the response surface, which minimise the error to the data points. To examine the fit of the response surface to the data points, a lack-of-fit analysis is conducted. Five lack-of-fit tools suited for the analysis of the response surface are represented below.

R-squared

One of the tools is the R-squared value, which is formed by:

$$R^2 = \frac{SS_R}{SS_T} \quad \text{Eq. 3.6}$$

With

$$\begin{aligned} SS_T &= SS_R + SS_E \\ SS_T &= \sum_{i=1}^n (y_i - \bar{y})^2 \\ SS_R &= \sum_{i=1}^n (\hat{y}_i - \bar{y})^2 \\ SS_E &= \sum_{i=1}^n (y_i - \hat{y}_i)^2 \end{aligned} \quad \text{Eq. 3.7}$$

Where y_i and \hat{y}_i are the experimental data and the estimated value respectively. The R-squared value is between zero (no correlation) and one (perfect fit). Some caution should be taken, when using the R-squared value. When adding extra terms to the model, the R-squared value will always increase. This does not necessary imply a better model.

Adjusted R-squared

A variant of the above is the adjusted R-squared, which accounts for the number of terms in the model and the available experimental data:

$$\begin{aligned} \bar{R}^2 &= 1 - \left(\frac{n-1}{n-p} \right) (1 - R^2) \\ &= 1 - \left(\frac{n-1}{n-p} \right) \frac{SS_E}{SS_T} \\ &= 1 - \left(\frac{n-1}{SS_T} \right) MS_E \end{aligned} \quad \text{Eq. 3.8}$$

Where n is the number of data points, p the number of terms in the regression model and MS_E is the mean square error, i.e. sum of square error divided by the number of degrees of freedom. The adjusted R-squared value can both increase and decrease by adding terms to the model. The decrease of the adjusted R-squared value occurs when the decrease of the error is not compensated by the loss of degree of freedom of the regression.

The maximum of the adjusted R-squared value is reached when MS_E is at its minimum. This is derived from the believe that the sum of squares of the new model must reduce by an amount equal to the mean square error of the old model to gain a better model:

$$SS_{E,old} - SS_{E,new} < MS_{E,old} \quad \text{Eq. 3.9}$$

The MS_E will increase if this is not the case due to the loss of a degree of freedom. Therefore the model with the lowest MS_E is considered to be the best model, corresponding to a maximum of the adjusted R-squared value.

F-stat

Another way of investigating the model is the F -stat, which is not an actual lack-of fit test but a test for significance of regression. This statistical tool uses a hypothesis test for an F -distribution. The response model is represented as:

$$\hat{y} = \beta_0 + \beta_1 x_1 + \beta_2 x_2 \dots \quad \text{Eq. 3.10}$$

The hypothesis test:

$$\begin{aligned} H_0 : \beta_1 = \beta_2 = \dots = \beta_k = 0 \\ H_1 : \beta_i \neq 0 \text{ for at least one } i > 0 \end{aligned} \quad \text{Eq. 3.11}$$

The hypothesis H_0 is rejected when with a confidence of $(1 - \alpha) \cdot 100\%$ at least one effect is significant, i.e. not zero. To satisfy H_1 , the F value of Eq. 3.12 is above a critical value, determined from statistical tables for the distribution of $F_{(1-\alpha),k,n-k-1}$. The test statistic is formed by:

$$F = \frac{SS_R/k}{SS_E/(n-k-1)} = \frac{MSR}{MSE} \quad \text{Eq. 3.12}$$

Where k is the degree of freedom of the regression model.

p-value

The p-value is the probability of wrongly rejecting the null hypothesis if it is in fact true. The p-value is compared to the confidence interval, formed by $(1 - \alpha)$. The p-value must be smaller than α to confirm the hypothesis test of Eq. 3.11.

t-test

The F statistic tells us something about the model in general. The following step is to look at the individual effects. For this a new hypothesis test is used:

$$\begin{aligned} H_0 : \beta_i &= 0 \\ H_1 : \beta_i &\neq 0 \end{aligned} \quad \text{Eq. 3.13}$$

Where the hypothesis H_0 is rejected if t is above or below a critical value, formed by $t_{\alpha/2, n-k-1}$ and $t_{(1-\alpha/2), n-k-1}$ respectively. The t value is formed by:

$$t = \frac{\beta_i}{S_{\beta_i}} \quad \text{Eq. 3.14}$$

Where β_i is the estimated effect and S_{β_i} the standard error.

3.5.4 Optimisation Algorithms

In this section the algorithms used by Matlab in the function *fmincon* is briefly discussed [1]. For comparison between different algorithms is referred to the work of Martijn Bonte [5]. *fmincon* is a Matlab routine for constrained optimisation, suited for Response Surface Methodology. The constraints can be both equality and inequality constraints and are of the same form as described in section 3.3.

The Matlab routine is divided in large-scale and medium-scale optimisations. For large-scale optimisations a trust region method is used, based on the interior-reflective Newton method described in [8] and [9].

The strategy of a trust region method is to optimise the objective function $f(x)$ around iterate x_k by approximating the objective function by a model function q_k . In a standard trust region, the quadratic approximation q_k is defined by the first two terms of the Taylor approximation of the objective function around x_k :

$$q_k(x_k + p) = f_k + p^T \nabla f_k + \frac{1}{2} p^T H_k p \quad \text{Eq. 3.15}$$

Where H is the Hessian matrix containing the second order derivatives of the objective function:

$$H = \begin{bmatrix} \frac{\partial^2 f}{\partial x_1 \partial x_1} & \dots & \frac{\partial^2 f}{\partial x_1 \partial x_n} \\ \vdots & \ddots & \vdots \\ \frac{\partial^2 f}{\partial x_n \partial x_1} & \dots & \frac{\partial^2 f}{\partial x_n \partial x_n} \end{bmatrix} \quad \text{Eq. 3.16}$$

The trust region method is based on the minimisation of

$$\min_p q_k(x_k + p) \quad \text{Eq. 3.17}$$

Where p is the direction within a trust region N around x_k , usually spherical or ellipsoidal of shape. If $f(x_k + p) > f(x_k)$, the trust region is reduced and minimised again according to Eq. 3.17. Subsequently x_k is updated.

For medium-scale optimisations the Matlab routine *fmincon* uses Sequential Quadratic Programming. This is based on Quadratic Programming (QP), which have the standard form:

$$\begin{aligned} \min f(x) &= x^T Hx + c^T x \\ \text{s.t.} : A_1 x - b_1 &= 0 \\ A_2 x - b_2 &\leq 0 \end{aligned} \quad \text{Eq. 3.18}$$

Sequential Quadratic Programming method solves a QP sub problem at each iteration. The basic idea is to solve the Karush-Kuhn-Tucker (KKT) conditions iteratively with Newton's method. This is a necessity condition for problems with mixed constraints, i.e. both equality and inequality constraints:

$$\begin{aligned} h(x^*) &= 0, g(x^*) \leq 0 \\ \nabla(f^*) + \lambda^T \nabla h^* + \mu^T \nabla g^* &= 0^T, \lambda \neq 0, \mu^T \geq 0, \mu^T g = 0 \end{aligned} \quad \text{Eq. 3.19}$$

For a problem with only equality constraints, Newton's method leads to the following set of equations.

$$\begin{pmatrix} \nabla^2 L_k & (\nabla h)_k^T \\ (\nabla h)_k & 0 \end{pmatrix} \begin{pmatrix} p_k \\ \lambda_{k+1} \end{pmatrix} = - \begin{pmatrix} \nabla f_k \\ h_k \end{pmatrix} \quad \text{Eq. 3.20}$$

With L the Lagrangian in which only equality constraints h are present, λ the Lagrange multipliers and f the objective function. A related quadratic programming problem can now be solved for the k^{th} iteration step:

$$\begin{aligned} \min Q(p) &= \nabla f_k p + \frac{1}{2} p^T (\nabla^2 L_k) p \\ \text{s.t.} : (\nabla h)_k p - h_k &= 0 \end{aligned} \quad \text{Eq. 3.21}$$

The Hessian matrix is obtained by a Broyden-Fletcher-Goldfarb-Shannon (BFGS) Quasi-Newton method. This method is used for updating the Hessian matrix in a numerically cheap way.

The Matlab routine *fmincon* is suited for finding local optima. For the global optimum the following assumption is made:

When optimising with the Matlab routine 'fmincon' from every point of the experimental design, at least one of the solutions is the global optimum.

The response surfaces are of a maximum order of two. This means that for an unconstrained problem (only bounded by the boundaries of the feasible domain), the surface has only one optimum and is therefore the global optimum. The implicit constraints are also of a maximum order of two. Therefore in this case it is believed the assumption is valid.

In the next chapters the theory discussed in the sections above is applied to a case study, the optimisation of the metal forming process of chapter two; tube hydroforming.

4 Experimental Simulations

This chapter and the following two chapters discuss an application of the theory described in chapter 3: The optimisation of the initial tube geometry for hydroform tubes. For the simulations of the hydroform process a die with a square geometry is used, which is depicted in Figure 4.1. The simulations are conducted in plane strain conditions, a common situation in the hydroforming processes due to the absence of axial feeding as indicated in section 2.3. The parameters, which are altered to find the optimum, form the description of the initial tube geometry (section 4.1) and the objective of the optimisation problem is a uniform wall thickness distribution. Several formulations for the objective are used to investigate the influence on the optimum.

The boundaries of the problem are described in section 4.3. Besides explicit constraints, an implicit constraint is introduced formed by the margin to failure. In this case necking. The chapter concludes with the implementation of an experiment design, namely Face Centred Central Composite Design.

4.1 Choice of Design Parameters

As mentioned in the introduction, the goal of the thesis is to optimise the initial tube geometry for hydroforming. Applying the theory discussed in chapter 3, would imply the initial tube geometry as the objective function. Even though this kind of formulation is commonly used, the actual goal (objective) of the optimisation problem is a uniform wall thickness distribution and the initial tube geometry is used to achieve this goal. Therefore the parameters used to describe the initial tube geometry are the design variables. Parameters that are variable but kept constant for this optimisation problem are called design parameters.

4.1.1 Design Variables

As mentioned above, the parameters describing the initial tube geometry are design variables. It is possible to describe the initial tube geometry in several different ways. For this project a Cartesian coordinate system is used.

The geometry is based on the estimated practical limitations of the tubular blank process (section 2.2.1). At this moment the tubular blank machine is designed to produce round tubes. For applying non-round tubes in the future, the practical and economical limitations of the machine needs to be described in detail. For now the limitation is set on two different dimensions for radii, implying two different tool sets. Furthermore, the tube is assumed to be prismatic.

The die used for the experiments is square with rounded corners, depicted in Figure 4.1. The height of the square is 60 millimetres with corner radii of 6 millimetres. The lines of symmetry are marked in red.

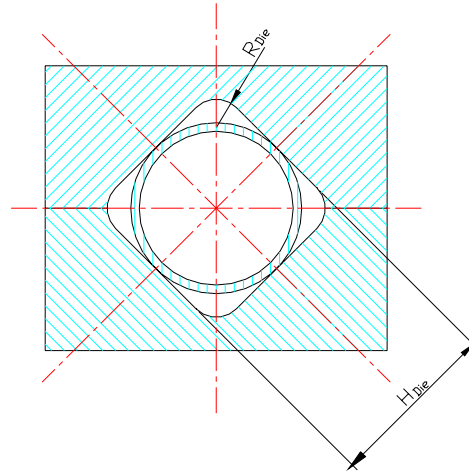


Figure 4.1. Die-shape for "corner filling" tests

The finite element models will consist of a quarter tube, to simulate the plane strain deformation of the tube during hydroforming. A possible initial tube is depicted in Figure 4.2. The geometry is described using seven variables, three lengths (H , L , δ), the thickness (t) two radii (ρ_1 , ρ_2) and one angle (β). The radii will be described using the radius of curvature κ , to be able to describe both concave and convex radii for ρ_2 . This is due to the discontinuity of the radius in the transition from a concave to a convex radius and visa versa.

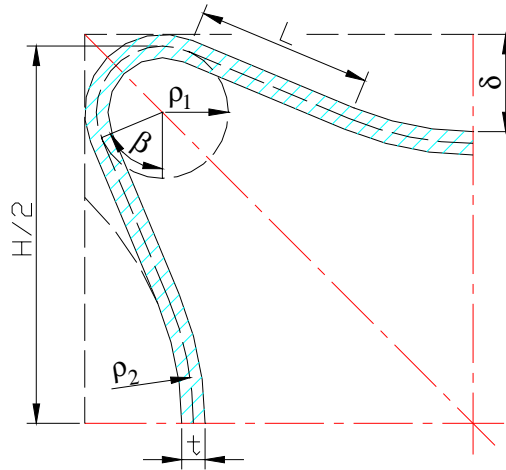


Figure 4.2. Design variables to describe the initial tube geometry

The relation between the design variables depicted in Figure 4.2 is formed by the following two equations:

$$\frac{H}{2} = \frac{1}{\kappa_1} + \frac{\kappa_2 - \kappa_1}{\kappa_1 \kappa_2} \cos \beta + L \sin \beta \quad \text{Eq. 4.1}$$

$$\delta = -\frac{\kappa_2 - \kappa_1}{\kappa_1 \kappa_2} (1 - \sin \beta) - L \cos \beta \quad \text{Eq. 4.2}$$

Where

$$\kappa_1 = \frac{1}{\rho_1} \quad , \quad \kappa_2 = \frac{1}{\rho_2} \quad \text{Eq. 4.3}$$

The derivation of the equations can be found in Appendix B. From Eq. 4.1 and Eq. 4.2 it is seen that there are five degrees of freedom instead of the seven variables depicted in Figure 4.2. Thus the initial geometry from Figure 4.2 can be described with five design variables. For this optimisation problem the following design variables are chosen: the height H , the radius of curvature κ_1 , the radius of curvature κ_2 , the length L and the wall thickness t .

4.1.2 Design Parameters and Constants

The design variables are established and the remaining parameters for hydroforming are constant. This includes material parameters, geometrical parameters (initial geometry) and process parameters. The remaining geometrical parameter is the length of the tube, which is trivial due to the assumption of plane strain and prismatic geometry.

The plane strain situation implies also that no axial feeding is applied. The axial force however is not zero and provides stress in the length of the tube. This is due to the self-feeding character of tubes during hydroforming. Another process parameter is the friction. The lubrication and most of all the pressure determine amongst other things the friction force during the hydroform process. For the simulations for this project Coulomb friction is assumed, with a constant friction coefficient of $\mu = 0.1$.

In the beginning of the project the material parameters of DP600 were used for the optimisation problem. DP600 is a dual phase high strength steel and of high interest for hydroform applications. Due to the low work hardening coefficient n , the maximum strain before failure is relatively low. This leads to convergence problems for a wide range of settings for the design variables. Therefore another type of material was used with a higher work hardening coefficient (see Table 4.1), namely the mild steel DC04. This material has a higher strain before failure and is more stable during numerical simulations.

Table 4.1. Material properties

	DP600	DC04
σ_{y0}	431	174
n	0.151	0.213
C	1004	542
ε_0	0.0037	0.0048

4.2 Objective Function

The aim of an optimisation problem is to minimise or maximise an objective, named the objective function. The optimum of the objective function corresponds to a set of values for the design variables. In the next subsections the formulation of objective functions for a wall thickness distribution is discussed.

4.2.1 Wall Thickness Distribution

The wall thickness distribution of a hydroformed tube influences the properties of the product. A uniform or an almost uniform wall thickness distribution provides a more uniform stiffness and strength of the tube wall. In case of a plane strain situation a uniform wall thickness distribution implies an equal plastic deformation in the entire tube. Let us consider the invariance of volume for an infinitesimal cube.

$$\begin{aligned}
 \varepsilon_1 + \varepsilon_2 + \varepsilon_3 &= 0 \\
 \text{Plane strain} &\rightarrow \varepsilon_2 = 0 \\
 \Rightarrow \varepsilon_3 &= -\varepsilon_1 \\
 \Rightarrow \varepsilon_{\text{thickness}} &= -\varepsilon_{\text{hoop}}
 \end{aligned}
 \tag{Eq. 4.4}$$

Eq. 4.4 implies a uniform strain in circumferential direction, when the wall thickness is uniformly distributed over the tube perimeter. This holds only for tubes with a small wall thickness compared to the diameter of the tube, where the bending effect becomes secondary.

In this section the quantification of the wall thickness distribution is derived in the form of an objective function. The wall thickness is a continuous function of the tube perimeter and for the determination of the distribution a finite number of observations is used. The number of observations is denoted with N and is related to the number of elements used in a finite element model of the tube. The i^{th} observation is denoted with $t_i(\mathbf{x})$ dependent of the design variables \mathbf{x} . The finite element model will be further discussed in section 5.1.

4.2.2 Absolute Difference

An overall measure for the observations of the wall thickness is the average wall thickness, $\bar{t}(\mathbf{x})$, dependent on the design variables \mathbf{x} . The wall thickness of the tube in an arbitrary point i along the perimeter of the tube is equal to the average wall thickness plus a variation:

$$t_i = \bar{t} + \delta t_i \tag{Eq. 4.5}$$

The variation δt_i represents the deviation to the average wall thickness. The comparison of variations for all points i is an quantification for the wall thickness distribution and forms the basis for the first group of objective functions. The simplest form is the summation of all variations:

$$f_1(\mathbf{x}) = \sum_{i=1}^N (\delta t_i)^\alpha = \sum_{i=1}^N (t_i(\mathbf{x}) - \bar{t}(\mathbf{x}))^\alpha \tag{Eq. 4.6}$$

Where α is a scaling factor. For $\alpha = 1$, Eq. 4.6 is always equal to zero, independent of the number and values of the observations. Odd values of α result in a summation of negative and positive values of δt_i , which lead to a meaningless evaluation of the wall thickness

distribution, i.e. high values for f could be assigned to uniform distributions and low values to coarse distributions and visa versa. To obtain an objective function with a value of zero for f for a sample with equal observations and increased values for f when the variation of the observations increase, the scaling factor α needs to be even. For the remaining objective functions the following count, unless stated otherwise: $\alpha = 2, 4, 6, \dots$

For small variations between the observations the values of δ_i are small. Due to the power of Eq. 4.6, especially for high values of α , the summation will consist of small values and lead to small variations of f between the experiments. To improve the distinction between the experimental results the inverse power of α is added:

$$f_2(\mathbf{x}) = \left(\sum_{i=1}^N (t_i(\mathbf{x}) - \bar{t}(\mathbf{x}))^\alpha \right)^{\frac{1}{\alpha}} \quad \text{Eq. 4.7}$$

Where $\alpha = 2$ and ∞ respectively represent the L_2 and L_∞ -norm. These are norms commonly used for evaluating properties of vectors.

The objective functions of Eq. 4.6 and Eq. 4.7 do not account for the number of observations, which will result in incomparable values for the objective function. The number of observations is not equal for all models due to different wall thicknesses and perimeters. Therefore the objective function is divided by the number of observations N :

$$f_3(\mathbf{x}) = \frac{\left(\sum_{i=1}^N (t_i(\mathbf{x}) - \bar{t}(\mathbf{x}))^\alpha \right)^{\frac{1}{\alpha}}}{N} \quad \text{Eq. 4.8}$$

An in the statistics common used and important measure of the spread of observations is the variance. This is roughly the arithmetic average of the squared distance from the mean. Written in general form, where $\alpha = 2$ represents the variance:

$$f_4(\mathbf{x}) = \frac{\sum_{i=1}^N (t_i(\mathbf{x}) - \bar{t}(\mathbf{x}))^\alpha}{N - 1} \quad \text{Eq. 4.9}$$

The standard deviation is the square root of the variance. This restores the unit of the spread to the original data units. Again written in general form, where $\alpha = 2$ represents the standard deviation:

$$f_5(\mathbf{x}) = \left(\frac{\sum_{i=1}^N (t_i(\mathbf{x}) - \bar{t}(\mathbf{x}))^\alpha}{N - 1} \right)^{\frac{1}{\alpha}} \quad \text{Eq. 4.10}$$

In the equation for the variance and standard deviation is divided by $N - 1$ instead of N . This results from the statistical fact that the average $\bar{t}(\mathbf{x})$ is not the true average, but an approximation. The true average is obtained when using an infinite number of observations. Due to this approximation the variance and standard deviation lose one degree of freedom, i.e. it is possible to calculate the N^{th} observations when $N - 1$ observations and the average are known. By using $N - 1$ the variance and standard deviations become bias corrected.

To represent the behaviour of the above described objective functions the course of the penalty for the observations is shown in Figure 4.3 for three values of α . The penalty is the value, which an individual observation contributes to the summation of the objective function. The penalty is zero when the observation t_i is equal to the average value \bar{t} . For the figure it is seen that for higher values of α the emphasis is on larger values for δt_i , but that the penalties self are lower. They only will be higher for higher values of α when δt_i becomes larger than \bar{t} . This would imply a thickness smaller than zero, which is impossible.

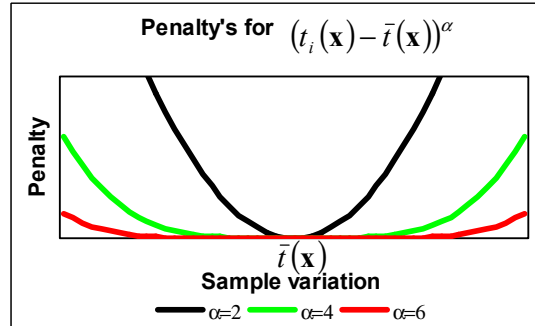


Figure 4.3. Penalty profile for objective functions

To obtain a penalty profile with more emphasis on small variations around the average value, but without exorbitant penalty values on a further distance to the average value, the following objective function is formulated:

$$f_6(\mathbf{x}) = \frac{\sum_{i=1}^N \left(1 - \left(e^{-\left(t_i(\mathbf{x}) - \bar{t}(\mathbf{x}) \right)^2} \right)^\alpha \right)}{N} \quad \text{Eq. 4.11}$$

The maximum value for a penalty is 1 and for higher values for α this value is reached for smaller variations around the average $\bar{t}(\mathbf{x})$. The penalty profile is depicted in Figure 4.4. Note that α can now assume all possible real values.

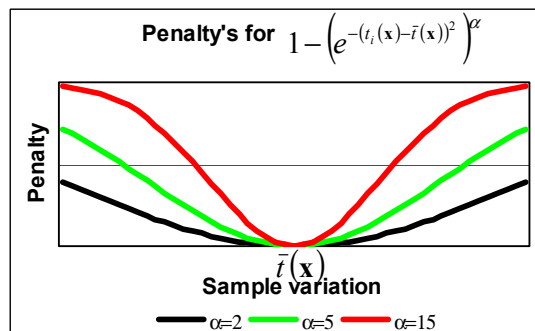


Figure 4.4. Penalty profile for objective functions of f_6

4.2.3 Relative Difference

Until this moment the absolute difference between the observations is considered. Another possibility for quantifying the wall thickness distribution is using the relative difference between the wall thickness in point i and the average wall thickness.

$$f_7(\mathbf{x}) = \left(\frac{\sum_i^N \left(\frac{t_i(\mathbf{x}) - \bar{t}(\mathbf{x})}{\bar{t}(\mathbf{x})} \right)^\alpha}{N} \right)^{\frac{1}{\alpha}} \quad \text{Eq. 4.12}$$

This function was derived using the objective function of Revuelta en Larkiola (2004) [29]. They used the initial wall thickness, $t_{0,i}$, instead of the average wall thickness. The emphasis of their objective function is not so much on the wall thickness distribution, but on the decrease of the wall thickness. This means that a uniform distribution with high strains in wall thickness direction can be considered worse than a coarse distribution with low strains. The objective function for this report focuses on the distribution only and for high strains a necking criterion is used (see section 4.3).

$$f_8(\mathbf{x}) = \frac{\sqrt{\sum_i^N \left(\frac{t_i(\mathbf{x}) - t_{0,i}}{t_{0,i}} \right)^2}}{N} \quad \text{Eq. 4.13}$$

The penalty profile for the objective function of f_7 (Eq. 4.12) is the same as Figure 4.3 with one difference. The penalty value is now no longer dependent on the absolute value of the average wall thickness, which is related to the initial wall thickness. This means objective function f_7 is not biased concerning initial wall thickness, which is a design variable.

4.2.4 Quotient

A third option for the formulation of objective functions for the wall thickness distribution is the quotient between $t_i(\mathbf{x})$ and $\bar{t}(\mathbf{x})$ as stated in Eq. 4.14 and Eq. 4.15. The former objective function emphasis on the observations with values higher, while the latter emphasis on the observations with values smaller than the average value.

$$f_9(\mathbf{x}) = \frac{\left(\sum_i^N \left(\frac{t_i(\mathbf{x})}{\bar{t}(\mathbf{x})} \right)^\alpha \right)^{\frac{1}{\alpha}}}{N} \quad \text{Eq. 4.14}$$

$$f_{10}(\mathbf{x}) = \frac{\left(\sum_i^N \left(\frac{\bar{t}(\mathbf{x})}{t_i(\mathbf{x})} \right)^\alpha \right)^{\frac{1}{\alpha}}}{N} \quad \text{Eq. 4.15}$$

Endelt and Nielsen (2001) [10] formulated an objective function based on the quotient of $t_i(\mathbf{x})$ and $\bar{t}(\mathbf{x})$. Their objective function consists of two parts namely $f_{th}(\mathbf{x})$ and $f_{geo}(\mathbf{x})$. The former determines the distribution of the wall thickness and the latter the geometric error of the fit to the die, i.e. how close the tube follows the shape of the die. The last stated is not

an objective for this project, but a constraint. The tube must fit to the die perfect at all times. The objective function is:

$$f_{11}(\mathbf{x}) = f_{th}(\mathbf{x}) + f_{geo}(\mathbf{x})$$

$$f_{11}(\mathbf{x}) = \frac{1}{2} \sum_{i=1}^N \left(\frac{\left(1 - e^{\left(\frac{\bar{t}(\mathbf{x})}{t_i(\mathbf{x})} \right)^{\alpha_1} - 1} \right)^2}{\alpha_2} \right) + \frac{1}{2} \sum_{i=1}^N \left(\frac{t_i(\mathbf{x})}{2\beta} - \frac{d_i(\mathbf{x})}{\beta} \right) \quad \text{Eq. 4.16}$$

Where α_1 , α_2 , β are scaling factors and d_i the distance between the die and the nodes. The penalty profiles for all three objective functions (f_9 , f_{10} and f_{11}) are asymmetric. In Figure 4.5 the penalty profile for Eq. 4.16 is depicted. The asymmetric characteristic of the objective function lead to a different evaluation of asymmetric distributions, dependent on which side of \bar{t} the largest variation is. For hydroform tubes this means that wall thickness reduction on small parts of the tube perimeter lead to high values for the objective function. The emphasis for this objective function is besides on the distribution also on the necking of the tube. As applied to the objective function of Eq. 4.13, only the wall thickness distribution is considered.

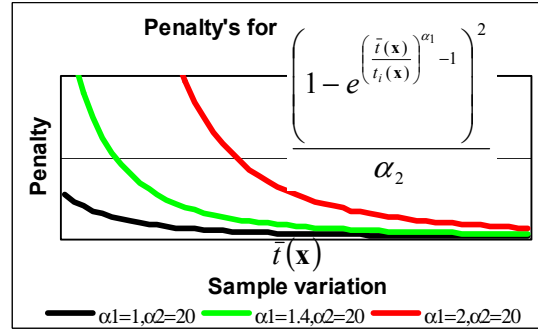


Figure 4.5. Penalty profile for the objective function of Eq. 4.16

4.2.5 Objective Function Selection

All objective functions mentioned above are some sort of measurements for the wall thickness distribution for a hydroformed tube, divided into three categories. The objective functions based on absolute and relative difference do not differ much in their evaluation of the wall thickness with the exception of the biasing effect of the objective functions based on the absolute difference. They are biased in favour of small values of $|\delta t_i|$. This has nothing to do with the strain in thickness distribution, but the initial wall thickness. Since, for a given strain distribution in wall thickness direction along the perimeter of the tube, a small initial wall thickness leads to small values of $|\delta t_i|$, while a high initial wall thickness will lead to high values.

The third group of wall thickness distributions has an asymmetric character and as a consequence less suitable for evaluating the distribution. For the remainder of the report three objective functions are examined in more detail. That is f_7 (Eq. 4.12) for the unbiased character towards the design variables, f_5 (Eq. 4.10) to investigate the influence of the biasing effect and f_6 (Eq. 4.11) for the emphasis on small variations around the average value of the wall thickness.

4.3 Constraints

All the design variables, parameters and objective functions are now known. In this section the boundaries conditions (constraints) are formulated, starting with the constraints depending on the design variables only. These explicit constraints form the boundaries of the feasible domain, for which the design of experiments are determined. First let us describe the constraints before formulating them in mathematical form.

1. The initial tube must fit in the die cavity of the closed die,
2. The minimum radius applied to the tube must be at least two times the wall thickness,
3. The (outside) perimeter of the tube must be at least 2 percent smaller than the perimeter of the die cavity,
4. After hydroforming the tube must have adopted the shape of the die,
5. Necking of the tube is not allowed.

The first three constraints are explicit constraints and are geometrical based. The last two constraints are implicit constraints. Endelt and Nielsen (2001) combined the fourth constraint with the evaluation of the wall thickness in the objective function of Eq. 4.16. With the theory of section 3.3 the second part of this objective function can be transformed into a constraint. However, for the simulations conducted for this project only a visual inspection of the mesh is performed. This is possible due to the simplicity of the die, for both two- and three-dimensional simulations.

Now the explicit constraints are formulated in a mathematical form, using the design variables of Figure 4.2 (initial tube) and the parameters of the die depicted in Figure 4.1.

Constraint 1.a: The total height of the initial tube, H_{tot} , is restricted to the height of the die cavity H_{die} .

$$\begin{aligned}
 H_{tot} &\leq H_{die} && \text{Eq. 4.17a} \\
 \Downarrow &&& \\
 H + t &\leq H_{die}, \quad \delta \leq 0 && \text{b} \\
 H + 2\delta + t &\leq H_{die}, \quad \delta \geq 0 && \text{c}
 \end{aligned}$$

Constraint 1.b: The length L cannot adopt negative values

$$L \geq 0 \quad \text{Eq. 4.18}$$

Constraint 2: The radius (measured on the outside of the bend) is not allowed to be smaller than two times the wall thickness. Note that the radii of curvatures are measured from the centre of the tube wall.

$$\begin{aligned}
 \frac{1}{\kappa_1} &\geq \frac{3}{2}t && \text{Eq. 4.19a} \\
 \frac{1}{\kappa_2} &\geq \frac{3}{2}t && \text{b}
 \end{aligned}$$

Constraint 3: The (outside) perimeter of the initial tube is restricted to a maximum of 98% of the perimeter of the die cavity. This boundary condition is created to prevent simulations of an almost filled die cavity.

$$P_{tube} \leq 0.98 \cdot P_{Die} \quad \text{Eq. 4.20}$$

In Appendix B the derivation of the explicit constraints is described in more detail. Constraint 5 restricts necking of the tube. Necking is one of the failure modes discussed in chapter 1 and can be simulated in the form of mesh localisation. This is however dependent on the mesh of the finite element model. For this reason a constraint is formulated, which is dependent on the response of the simulation. Therefore the constraint is implicit. Necking occurs when the strains exceed a certain limit, dependent on the strain ratio and strain path. In Figure 4.6 a forming limit diagram is displayed. The vertical and horizontal axis represents the first and second principal strain respectively. The line in the diagram is called the forming limits curve. When the strains of a point in the tube exceed the forming limit curve, the tube will neck at this point. For a plane strain situation, as used in this report, the second principal strain is always equal to zero. Therefore all points in the tube are situated on the vertical axis.

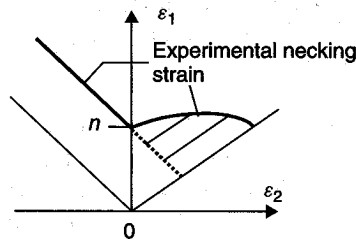


Figure 4.6. Forming limit diagram

The right side of the forming limit curve can be described with the Marciniak-Kuczynski criterion, based on the ratio of the strain rates. For the purpose of this report a criterion is used to describe the left side of the forming limit curve, given in Eq. 4.21. The derivation is described in Appendix C.

$$\varepsilon_1 + \varepsilon_2 = n \quad \text{Eq. 4.21}$$

This criterion is independent of the anisotropic effects of the material (assuming strain rate independent work hardening behaviour). The information can be obtained from the finite element package DiekA by using the equivalent strain. For a plane strain situation the following holds:

$$\begin{aligned} \bar{\varepsilon} &= \sqrt{\frac{2}{3} \{ \varepsilon_1^2 + \varepsilon_2^2 + \varepsilon_3^2 \}} \\ \text{plane strain: } \quad \varepsilon_2 &= 0, \quad \varepsilon_3 = -\varepsilon_1 \\ \Rightarrow \bar{\varepsilon} &= \sqrt{\frac{4}{3} \varepsilon_1^2} \\ \varepsilon_1 &= \pm \frac{\sqrt{3}}{2} \bar{\varepsilon} \end{aligned} \quad \text{Eq. 4.22}$$

Necking appears only on a small section of the tube wall. Therefore the node with the highest equivalent strain is used. With the information of all simulations a metamodel is formed, described with:

$$g(\mathbf{x}) = \max\left(\frac{\sqrt{3}}{2} \bar{\epsilon}_i(\mathbf{x})\right) \quad \text{for } i = 1 \dots N \quad \text{Eq. 4.23}$$

To transform this into an implicit constraint the theory of section 3.3 is used, applied on Eq. 4.21 and Eq. 4.23.

$$\begin{aligned} g(\mathbf{x}) &= \max\left(\frac{\sqrt{3}}{2} \bar{\epsilon}_i\right) \leq n \\ \Rightarrow g_{impl}(\mathbf{x}) &= \max\left(\frac{\sqrt{3}}{2} \bar{\epsilon}_i\right) - n \leq 0 \end{aligned} \quad \text{Eq. 4.24}$$

The optimisation problem is now fully constrained. The boundaries for the design variables in the experimental design can now be determined.

4.4 Interpretation of the Design of Experiments

In section 3.5.1 the choice of the experimental design was indicated. In this section the values for the design variables and the settings for the experimental runs are discussed. Together they form the experimental design. The design is called Face Centred Central Composite Design and is depicted in Figure 3.6. For the optimisation problem the solution space is formed by five design variables and one objective function. As described in section 3.5.1 the corners of the design are formed by a two-level full factorial design. These points form the first $2^n=2^5=32$ runs, followed by the $2*n=2*5=10$ star points and the last run is the centre run. The experimental runs are shown in Table 4.2.

Table 4.2. Face Centred Central Composite Design for 5 design variables

	$\frac{H}{2}$	L	t	κ_1	κ_1
ff	1	-1	-1	-1	-1
ff	2	-1	-1	-1	+1
ff	3	-1	-1	-1	+1
ff	4	-1	-1	-1	+1
ff	5	-1	-1	+1	-1
ff	6	-1	-1	+1	+1
ff	7	-1	-1	+1	+1
ff	8	-1	-1	+1	+1
ff	9	-1	+1	-1	-1
ff	10	-1	+1	-1	+1
ff	11	-1	+1	-1	+1
ff	12	-1	+1	-1	+1
ff	13	-1	+1	+1	-1
ff	14	-1	+1	+1	+1
ff	15	-1	+1	+1	+1
ff	16	-1	+1	+1	+1
ff	17	+1	-1	-1	-1
ff	18	+1	-1	-1	+1
ff	19	+1	-1	-1	+1
ff	20	+1	-1	-1	+1
ff	21	+1	-1	+1	-1
ff	22	+1	-1	+1	+1
ff	23	+1	-1	+1	+1
ff	24	+1	-1	+1	+1
ff	25	+1	+1	-1	-1
ff	26	+1	+1	-1	+1
ff	27	+1	+1	-1	+1
ff	28	+1	+1	-1	+1
ff	29	+1	+1	+1	-1
ff	30	+1	+1	+1	+1
ff	31	+1	+1	+1	+1
ff	32	+1	+1	+1	+1
ff	33	-1	0	0	0
ff	34	+1	0	0	0
ff	35	0	-1	0	0
ff	36	0	+1	0	0
ff	37	0	0	-1	0
ff	38	0	0	+1	0
ff	39	0	0	0	-1
ff	40	0	0	0	+1
ff	41	0	0	0	0
ff	42	0	0	0	0
ff	43	0	0	0	0

For the two-dimensional experiments, a fractional factorial design will be used as a validation of the design. As will be shown later in the text the fraction will lead to a resolution V design, which must result in the same model for the used regression models. For a half fraction the number of runs decreases with 16. This time only the experimental runs denoted with "ff" in Table 4.2 form the experimental design.

The basis of the design consists out of a two-level full factorial design for *four* variables. Multiplying the four variables per run, the fifth variable (column) is formed. The star points and centre run remain the same. Using the theory of Appendix A the confounding is determined. The multiplication is written as 5=1234, forming the word I=12345 (resolution V design). Using some math, the following can be formed:

$$\begin{array}{lllll}
 1=2345 & 12=345 & 23=145 & 34=125 & 45=123 \\
 2=1345 & 13=245 & 24=135 & 35=124 & \\
 3=1245 & 14=235 & 25=134 & & \\
 4=1235 & 15=234 & & & \\
 5=1234 & & & &
 \end{array}
 \tag{Eq. 4.25}$$

The main effects are therefore confounded with four-factor interactions and the two-factor interaction with the three-factor interactions. The order of the response surface fitted through the experimental data is not higher than quadratic. Thus only linear, pure quadratic and two-factor interactions are considered. The higher order terms are assumed to be insignificant. Therefore the fractional factorial design should lead to the same result as the entire design of Table 4.2.

Both designs form a hyper cube of five dimensions, which is to be fitted into the feasible domain. Due to the complexity of some constraints, the boundaries for the design are chosen in an iterative manner. Increasing the range of one variable can lead to the decrease of the range of one or more variables. Therefore it is impossible to indicate if the design forms the largest space possible in the feasible domain. In the table below the ranges for the design space are indicated:

Table 4.3. Ranges for the design variables

	-1	0	-1
$H/2$	26.4	27.1	27.8
L	1	3	5
t	1	1.3	1.6
κ_1	1/15	7/60	1/6
κ_2	-1/40	-9/800	1/400

The next step for the optimisation of the problem described in this chapter is conducting the numerical experiments. In the next two chapters the experiments are modelled and the results optimised using RSM.

5 Two-Dimensional Experiments

In this chapter the experimental results are discussed of two-dimensional simulations conducted in the finite element programme DiekA, developed at the University of Twente. The chapter is divided into two groups. In the first sections the optimisation problem of chapter 4 for two-dimensional simulations is discussed, starting with the formulation of the finite element model in section 5.1. Also a few comments are made concerning the simulation results. In section 5.2 the results are used to build a metamodel, which is subsequently optimised with a Matlab routine.

The second group concentrates on the validation of the optimisation. At first the optimum is compared with the simulation results. To validate the finite element model, two methods are used. First a mesh convergence check is preformed. For this the optimisation is repeated for two new finite element models with different mesh densities. For the second validation a model is used taking in account initial work hardening, representing the tube-forming step. To investigate the possibility of reducing the number of finite element simulations a fractional factorial design is used for the optimisation to see if this kind of model is sufficient and detect possible influence on the optimum. This is described in section 5.3.3.

5.1 Finite Element Model

The tube geometries according to the experimental design of Table 4.2 and the settings of the design variables of Table 4.3 are modelled with two dimensional plane strain elements. Each element consists of four nodes with two degrees of freedom, namely the x and y displacement. A quarter of the tubes are modelled with five elements across the wall thickness. The aspect ratio of these elements is as close to one as possible. A meshed tube with die contour is depicted in Figure 5.1. The other meshed tube geometries according to the experimental design are described in Appendix D.

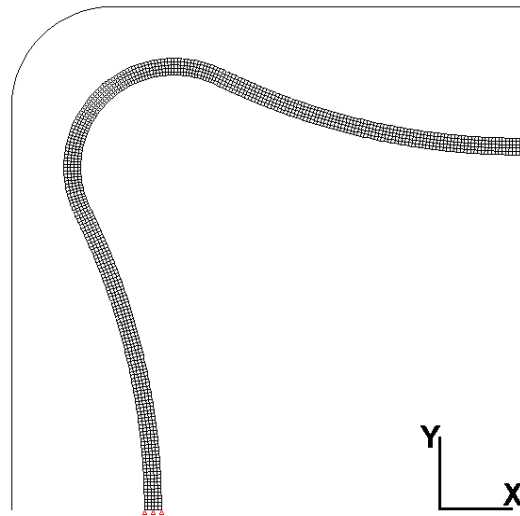


Figure 5.1. Finite Element Model

The plastic deformation is described using a von Mises yield locus with a Nadai work hardening model. This model describes an isotropic material behaviour. The material used for the simulations (DC04) is an anisotropic material however. In this case the r-values

(anisotropy parameters) are of no influence on the strain distribution. This is a result of the plane strain assumption; therefore an isotropic material model is sufficient.

The contact is described using four node contact elements in combination with a Coulomb friction model. The contact stress and friction are calculated using the penetration of the elements in the die contour in combination with a prescribed contact stiffness. This results in a geometrical error of the final tube. An implicit constraint in section 4.3 stating the adoption of the die shape of the tube at the end of the forming process, which cannot be fully met with the contact algorithm. The influence of the penetration on the wall thickness distribution however is expected to be low.

The simulation is stopped when the middle node of the outside tube perimeter reaches the die wall. This is possible due to the corner filling aspect of the process. The small radius of the die is likely to be the last spot of the die cavity that is completely filled. A visual inspection is used to ensure a correct filling of the die cavity.

5.1.1 Extracting Simulation Data

The information needed for the optimisation problem is limited by the objective functions and the implicit constraint. This is only the geometry of the final model and the equivalent strain. The rest of the simulation data is not used, except for globally checking the validity of the model compared with existing results, like the maximum pressure occurring in the simulations.

Wall Thickness

The distance between a node on the outside of the mesh and a node on the inside of the mesh is used to extract the wall thickness from the model at the end of the simulation. This is derived from the position of the nodes using Pythagoras:

$$t_i = \sqrt{(x_{i,j} - x_{i,k})^2 + (y_{i,j} - y_{i,k})^2} \quad \text{Eq. 5.1}$$

With j the node number on the outside and k the node number on the inside of the mesh, belonging to the i^{th} observation of the wall thickness. The wall thickness t_i will overestimate the true wall thickness of the model t'_i due to uneven elongation strains across the thickness. The correlation between t_i and t'_i is:

$$t' = \cos \alpha \cdot t_i \quad \text{Eq. 5.2}$$

With α the angle as depicted in Figure 5.2.

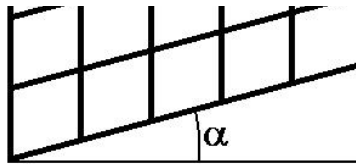


Figure 5.2. Obliqueness of the Mesh

The deflection of t_i is however negligible for small angles of α , even less than 1% for angles up to 8 degrees. α is assumed to be small, therefore t_i may be used as the real thickness of the model.

Necking Criterion

The implicit constraint of Eq. 4.24 uses the maximum equivalent strain of the model. This data is easily extracted from the output files of DiekA. In hydroforming the major part of the strain is caused by elongation of the tube wall and only for a small part by bending. Only in the last part of the simulation, during the corner filling, the strains can be dominated by bending. (Thin walled versus thick walled theory). It is reasonable to assume a constant increasing strain in the model; therefore the output of the last step is used.

5.1.2 Results of the Simulation

With the experimental design of section 4.4 and the model setting mentioned above, all the necessary information is present to execute the finite element simulations. The simulations are run with all the constraints mentioned in section 4.3. The implicit constraint for necking is not used for stopping the simulations; the simulations only stop when numerical instability occurs. For two-dimensional simulations this occurs when the mesh starts to show localisation, thus necking. From the results of J. Bakker [3] it is seen that a round tube of DC04 with a wall thickness of 1.5 mm and diameter of 60 mm completely fills the die cavity, without mesh localisation. The experimental design was chosen in such way that the perimeter of the smallest tube is equal or larger compared to the mentioned round tube, to prevent mesh localisation to occur. However, for four simulations the mesh localised, indicating necking. The perimeters of the localised finite element models are the four smallest perimeters and the models have a wall thickness of 1 mm. This indicates an increased sensitivity for necking for tubes with small perimeters and small wall thicknesses.

The wall thicknesses as function of the perimeter of the converged simulations are depicted in Figure 5.3. In Appendix E a larger version of this figure is incorporated. The three levels of the experimental design for the design variable t are clearly recognisable, namely 1, 1.3 and 1.6 mm.

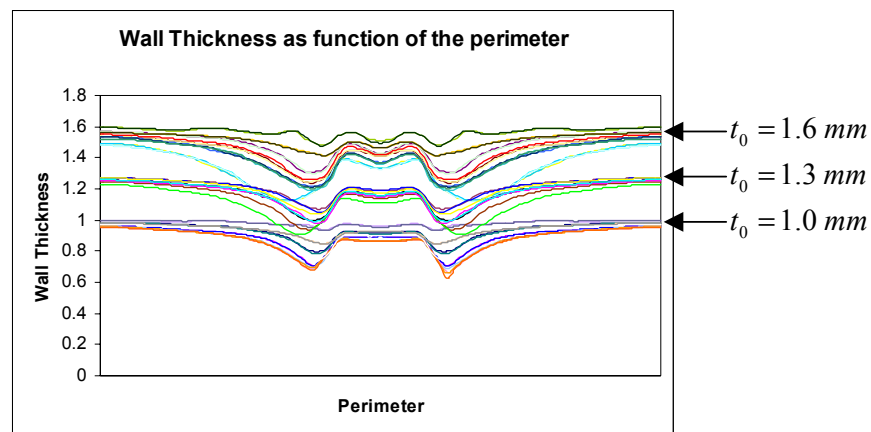


Figure 5.3. Wall thickness of the completed simulations

In Figure 5.4 the wall thickness as a function of the perimeter for a round tube is depicted. The wall thicknesses in both figures show a similar patron. The plateau in the middle of the function for the wall thickness corresponds to the corner of the die. The dent in the middle of the plateau is caused by the bending effect during hydroforming, which is less obvious for tubes with smaller initial wall thicknesses. The two dents on either side of the plateau correspond to the area next to the radius of the die. These points of the tube experience the highest strain in the wall thickness direction and are likely the points where necking occurs.

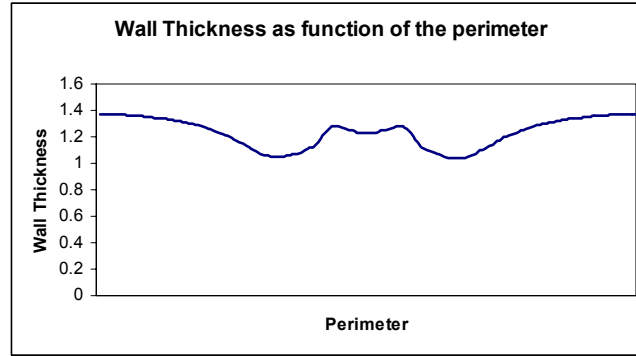


Figure 5.4. Wall thickness for a round tube with an initial wall thickness of 1.5 mm

5.2 Response Surface Methodology

In this section the approximation method Response Surface Methodology (RSM) is used to find the optimum of the wall thickness distribution and give an estimation of the effects. As mentioned in section 4.2.5 three objective functions are evaluated (Note that the values for α are 2, 20 and 2 respectively):

$$f_5(\mathbf{x}) = \sqrt{\frac{\sum_{i=1}^N (t_i(\mathbf{x}) - \bar{t}(\mathbf{x}))^2}{N-1}} \quad \text{Eq. 4.10}$$

$$f_6(\mathbf{x}) = \frac{\sum_{i=1}^N \left(1 - \left(e^{-(t_i(\mathbf{x}) - \bar{t}(\mathbf{x}))^2}\right)^{20}\right)}{N} \quad \text{Eq. 4.11}$$

$$f_7(\mathbf{x}) = \sqrt{\frac{\sum_i \left(\frac{t_i(\mathbf{x}) - \bar{t}(\mathbf{x})}{\bar{t}(\mathbf{x})}\right)^2}{N}} \quad \text{Eq. 4.12}$$

The first step is the forming of a metamodel followed by the optimisation of this model (section 5.2.1 and 5.2.2 respectively). For the optimisation the criterion of section 4.3 (implicit constraint) is used to see the influence on the optimum.

5.2.1 Metamodel

The metamodel is fitted using linear regression analysis as mentioned in section 3.5.2. In Table 5.1 the results for the lack of fit tests are displayed. The R-squared values are above 0.9 for all models and objective functions, which indicated a good fit.

Table 5.1. Lack-of-fit tests

	Linear model	Linear model with interactions	Quadratic model	Quadratic model with interactions		Linear model	Linear model with interactions	Quadratic model	Quadratic model with interactions
R^2	0.9511	0.9936	0.9527	0.9981		0.9564	0.9955	0.9634	0.9979
F-statistic	128.5	238.7	56.41	482.7		144.7	342.9	73.68	437.2
p-value	0	0	6e-16	0		0	0	0	0
Adjusted R^2	0.9453	0.9899	0.9380	0.9962		0.9513	0.9929	0.9520	0.9959
	Lack-of-fit for f_5					Lack-of-fit for f_6			
R^2	0.9279	0.9921	0.9313	0.9953					
F-statistic	84.88	191.5	37.98	191.5					
p-value	0	0	1e-13	0					
Adjusted R^2	0.9194	0.9875	0.9100	0.9906					
	Lack-of-fit for f_7								

The same applies to the F-statistic. The critical values are depicted in Table 5.2. The values for the fitted models are all ample above the critical values, which results in the low p-values. Thus the probability is nearly zero to have falsely rejected the null hypothesis H_0 of Eq. 3.11. This means that at least one term of the metamodels is significant. Due to the similarities between the models (repetition of terms), a statement can be made for the significance of at least one term of all models if the linear model has an F value above the critical value. If the null hypothesis H_0 is rejected for the linear model, all models will reject the null hypothesis H_0 .

Table 5.2. Critical F-values

	Critical $F_{(1-\alpha),k,n-k-1}$ value	
	$\alpha = 0.05$	$\alpha = 0.01$
Linear model	2.4558	3.5277
Linear model with interactions	2.0839	2.8139
Quadratic model	1.9313	2.5350
Quadratic model with interactions	1.8459	2.3824

Of the four models presented the 'linear model with interactions' is considered as the best model and will be used for the optimisation. Below the choice will be explained on the basis of the lack-of-fit test of Table 5.1.

The 'linear model' already has a good fit. If interaction terms are added to this model, the R-squared value increases significantly. The increase of the R-squared value is always the case when adding terms to a model. Therefore the adjusted R-squared value is examined, which considers the reduction of the sum of squares error (SSE) against the reduction of the

degrees of freedom of the regression model. In this case an evident increase of the adjusted R-squared is observed, indicating a better model.

The next step is the comparison between the 'linear model with interactions' and the 'quadratic model with interactions'. The increase in the R-squared value is small, although the values for both models are high. The same holds for the adjusted R-squared value. For the first two objective functions the F-statistic increases, which *can* indicate a relative larger amount of significant terms. For the third objective functions the F-statistic remains the same. The choice between these two models is not obvious. The quadratic effects added to the 'linear model' show a small increase in the R-squared value, a decrease of the F-statistic and for the first and third objective function a decrease of the adjusted R-squared value, while the increase for the second objective function is very small. From this it can be concluded that there are no major quadratic effects present in the metamodel.

Above the regression models are compared with the use of the lack-of-fit tests. These models consist of a number of effects, dependent on the choice of model. The four models consists either of all effects of a type or none of these. This means that all interaction effects are considered or none. The preference of one model above another model does not imply a contribution of all added effects to a better model. The significance of each individual effect is tested with the t-test of section 3.5.3. With this test a 95% confidence interval is determined, which implies a probability of 95% that an effect has a value within this interval. When zero is included within an interval the corresponding effect is considered insignificant. In Figure 5.5 the confidence intervals for the 'linear model with interactions' (Eq. 5.2) is shown, where the significant effects are marked in a red font. In Appendix F the parameters of the metamodels with corresponding confidence intervals for all models are enclosed.

$$\begin{aligned}
 f(\mathbf{x}) = & \beta_0 + \beta_1 H + \beta_2 L + \beta_3 t + \beta_4 \kappa_1 + \beta_5 \kappa_2 + \\
 & \beta_{12} HL + \beta_{13} Ht + \beta_{14} H\kappa_1 + \beta_{15} H\kappa_2 + \beta_{23} Lt + \\
 & \beta_{24} L\kappa_1 + \beta_{25} L\kappa_2 + \beta_{34} t\kappa_1 + \beta_{35} t\kappa_2 + \beta_{45} \kappa_1 \kappa_2
 \end{aligned}
 \tag{Eq. 5.3}$$

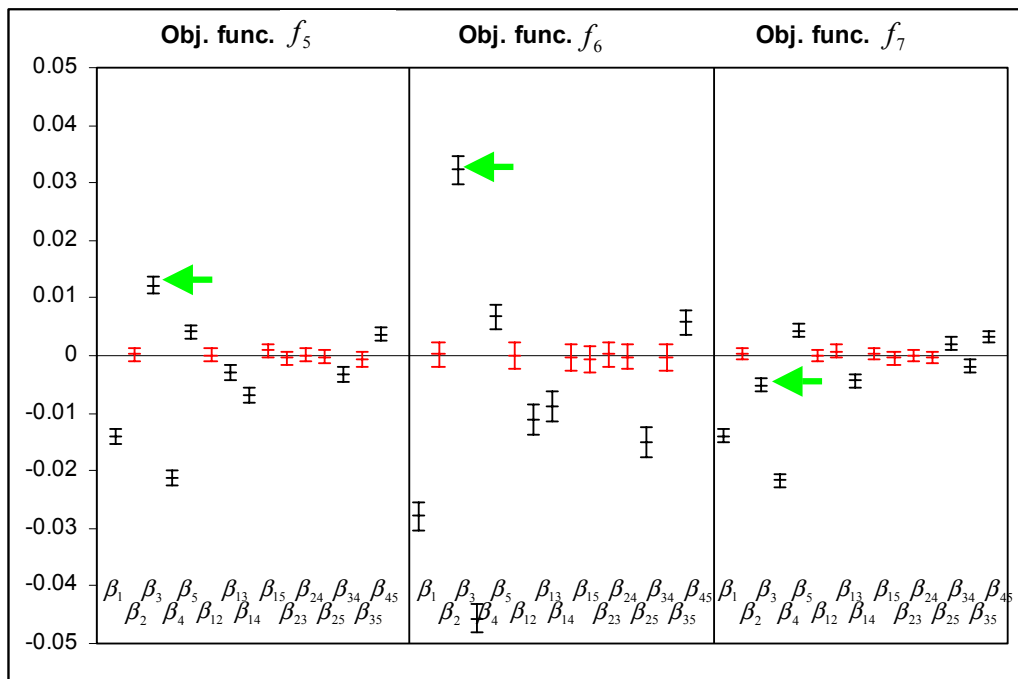


Figure 5.5. 95% confidence intervals of the linear model with interactions

In the Matlab routine the parameters of the regression model is scaled to coded variables. This means all variables have a lower bound of '-1' and an upper bound of '+1', like in the experimental design of Table 4.2 and NOT the lower and upper bound of Table 4.3. When the confidence intervals are examined the insignificance of a group of effects is noticed. This concerns the linear and interaction effects of the design variable L , which implies an insignificant effect of this design variable on the wall thickness distribution. Furthermore the significant interaction effects are globally three times smaller than the linear effect, which corresponds to the already high R-squared for the linear model. Another comment is in place regarding the difference between the models, the objective functions based on the absolute difference between $t_i(\mathbf{x})$ and $\bar{t}(\mathbf{x})$ (Eq. 3.10 and Eq. 3.11) on one side and the objective function based on the relative difference on the other side (Eq. 3.12). The dissimilarity concerns the design variable t (the green arrows in Figure 5.5). The sign of the significant effects are opposite, both linear and interactive. Furthermore the significance of the interaction effects Ht and $t\kappa_2$ is not equal for the two groups. The most striking difference is the value of the linear effect for t compared to the other significant linear effects. For the objective function of Eq. 3.12 the effect is much smaller compared to the other two, this is probably due to the biasing effect of the objective function based on the absolute difference. The significance of the design variable t is apparently not as high as the other two objective functions indicate. Overall speaking, the design variables with the highest significance are the height H and the radius of curvature κ_1 , see Figure 4.2 for the geometry of the initial tube. This counts for both the individual linear effects as the interaction effect between the two design variables. Below the metamodel is depicted for the two design variables for the objective function f_5 . The linear behaviour of the metamodel is clearly shown and the effect of the interactions is small, shown as a twist of the surface.

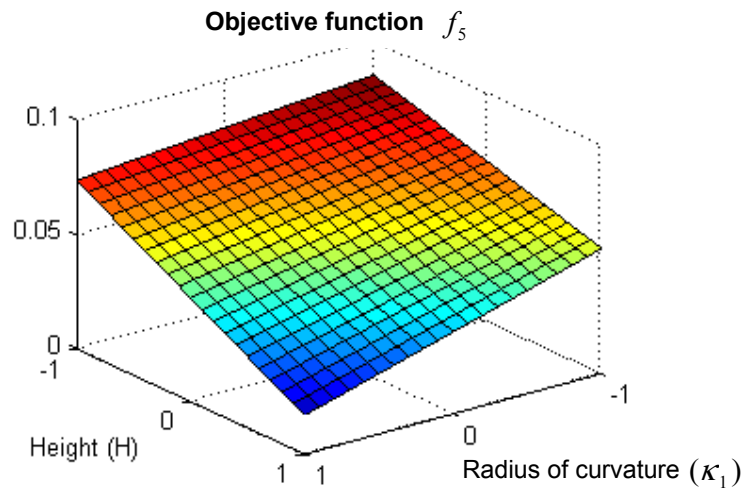


Figure 5.6. Metamodel of the objective function f_5

5.2.2 Optimisation

The optimisation of the metamodel is conducted in Matlab using the *fmincon* command. First the model is optimised without the use of the implicit constraint, which is added later to see the influence on the optimum. In Figure 5.7 the behaviour of the metamodel around the optimum is depicted for the three objective functions.

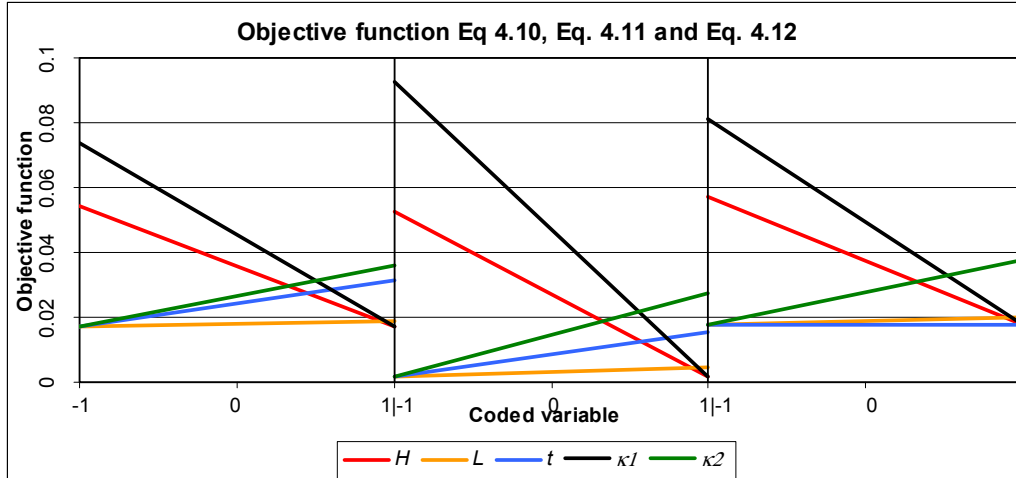


Figure 5.7. Behaviour around the optimum

Each line represents a variable varied between -1 and $+1$ (coded variables), for which the other variables are kept constant and equal to the optimum value. All lines are linear as expected from the choice of metamodel. The optimum is consequently located on the border of the feasible domain for all design variables. The values of the variable in the optimum for the three objective functions are shown in Table 5.3 and the initial tube geometry is depicted in Figure D.19 in Appendix D. The location of the optimum is equal for the three objective functions. A remark must be made concerning the objective function of Eq. 4.12. The negative sign for the linear effect of the design variable t is different from the other objective functions and indicates a preference for the upper bound ($+1$) of the design variable, while the optimum is formed by the lower bound (-1). The line for t in the right objective function in Figure 5.7 is almost horizontal with a minimum at the lower bound. This is caused by the interaction effects, which tend to twist the response surface (metamodel).

Table 5.3. Optima for three objective functions

	$H/2$ (mm)	L (mm)	t (mm)	κ_1 (mm^{-1})	κ_2 (mm^{-1})
f_5	27.8 (+1)	1 (-1)	1 (-1)	1/6 (+1)	-1/40 (-1)
f_6	27.8 (+1)	1 (-1)	1 (-1)	1/6 (+1)	-1/40 (-1)
f_7	27.8 (+1)	1 (-1)	1 (-1)	1/6 (+1)	-1/40 (-1)

The optimum is located in a corner of the experimental design and corresponds to an experimental run of the design (run number 19 of Table 4.2). This means the actual values for the objective functions are known. In Table 5.4 the values for the optimum of the metamodel are compared to the values of the simulation. It is seen that the metamodel differs to the value of the simulations, which is caused by the regression analysis.

Table 5.4. Optima for three objective functions

	Metamodel	Simulation
f_5	0.0169	0.0154
f_6	0.0179	0.0157
f_7	0.0017	0.0047

The next step is the implementation of the implicit constraint of Eq. 4.24

$$g_{impl}(\mathbf{x}) = \max\left(\frac{\sqrt{3}}{2}\bar{\epsilon}_i\right) - n \leq 0 \quad \text{Eq. 4.24}$$

The data of the simulations concerning the implicit constraint are formed into a metamodel as done with the objective functions. The metamodel is subsequently used to determine the course of the constraint through the solution space. The model is fitted using regression analysis. The lack-of-fit results are shown in Table 5.5.

Table 5.5. Lack-of-fit tests for Eq. 4.24

	Linear model	Linear model with interactions	Quadratic model	Quadratic model with interactions
R ²	0.8522	0.9714	0.8586	0.9774
F-statistic	38.04	52.08	17.0	38.9
p-value	0	0	0	0
Adjusted R ²	0.8348	0.9547	0.8147	0.9548

All models show a good fit, even though the R-squared, adjusted R-squared and F-statistic values are lower compared to the objective functions. With the help of the table above the model for the implicit constraint is set on the 'linear model with interactions', for which the F-statistic and adjusted R-squared value are the highest of all four models.

The results of the optimisation for the objective function f_5 in combination with the implicit constraint of Eq. 4.24 are depicted in Figure 5.8 and are of the same sort as Figure 5.7. Note that the metamodel for the implicit constraint is independent of the objective functions. The solid and dashed lines represent the metamodel of the objective function and implicit constraint respectively. The horizontal dotted line indicates the boundary of the implicit constraint. When the metamodel of the implicit constraint is located above the dotted line, the tube will fail due to necking. From the figure it is seen that for the variation around the optimum the implicit constraint has values above zero for H and κ_1 only. Furthermore at the optimum point for the objective function the implicit constraint is satisfied.

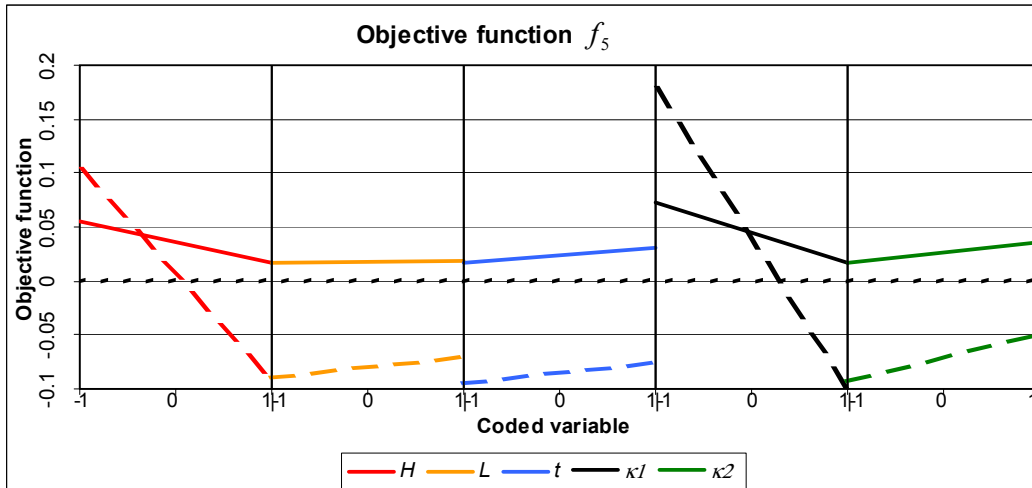


Figure 5.8. Behaviour of the implicit constraint around the optimum

From the figure it is shown that the metamodels around the optimum have the same direction. This is due to the relationship with the strains of both the objective function and the implicit constraint. The wall thickness distribution becomes more uniform if the maximum strain in the tube is small. As mentioned for Figure 5.3, the wall thickness distribution show for all tubes a similar patron. Also seen for the round tube. In the first stage of the process the tubes are inflated in a bending mode, without any wall thickness reduction. Until contact occurs with the die wall, the tubes attempt to obtain a round shape. From the moment of contact the elongation of the tube wall starts, resulting in reduction of the wall thickness. This reduction only occurs for those regions, which are not in contact with the die wall. This is the reason why the optimal initial tube geometry has the largest possible perimeter within the domain of the experimental design.

A last remark is in place concerning the metamodel for the implicit constraint. The minimum for this metamodel is located for small values of the design variable t . A higher sensitivity for necking was mentioned in section 5.1.2 concerning small values of t also. Apparently the combination with the perimeter length is of more importance than the wall thickness only.

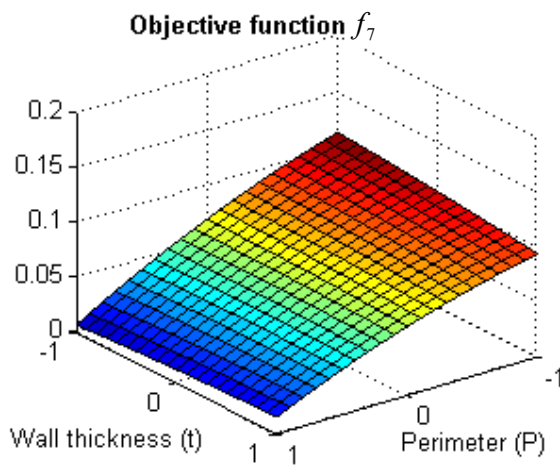


Figure 5.9. Metamodel as function of the perimeter

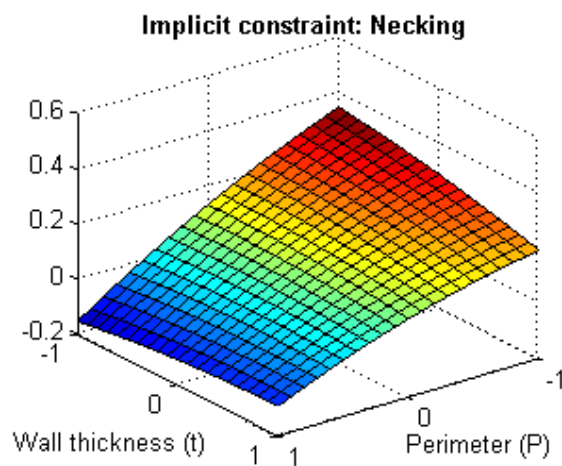


Figure 5.10. Metamodel of the implicit constrain

The relation between the initial tube perimeter P and the initial wall thickness t is depicted in Figure 5.10 and is a transformation of the metamodel for the implicit constraint. The mentioned interaction between the wall thickness and the perimeter is clearly shown. The dark blue area and the dark red area stand for low risk and high risk for necking respectively. Thus a combination between a low wall thickness and a low perimeter increase the change on necking.

In Figure 5.9 the metamodel for the objective function f_5 is depicted as function of the same variables. Note that the outside perimeter is a function of all five design variables. The influence of the perimeter is linear on the wall thickness distribution. For this objective function the role of the initial wall thickness t is also good represented. For low perimeters a high wall thickness is preferred, while for high perimeters a low wall thickness is preferred. The former is caused by the linear effect of t in the metamodel and the interaction effects causing the twist in the metamodel.

The location of the optimum is now known and the influence of the parameters is globally known. In the next section the optimum is validated using several methods. In chapter 7 the influence of the design variables is further discussed.

5.3 Validation of the Optimisation

In this section the results of the optimisation is validated. At first the behaviour around the optimum is investigated using the simulation data to see if it is in accordance with Figure 5.7. To see if the used finite element model is accurate enough for the optimisation a mesh refinement is applied to conduct a mesh convergence check. Furthermore an initial condition is added, representing the tube-forming step.

In the previous sections the optimisation of three objective functions was discussed using the Face Centred Central Composite Design (CCD) of Table 4.2. In the same table a design with less experimental runs was presented, indicated with 'ff'. In section 5.3.3 the influence of this fractional design on the optimum is discussed.

5.3.1 Comparison with the Results of the Simulations

In Figure 5.7 the behaviour around the optimum was shown. The optimum of the metamodel is in accordance with the minimum value of the objective functions determined from the experimental runs. In Figure 5.11 the same behaviour is shown, by plotting the wall thicknesses as function of the perimeter. The magenta coloured line corresponds to the optimum derived in the previous section. The other lines correspond to the initial geometries for which one design variable is altered compared to the optimum. The numbers mentioned in the legend correspond to the experimental runs of Table 4.2.

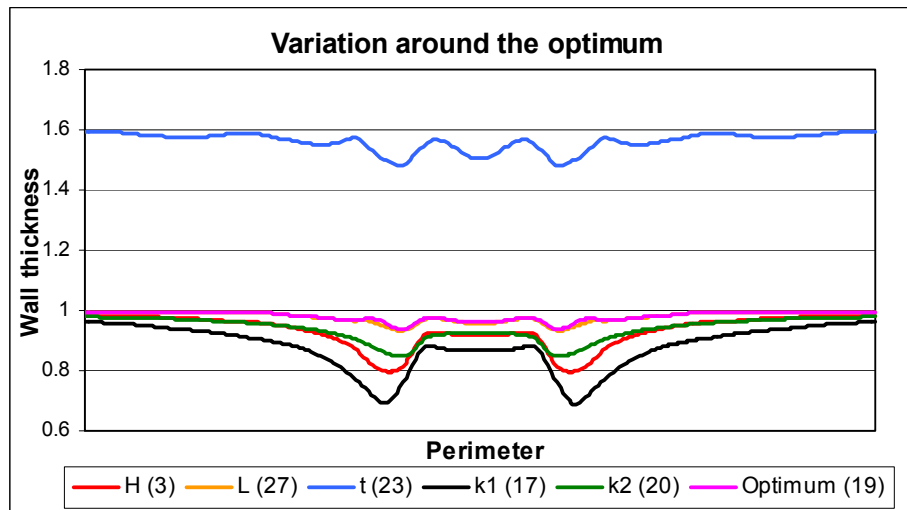


Figure 5.11. The behaviour of the wall thickness around the optimum

The largest difference in the wall thickness is caused by the change of κ_1 , followed by H . Which corresponds to the largest slope of these two design variables in Figure 5.7, where the slope for L is almost horizontal. This matches to the almost same wall thickness for L in Figure 5.11, represented with the orange line. The slope for k_2 is between the slopes of H and L in Figure 5.7, which corresponds to the distribution of the green line compared to the red and orange line in the figure above. The line for the wall thickness of t (blue line) is harder to judge. Absolute the spreading is larger compared to the optimum, but relatively the difference is not so obvious. This explains the difference in the slope for the three objective functions in Figure 5.7 concerning the design variable t .

5.3.2 Finite Element Model Validation

The optimisation of the wall thickness distribution for hydroform tubes as conducted in this chapter is based on finite element models. These models are approximations of the reality and are based on several assumptions and simplification. The best way to validate finite element simulations is by physical experiments. This is however not possible for this project. Therefore the finite element model is validated on the field of convergence. Further more the influence of initial work hardening is investigated, which is neglected in the simulations used until this point.

Mesh Convergence

To validate the accuracy of the model, without the possibility of comparison with physical experiments a mesh convergence check is performed. The characteristic of finite element simulations is the mesh dependent accuracy [11]. Generally speaking, the more elements used the more accurate the mesh. The same applies to the complexity of the elements. A mesh consisting of elements with a higher order interpolation function will generally result in a more accurate result. Increasing the number or the complexity of the elements eventually leads to no significant improvement of the model. For this project a convergence check is conducted using mesh refinement. Three different mesh densities, depicted in Figure 5.12 are modelled:

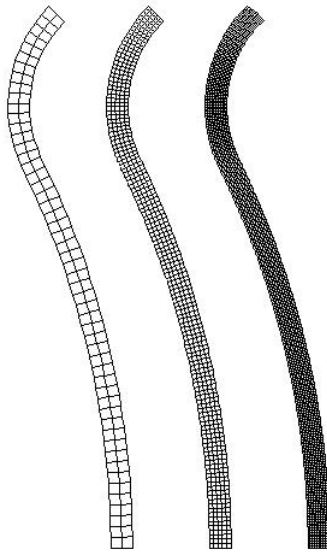


Figure 5.12. Mesh Refinement

The model on the left consists of two elements across the tube wall; the middle model is the original model with 5 elements across the tube wall and the model on the right consists of 10 elements across the tube wall.

The first difference between the models emerged during the simulations. The models with smaller elements are subjected more to mesh localisation. This is due to the capability of better predicting local behaviour. In this case necking. Table 5.6 represents the number of simulations with mesh localisation.

Table 5.6. Mesh localisation

Number of elements across the tube wall	Number of simulations with mesh localisation
2	0
5	4
10	8

The values of the design variable t for the models subjected to localisation are all the same, namely 1mm. And have the smallest perimeters of the simulated tubes. This corresponds to the metamodel of the implicit constraint (see Figure 5.10).

The convergence of the simulation and the influence of this on the objective function are investigated only. In this case the objective functions are all based on geometric properties of the mesh. Displacements in simulation have the tendency to converge much faster than stresses when applying mesh refinement. The convergence effect is probably stronger for the stresses and of influence for the failure criteria (implicit constraint).

To examine the influence of the mesh on the objective function the results of the simulations are plotted in Figure 5.13 and Figure 5.14. Each dot represents one setting of the experimental design for two mesh densities. On the axes the value for the objective function is displayed. The dotted line in the plot denotes the line for which both type of simulations

obtain equal values for the objective function. The green and red lines denote the upper and lower bound of the 25% and 50% diversion respectively.

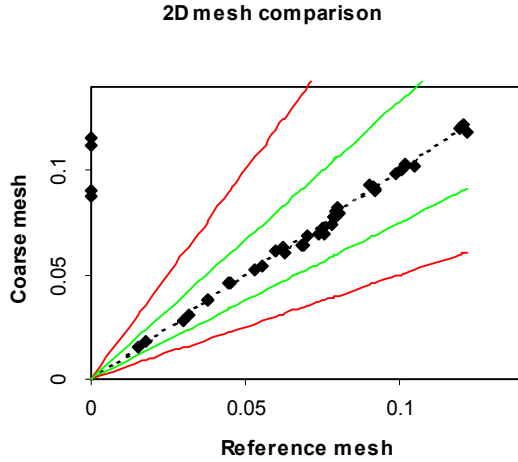


Figure 5.13. Coarse and reference mesh

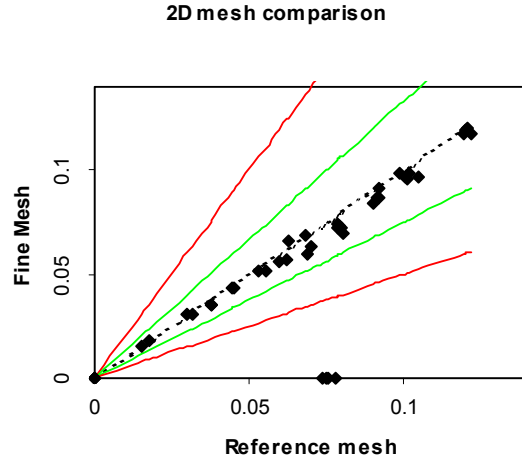


Figure 5.14. Reference and fine mesh

The plots above are for the objective function f_5 . The other two objective functions produce similar plots. The dots on the horizontal axis denote the lack of convergence of the mesh plotted on the vertical axis and visa versa. The dot(s) in the origin denote lack of convergence of both mesh types. In both plots the dots are concentrated around the dotted line, indicating a good match between the three meshes. Due to this placement of the dots it is believed there is no influence of the mesh density in combination with the objective functions on the position of the optimum in the feasible domain. This is checked with the Matlab routine and confirms the statement.

The reference model of Figure 5.1 is accurate enough for the optimisation problem; the coarse mesh however is accurate enough also. The use of this mesh would save a lot of time, when additional runs are necessary.

Influence of the Initial Work Hardening

As shown in chapter two, several forming steps are potentially conducted before hydroforming, of which forming of the tube is always present. The forming steps cause strain hardening and decrease the formability of the material during hydroforming. The model of Figure 5.1 is compared to a similar model with initial work hardening to investigate the model behaviour. The initial work hardening is derived from the tube-forming step. Especially for small radii the work hardening is large and the difference between the non-work hardening sections can become important. The other forming steps are not considered, because this project aims at excluding them from the process cycle.

The tube-forming process is the tubular blank process of section 2.2.1 and only consists of bending of the sheet. The strain in the sheet depends on the radius and the wall thickness only and is formed by the relation:

$$\varepsilon_1 \approx \frac{y}{\rho_0}, \quad \varepsilon_2 = 0, \quad \varepsilon_3 \approx -\frac{y}{\rho_0}. \quad \text{Eq. 5.4}$$

With ρ_0 the radius of the neutral line and y the distance from the neutral line. From this the equivalent strain needed for the input of the simulation programme is determined:

$$\bar{\epsilon} = \sqrt{\frac{2}{3}(\epsilon_1^2 + \epsilon_2^2 + \epsilon_3^2)}$$

$$\Downarrow$$

$$\bar{\epsilon} = \left| \frac{2y}{\sqrt{3}\rho_0} \right| \quad \text{Eq. 5.5}$$

For the derivation is referred to Appendix G.

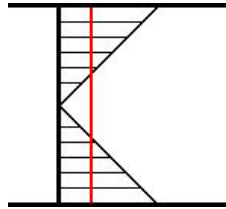


Figure 5.15. Initial Work Hardening

In Figure 5.15 the variation of the strain hardening across the tube wall is depicted. For the simulations the model is simplified to a uniform strain hardening across the wall thickness, indicated with the red line, and is chosen half of the maximum strain hardening.

For the comparison between the reference model and the model with initial work hardening a similar plot as for the mesh convergence check is used, depicted in Figure 5.16.

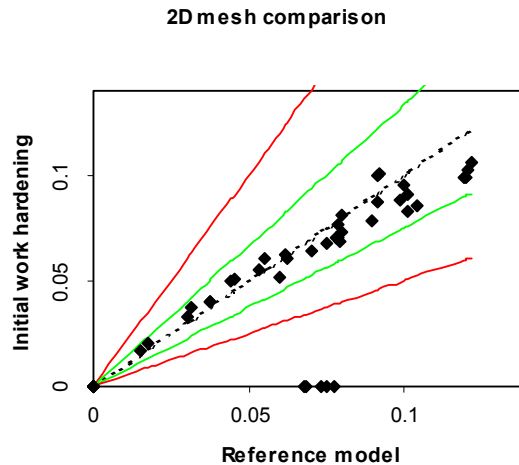


Figure 5.16. Influence of initial work hardening

The dots are ones more concentrated around the dotted line, but more diverted as the mesh density comparison. All dots are placed between the green lines indicating a diversion of less than 25%. Notable is the difference in diversion between the dots with high and low value of the objective function. This means the initial work hardening has a positive effect on the wall thickness distribution for tubes with high elongation and negative effect for tubes with low elongation. From this a difference between the metamodel is expected. The linear effects become a little smaller and the interaction effect larger for the finite element models accounting for the initial work hardening. Globally speaking, the simulations of the initial work

hardening have no influence on the location of the optimum, similar as the mesh density. Therefore it is believed the used model of Figure 5.1 (without work hardening) is accurate enough for the optimisation problem.

5.3.3 Fractional Factorial Design

The Face Centred CCD of Table 4.2 consists of 43 experimental runs. To lower the computational cost the number of runs is decreased. To realise this a fraction of the experimental design is used, denoted with 'f' in Table 4.2. As mentioned in section 4.4 the design is of resolution V. This implies no confounding of main and two-factor interaction effects with each other. This new design should lead to the same optimum as obtained in the analysis of section 5.2.2.

In Table 5.7 the lack-of-fit tests are displayed for the fractional design. The lack-of-fit table shows similar results as the lack-of-fit of the original design (see Table 5.1), except for the F-statistic. These values are all lower, but still ample above the critical values. This is caused by the reduction of the number of experiments, which leads to the reduction of the degrees of freedom of the Mean Square Error (see section 3.5.3). Overall the choice of metamodel is the same as for the original experimental design, the 'linear model with interactions'.

Table 5.7. Lack-of-fit tests

	Linear model	Linear model with interactions	Quadratic model	Quadratic model with interactions		Linear model	Linear model with interactions	Quadratic model	Quadratic model with interactions
R^2	0.9499	0.9927	0.9529	0.9981		0.9518	0.9937	0.9631	0.9986
F-statistic	72.11	81.18	28.32	102.7		74.99	94.90	36.54	138.1
p-value	1e-11	9e-8	1e-7	2e-4		7e-12	4e-8	2e-8	1e-4
Adjusted R^2	0.9399	0.9825	0.9246	0.9901		0.9422	0.9849	0.9410	0.9933
Lack-of-fit for f_5					Lack-of-fit for f_6				
R^2	0.9327	0.9919	0.9391	0.9976					
F-statistic	52.64	73.26	21.59	83.14					
p-value	1e-10	1e-7	8e-7	3e-4					
Adjusted R^2	0.9192	0.9806	0.9026	0.9885					
Lack-of-fit for f_7									

The small difference in the lack-of-fit compared to the original model indicates a small difference of the metamodels. The influence on the optimum is however negligible, the optima for the objective functions of Eq. 4.10 and Eq. 4.11 are even the same. The only difference is the location of the optima for the design variable L and t for the objective function of Eq. 4.12, marked in bold in Table 5.8. This variation for the former one however is of no influence due to the insignificance of all effects concerning the design variable L (linear and interaction effects), for both the original as the fractional design.

Table 5.8. Optima for three objective functions

	$H/2$ (mm)	L (mm)	t (mm)	κ_1 (mm ⁻¹)	κ_2 (mm ⁻¹)
f_5	27.8 (+1)	1 (-1)	1 (-1)	1/6 (+1)	-1/40 (-1)
f_6	27.8 (+1)	1 (-1)	1 (-1)	1/6 (+1)	-1/40 (-1)
f_7	27.8 (+1)	5 (+1)	1.6 (+1)	1/6 (+1)	-1/40 (-1)

The latter one is a bad approximation of the metamodel. The combination of the linear and interaction effects for t is not captured in the metamodel. If the original data is examined (thus not the metamodel), the minimum value corresponds to the optimum of section 5.2.2. In this case the results of the corresponding simulations is not evaluated in this design. This means that, even though the design is of resolution V and the major linear and interaction effects are found, small effects can be missed, which can lead to a different optimum.

6 3D Simulations

The geometry of most hydroformed products vary in three dimensions and are not suited for simulations using two-dimensional elements. In this chapter the optimisation problem of chapter 5 is repeated with three-dimensional elements to investigate the influence on the optimum. The study of J. Bakker [3] showed a worse reproduction of the wall thickness distribution, compared to two-dimensional simulations. This is caused by the formulation of the elements, which do not have the capacity of coupling the wall thickness between the elements and assume a plane stress conditions.

6.1 Finite Element Model

The finite element model consists of three-dimensional discrete Kirchhoff triangles with three integration points in the plane and five integration points in thickness direction. The elements take into account the membrane stresses and the bending stresses. Each element has six degrees of freedom. The material parameters and the contact formulation are similar to the two-dimensional simulations.

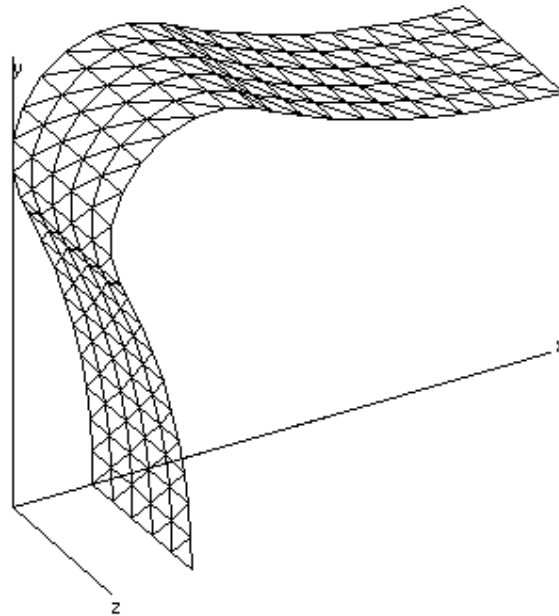


Figure 6.1. 3D finite element model

In Figure 6.1 a finite element model is presented. The length of the tube is limited to 10 mm to minimise the computational costs. The boundary conditions on the edge of the model restrict movement in the z-direction to simulate a plane strain situation, corresponding to the two-dimensional elements. This allows us to compare the results with the results of chapter five.

The elements have a length of approximately two millimetres, which results in far less elements than for the two-dimensional simulations. This means a lower number of observations of the wall thickness to predict the wall thickness distribution.

The information needed for the objective functions, the wall thickness, is directly exported to the output files and no extra calculation is needed. To determine the wall thickness distribution, the wall thickness of all element nodes is used.

6.1.1 Results of the Simulation

With the experimental design of Table 4.2 (in combination with Table 4.3) and the model parameters of the previous section the simulations are executed. Figure 6.2 the wall thickness as a function of the perimeter is depicted. As with the two-dimensional simulations the three different initial wall thicknesses (1, 1.3 and 1.6 mm) can be clearly distinguished as three groups in the figure. Compared to the wall thickness distributions of the two-dimensional simulations, similar patterns are presents. The figures below however are less ordered. Numerous simulations show an asymmetric wall thickness distribution. The strains are concentrated on one spot of the tube, denoting localisation. Furthermore an increase in wall thickness variation is noticed, which indicates an overestimate of the thickness strain compared to the two-dimensional simulations. In Appendix D a larger version of the figure below is included.

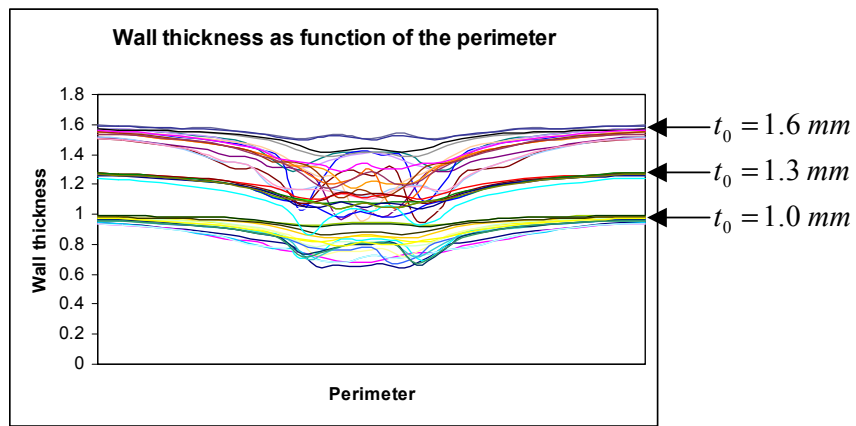


Figure 6.2. Wall thickness of the completed 3D simulations

In the next section the wall thickness distributions are evaluated with the objective functions and used to form metamodels for the optimisations.

6.2 Response Surface Methodology

This section follows the same strategy as section 5.2. Regression analysis is used to fit the data and form a metamodel, which is optimised using the Matlab routine *fmincon*. The implicit constraint for necking is not applied to the three-dimensional model. The results of the two-dimensional simulations already showed that this constraint has no influence on the optimum and is therefore not of any interest.

6.2.1 Metamodel

The results of the simulations are used in combination with the objective functions to fit a metamodel with regression analysis. The lack-of-fit for the four possible metamodels are presented below for the three objective functions (Eq. 4.10, Eq. 4.11 and Eq. 4.12).

Table 6.1: Lack-of-fit tests

	Linear model	Linear model with interactions	Quadratic model	Quadratic model with interactions		Linear model	Linear model with interactions	Quadratic model	Quadratic model with interactions
R ²	0.7898	0.9436	0.8080	0.9618		0.8279	0.9537	0.8511	0.9759
F-statistic	27.80	30.11	13.47	27.72		35.60	37.09	18.29	44.60
p-value	1e-11	5e-13	7e-9	3e-11		3e-13	4e-14	2e-10	2e-13
Adjusted R ²	0.7677	0.9154	0.7556	0.9302		0.8098	0.9305	0.8105	0.9560
	Lack-of-fit for f_5					Lack-of-fit for f_6			
R ²	0.8187	0.9338	0.8511	0.9662					
F-statistic	33.42	25.38	18.29	31.43					
p-value	9e-13	5e-12	1e-10	8e-12					
Adjusted R ²	0.7996	0.9007	0.8105	0.9383					
	Lack-of-fit for f_7								

The 'linear model' shows a worse fit compared to the two-dimensional model, and the quadratic effects have a larger influence on the improvement of this model. However the confidence intervals for all quadratic effects include zero, for both the 'quadratic model' and the 'quadratic model with interactions'. This means the quadratic effects are of no significance. This leads to the choice for the 'linear model with interactions', which show a better fit compared to the 'linear model'.

6.2.2 Optimisation

The metamodel of the section above is used to find the optimal wall thickness distribution. The linear behaviour of the metamodel indicates an optimum on the border of the feasible domain. Compared to the two-dimensional simulations the optimum (see Table 6.2) is the same for the three objective functions concerning three design variables. Two differences are noticed, namely the behaviour of the design variables L and t . For the former one this variation is unimportant, because all effects (linear and interaction) concerning L are insignificant. For the design variable t all effects are insignificant concerning the objective function of Eq. 4.12. The difference however is the significance of the linear effect and two interaction effects of the metamodel for the two-dimensional simulations, even though these effects are small. The metamodel for the three-dimensional simulations is not capable of estimating the small interactions between the effects of t , as the metamodel for the fractional factorial design. In this case the smaller number of observation and with it the more roughly estimation of the final geometry probably the caused the difference with the two-dimensional simulations.

Table 6.2: Optimal dimensions predicted by the three objective functions

	$H/2$ (mm)	L (mm)	t (mm)	κ_1 (mm ⁻¹)	κ_2 (mm ⁻¹)
f_5	27.8 (+1)	1 (-1)	1 (-1)	1/6 (+1)	-1/40 (-1)
f_6	27.8 (+1)	5 (+1)	1 (-1)	1/6 (+1)	-1/40 (-1)
f_7	27.8 (+1)	1 (-1)	1.6 (+1)	1/6 (+1)	-1/40 (-1)

Generally speaking with the insignificant design variables in mind it can be concluded that the three-dimensional simulations lead to the same result compared to the two-dimensional simulations. Although the confidence interval of the effects are larger, leading to insignificance of some effects compared to the two-dimensional simulations.

Table 6.3: Values of the objective function in the optimum

	Metamodel	Simulation
f_5	0.0166	0.0225
f_6	-0.003	0.0006
f_7	0.0123	0.0194

In Table 6.3 the values in the optima for the metamodel and the simulations are compared. They show a good resemblance. One comment must be made concerning the optimum value for the simulations concerning the objective function of Eq. 4.10. The minimum value for the simulations occurs for the same settings of the design variables as in Table 6.2 except for L , which is 1 mm. This is due to the low significance of L and the larger confidence interval compared to the two-dimensional simulations.

6.3 Data Comparison with 2D Simulations

In Figure 6.3 the results of the two-dimensional and three-dimensional simulations are plotted against each other to obtain a clear view of the difference between the models. The plot is made for the objective function of Eq. 4.10. The majority of the points are located above the dotted line (denoting similar results for both types of simulations). This means that the three-dimensional simulations predict a worse distribution of the wall thickness, especially for the simulations with small perimeters. These are the simulations with high elongations in circumferential direction and thus high strains in thickness direction. J. Bakker [3] showed a good resemblance of the wall thickness distribution for round tubes simulated using two-dimensional elements. Apparently the three-dimensional simulations overestimate the thickness strains.

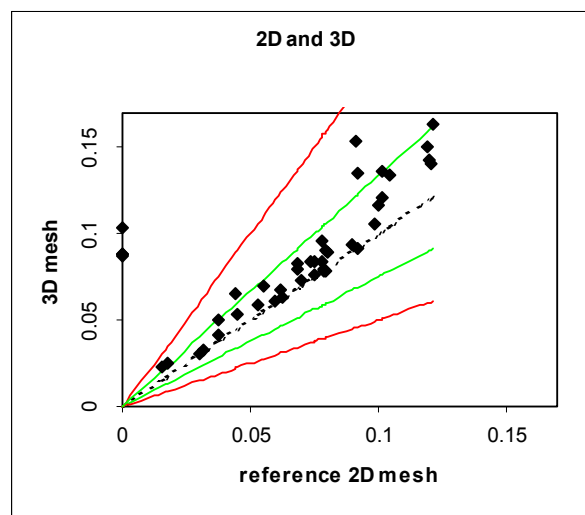


Figure 6.3. Comparison between two and three dimensional simulations for the objective function of f_6

From the results of this chapter, compared to the two-dimensional simulations of chapter 5, the three-dimensional simulations for optimisation (and simulation of hydroforming in general) is suitable in case of low strains in the wall thickness directions. When the strains increase the prediction of the wall thickness distribution becomes worse and the moment of necking occurs earlier compared to the two-dimensional simulations.

7 Discussion

In these chapter aspects of the optimisation of chapters 4 through 6 are discussed. This is divided into two groups. The first two sections focuses on the results of the optimisation. At first a screening of the design variables is applied to see if this kind of step in the optimisation routine would filter out the design variables, which are insignificant or small. Furthermore two new constraints are added, composed from the results of the optimisation of chapter 5.

In the last two sections some aspects of the used optimisation routine is discussed. The emphasis lies on the experimental design and the influence of implicit constraints.

7.1 Screening Design

The derived optima for the optimisation problem are formed by a set of design variables. The metamodel composed to describe the behaviour of the design variables contains a number of effects, which are not significant. In the case of the design variable L , all possible effects (main and two factor interaction effects) are insignificant and for κ_2 only a weak significance for the main effect and interaction with κ_1 is present.

The question is if it is possible to find the design variables with the largest effects on the model with the help of a screening design. This is a design consisting of a small number of experimental runs. The design is suited to find linear and two-factor interaction effects, but is not capable to estimate the effects. The design used in this section is a two-level fractional factorial design of resolution III (see Appendix A). This means the linear effects are heavily confounded with the interaction effects. For five design variables only eight experimental runs are needed. With the multiplications:

$$\begin{aligned} x_4 &= x_1x_2 \\ x_5 &= x_1x_3 \end{aligned} \tag{Eq. 7.1}$$

The following design is formed:

Table 7.1. Resolution III design

	H/2	L	t	k1	k2
1	-1	-1	-1	+1	+1
2	+1	-1	-1	-1	-1
3	-1	+1	-1	-1	+1
4	+1	+1	-1	+1	-1
5	-1	-1	+1	+1	-1
6	+1	-1	+1	-1	+1
7	-1	+1	+1	-1	-1
8	+1	+1	+1	+1	+1

Other designs are possible when the multiplications are altered. The experimental runs of Table 7.1 form a part of the experimental design of Table 4.2. Normally a screening design is the first step and the experimental runs can be used for the experimental design needed for the Response Surface Methodology. Also when a design variable appears to be insignificant, because the influence of the variable is negligible, the runs can be used.

7.1.1 Results of the Screening

The screening of the designs is performed with a DEX mean plot for a number of possible experimental designs amongst them the design of Table 7.1. The rest of the designs are mentioned in Appendix H together with the DEX mean plots for the three design variables (Eq. 4.10, Eq. 4.11 and Eq. 4.12). The DEX mean plot uses the average of the experimental data per level of a variable, represented in Eq. 7.2. These two points form a line and indicate the linear effect of the design variable.

$$f(x_i^-) = \frac{\sum_{k=1}^{n_{x_i^-}} f_k(\mathbf{x})|_{x_i=x_i^-}}{n_{x_i^-}} ; f(x_i^+) = \frac{\sum_{k=1}^{n_{x_i^+}} f_k(\mathbf{x})|_{x_i=x_i^+}}{n_{x_i^+}} \quad \text{Eq. 7.2}$$

In Figure 7.1 the DEX mean plot for the design of Table 7.1 is depicted.

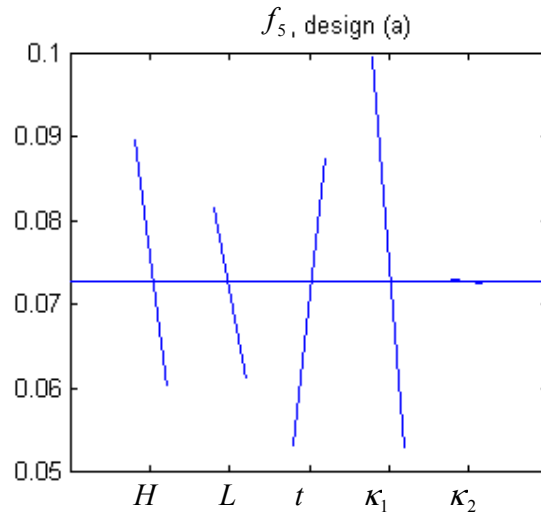


Figure 7.1. DEX mean plot of a screening design

In the figure the horizontal axis presents the design variables in the same order as the columns of the experimental design. From the figure the conclusion can be drawn that κ_2 is insignificant and the other design variables are significant. However the effects for κ_2 have a small significance and the effects for L have no significance at all. The conflicting results of the DEX mean plot above and the results of chapter 5 are caused by the nature of the screening design. In the design the main effects are confounded with the interaction effects. In case of L the linear effect is confounded with the interaction term $H\kappa_1$, which is a significant term.

In Appendix G the other DEX mean plots show similar confounding effects. This means that the engineer is dependent of the choice of screening design to find all insignificant terms.

7.2 Constant Mass of the Tube

In this section an extra constraint is added to the optimisation problem of the previous chapters. The constraint beholds a constant mass of the tube. Mass is an interesting parameter for the car industry and an increase of mass compared to the common round tube is not preferred. Therefore the mass of the tube is chosen almost equal to the mass of a round tube of diameter 60 mm (largest possible tube to fit in the die cavity of Figure 4.1)

To rewrite the constraint to the design variables the use is made of the proportionality of the mass to the area of the tube wall for a prismatic tube. The volume is approximated by the product of the wall thickness with the length of the neutral line of the tube, i.e. the tube is approximated as a rectangle, which is valid for thin walled tubes. The constraint in mathematical form becomes:

$$L_{middleline} \cdot t = \text{constant}$$

$$8 \cdot \left(\frac{1}{\kappa_1} \left(\frac{3\pi}{4} - \beta \right) + \frac{1}{\kappa_2} \left(\beta - \frac{\pi}{2} \right) + L \right) \cdot t = \text{constant} \quad \text{Eq. 7.3}$$

With this constraint a relation is formed between the 5 design variables. The optimisation problem loses one degree of freedom; therefore one design variable can be eliminated. In this case the wall thickness t is excluded. As a result only 25 experimental runs are needed for the experimental design (a Face Centred CCD) for this new optimisation problem. The boundaries for the design variables (except t) are the same as in Table 4.3 for comparison. The constant value for the (equality) constraint is set on 280 mm². This is slightly larger as a round tube with a diameter of 60mm and a wall thickness of 1.5 mm with an area of 275.7 mm².

Results

The fitting of the metamodel for the objective functions shows a more dominating quadratic effects and less influence of the interaction effects compared to the metamodel of chapter 5. This is due to the absence of the design variable t . In the metamodel of chapter 5 two interaction effects of t were significant and the quadratic effect of t was not significant. These terms are excluded from the new metamodel.

In chapter 5 the optimum implied a tube with a maximum perimeter. In this case the result is not much different with exception of t , which is now dependent of the new constraint. The result for the optimisation problem with the constraint denoting constant mass the optima for all objective functions are equal:

Table 7.2: Optimum for an optimisation involving tubes with constant mass.

$H/2$ (mm)	L (mm)	κ_1 (mm ⁻¹)	κ_2 (mm ⁻¹)
27.8 (+1)	1 (-1)	1/6 (+1)	-1/40 (-1)

Which forms the tube with the maximum perimeter.

Also in this case, there is no influence of the necking criterion, which influences only tubes with relatively small perimeters.

7.3 Decrease of Acceptable Maximum Perimeter

The optimum for the wall thickness distribution derived in chapter 5 is the initial tube with the largest perimeter within the investigated domain. In this domain the maximum perimeter is formed by a unique combination of design variables. To investigate the influence of the design variables on the optimum a restriction is added within the domain. The domain is bounded by the constraint (see section 4.3) restricting the perimeter to a maximum of 98% of the perimeter of the die cavity. The new constraint will restrict the perimeter to 90 % of the perimeter of the die cavity. This extra explicit constraint is used to form a boundary within the

domain of the experimental design. Therefore it is written in the same form as the implicit constraint for necking:

$$P_{tube} - 0.9 \cdot P_{Die} \leq 0 \quad \text{Eq. 7.4}$$

Where P_{tube} is the outside perimeter of the initial tube and P_{Die} the perimeter of the die cavity.

The metamodel for the constraint shows a perfect fit for a ‘quadratic model with interactions’, i.e. a R-squared value of one. This model is, in combination with the metamodel for the objective functions, subsequently optimised with the Matlab routine *fmincon*. The results are presented in Table 7.3.

Table 7.3. Optimum with a new constraint

	$H/2$ (mm)	L (mm)	t (mm)	κ_1 (mm ⁻¹)	κ_2 (mm ⁻¹)
f_5	26.5605	5	1	1/6	-1/98
f_6	26.4805	5	1	1/6	-1/74
f_7	26.4357	5	1.6	1/6	-1/185

The corresponding tubes are presented below:

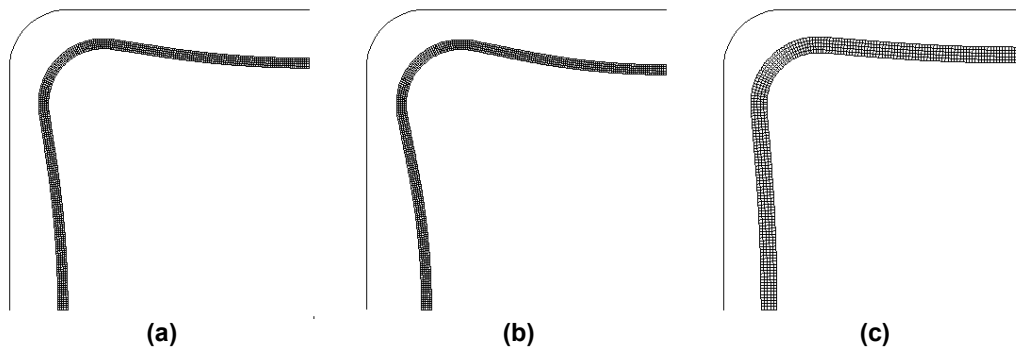


Figure 7.2. New optimum initial geometry for (a) f_5 , (b) f_6 and (c) f_7

The tubes presented above are almost alike. The biggest difference is found in the wall thickness of the objective function of Eq. 4.12, which has a preference for a wall thickness of 1.6 mm. This is due to the linear effect compared with the interaction effects concerning the design variable t . For a certain maximum allowable perimeter a change in preference occurs. This is seen in Figure 5.9.

The set of design variables forming the optimum are used to run a simulation. The results are used to determine the values of the objective functions. These are compared with the approximate values of the metamodels in Table 6.3.

Table 7.4: Values of the objective function in the optimum

	Metamodel	Simulation
f_5	0.0599	0.0605
f_6	0.0625	0.0635
f_7	0.0606	0.0630

The metamodels made a good approximation of the objective function in the found optimum. However the objective function of Eq. 4.10 shows a smaller value for the tube of Figure 7.2 (a) rather than (b). The metamodel for this objective function is not accurate enough in this region. The difference between the tubes are however small.

An overall conclusion from this constraint is the preference for a low box-like tube (H) with a sharp corner (κ_1) rather than a large box with a wide corner. Furthermore the box-like tube is dented in the middle of the sides (κ_2)

7.4 Data Point not satisfying an Implicit Constraint

In the previous sections the discussion was about the optimisation problem of the previous chapters. In this and the next section the discussion is shifted to the optimisation in general, starting with the influence of the implicit constraint on the optimum. It was not mentioned during the optimisation of chapter 5, but the introduced implicit constraints are treated in two different ways: An experiment not satisfying an implicit constraint

1. is excluded from the remainder of the optimisation, i.e. does not contribute to the metamodel;
2. together with the other experiments is used to build a metamodel to form a boundary on which the optimum can be located.

An example of the first point is the localisation of the mesh. In this situation the experiment does not satisfy two implicit constraints, namely the complete filling of the die cavity and the necking criterion. An example for the second point is the necking criterion used to build a metamodel. In the first case it is obvious that the experiment cannot be used for the optimisation, but it is not always so clear. It is all connected to the behaviour of the problem in consideration. The functions used to fit a metamodel through the data points are of a polynomial function with a maximum order of two. For most cases this model is sufficient to describe the considered phenomena. But this is restricted. When an experiment does not satisfy a constraint the behaviour of the experiment can alter to a more complex model. Necking is an example, which can be applied in both mentioned ways. Point two can be used when the strains in the model do not lead to mesh localisation. In that case point one applies. In chapter 5 initial work hardening was added to the finite element model. For some simulations the die cavity was completely filled, but the mesh showed localisation. The result for the simulation could be used to form a metamodel, but the localisation leads to an abnormality of the thinning behaviour of the tube, i.e. a peak in the wall thickness distribution. Therefore the simulations were excluded.

The necking criterion however excluded far more simulations, but the simulation of necking behaviour is less sensitive than the proposed criteria. Due to this the simulations followed normal thinning behaviour of the tube wall and can be used to form the metamodel.

7.5 Combination of the Feasible Domain and the Experimental Design

The constraints of an optimisation problem form the boundaries of the feasible domain. Within this domain the settings for the experimental runs are chosen according to an experimental design. In this report a classical design (Face Centred Central Composite Design) is used. The shape of the classical design limits the domain for the search to the optimum. When representing a classical design in an n -dimensional space formed by the n design variables, the shape of the classical design is either a hyper cube or a hyper sphere. In the case of the

classical design used in this report a hyper cube is formed. The classical design will only completely fill the feasible domain if the constraints forming its boundary are restricted to two conditions, namely:

- All constraints should be linear
- The in-product of the normal vectors of two constraints is either zero or one.

In practice however the constraints rarely meet both of the conditions. This leads to a difference between the domain size of the feasible domain and the experimental domain according to:

$$\text{Domain \{experimental design\}} \in \text{feasible domain}$$

Due to this the optimisation is performed on a smaller domain than possible with the risk of excluding the true optimum. Furthermore the domain of the experimental design can be small leading to a metamodel dominated by linear effects. Possible quadratic effect can be estimated, but the confidence interval will be large and lead to exclusion of the effects. This can explain the dominating linear behaviour of the metamodel for the wall thickness distribution of chapter 5 and 6.

8 Conclusions and Recommendations

8.1 Conclusions

The aim of this project was to gain more insight in optimisation of forming processes with finite element method in general, furthermore to improve the knowledge of the hydroforming process. In this section the conclusions are presented with a short explanation.

- The elements and element size have limited influence on the optimum.
Three mesh sizes for two-dimensional and a three-dimensional analysis were conducted. Each resulted in the same optimum. The three-dimensional simulations have the tendency to overestimate the wall thickness distribution (value of the objective function) and are less accurate due to overestimated maximum thinning. The same holds for the coarse mesh in the two-dimensional analysis. The overall picture however stays the same, which results in the same optimum.
- The optimal wall thickness distribution depends mostly on the perimeter of the tube.
As shown in chapter 5 the optimum is formed by the settings of the design variables, which form the largest perimeter for the initial tube. In chapter 7 the maximum perimeter was reduced. The optimum still beholds the tube with the largest allowable perimeter. The optimum tube is a box-like tube with a preference for a low side (H) and a sharp corner (κ_1) rather than a large box with a wide corner. Furthermore the box-like tube is dented in the middle of the sides (κ_2), forming a convex radius.
- An optimum located on the boundary of the domain can be misleading.
As mentioned before, the optimum depends on the maximum perimeter of the initial tube. For the domain used in chapters 4 through 6 the maximum perimeter is only reached for one combination of design variables. After the introduction of an extra restriction in section 7.3 in the form of an implicit constraint, the maximum allowed perimeter can be formed for several combinations of the design variables. Only in this situation the influence of the design variables on the optimum could be investigated.
- Applying a screening design to reduce the number of design variables is useful.
The screening designs of chapter 7 are capable of detecting insignificant design variables, but due to confounding of effects it is not certain that all insignificant variables are found.
- Insignificance of effects is influenced by the domain size
For the investigated optimisation problem the design variable L is insignificant for all effects (linear, interaction and quadratic) for the four possible metamodels. This is caused by the small variation of the length. When the domain is increased the design variable will be significant due to the influence on the perimeter length, especially in combination with the other design variables.
- The objective function should be unbiased with regard to the design variables.

In this report mostly two types of objective functions were investigated, biased and unbiased with respect to the initial wall thickness. When the initial wall thickness is used as a design variable the unbiased objective functions is preferred.

In the case the design variable is not linked to the objective function, as in section 7.2 the choice of objective function is less important due to the domination of the perimeter to the optimum initial tube geometry.

8.2 Recommendations

- Applying screening designs
When using a classical design, the screening design is a portion of the classical design. The results of the screening design can be used for the RSM, even if one design variable is insignificant. It is recommended to use a centre run in order to detect quadratic effects. These effects are not detected by a screening design and therefore the risk of excluding a variable with a weak linear but strong quadratic effect is present.
- (in)Significance of effects
With regression analysis the metamodel is fitted through the data points. For this project it was possible to choose from four different models, from which one was picked with the help of lack-of-fit tools. The effects forming the metamodel are (with the help of the confidence intervals) considered significant or insignificant. The influence of the insignificant is noteworthy. These effects contribute to the optimum, but are not entitled to. To lose the effect of the insignificant terms it is recommended to chance the value to zero. The fit of the model will deteriorate, but the chance of misinterpretation of the optimum is decreased.
- The necking criteria have no influence in the optimum
Despite of this it is useful to apply these criteria to the optimisation problem. If all simulations in the investigated domain do not meet the necking criteria, the metamodel can be used to gain insight into the necking behaviour of the tube(s) and help to find a new direction of search.
- Experimental design
The experimental design used in this project was a Face Centred Central Composite Design. This design is suited for predicting linear, interaction and quadratic effects needed for Response Surface Methodology. The domain of the design however is a limiting factor, concerning all classical designs. The domain of a classical design is rarely similar to the feasible domain formed by the constraints. This means that with the use of classical designs it is not possible to capture the behaviour of the process in the entire feasible domain. For this other designs are needed, which must be sought in the range of computer generated designs.

Acknowledgement

After graduation of my study mechanical engineering at the Saxion Hogeschool Enschede I decided to proceed my education of mechanical engineering at the University of Twente. To conclude this period I conducted my graduation at the CRD&T department at Corus staal B.V. in IJmuiden, of which this report is the end result.

I would like to thank professor Huétink of the department of applied mechanics to let me graduate at Corus RD&T. Furthermore I would like to thank my supervisors at Corus, Ruth van de Moesdijk and Maarten Kelder, and at the university, Ton van den Boogaard and Martijn Bonte, for constructive criticism and advise during my graduation period.

I would like to render thanks to all the employees in the PAC building at Corus for the pleasant time I spend there. I highlight Eisso Atzema for helping with DiekA and tips on the area of statistics, Rutger Peeters for the occasional support with my programming in visual basic and Ingrid van Stijn and Margot Klaassen for the two days of hydroform testing in Germany and to let me experience the practical and in particular the wet side of hydroforming.

Special thanks goes to Jelle Bakker, my roommate at Corus and fellow graduation student (graduated at 6 October 2004) for the support with the simulation software DiekA and the discussions of our projects. And of course my roommate for the last months, Jenny Venema, who will hunt me the rest of my life if she is not mentioned in this acknowledgement and who endured my grumpy moods during the final stage of writing my report.

And of course all the people who joint the relaxing games of soccer and volleyball on the beach with a nice beer afterwards.

As last but certainly not the least I would like to thank my parents to give me the opportunity to study at the university and of course the support they gave me in this period.

References

- [1] Matlab optimisation toolbox user guide, the Mathwork inc.
- [2] Alvarez, L.F., 2000, "Design Optimisation Based on Genetic Programming", Ph.D. Thesis, Department of Civil and Environmental Engineering, University of Bradford, UK.
- [3] Bakker, J., 2004, "Corner Filling in Tube Hydroforming", Graduation thesis, University of Twente, Department of Mechanical Engineering
- [4] Bauer, W., Sander, J., Bieling, P., 1999, "Creating a production process sequence for hydroforming", Hydroforming journal, sept 99, pp.50-54
- [5] Bonte, M.H.A., 2004, "Optimisation: An introduction", Internal report P04.1.047, Netherlands Institute for Metals Research, Delft, NL, 2004
- [6] Butler, N.A., 2000, "On Weighted Design Optimality Criteria and Response Surface Parameterizations", Statistics & Probability Letters, 51, pp. 41-46
- [7] Chang, F.C., Lay, C.F., 2002, "Optimal Designs for a Growth Curve Model", Journal of Statistical Planning and Inference, 104, pp. 427-438
- [8] Coleman, T.F. and Y. Li, "An interior, Trust Region Approach for Nonlinear Minimization Subject to Bounds", SIAM Journal on Optimization, vol. 6, pp. 418-445, 1996.
- [9] Coleman, T.F. and Y. Li, "On the Convergence of Reflective Newton Methods for Large-Scale Nonlinear Minimization Subject to Bounds", Mathematical Programming, Vol. 7, Number 2, pp./ 189-224, 1994.
- [10] Endelt Kristensen, B., Nielsen, K.B., 2001, "Least Square Formulation of the Object Function, Applied on Hydro Mechanical Tube Forming", Proceedings of the 9th International Conference on Sheet Metal, SheMet 2001, Mechanical Engineering Department Katholieke University Leuven, pp. 353-362
- [11] Fagan, M.J., 1992, "Finite Element Analysis, Theory and Practice", Longman, London
- [12] Gilmour, S.G., Mead, R., 2003, "A Bayesian Design Criterion for Locating the Optimum Point on a Response Surface", Statistics & Probability Letters, 64, pp. 235-242
- [13] Han, C., Chaloner, K., 2003, "D- and c-optimal Designs for Exponential Regression Models used in Viral Dynamics and other Applications" Journal of Statistical Planning and Inference, 115, pp. 585-601
- [14] Heizmann, J., 2003, "Activator Assisted Forming Technologies – Status and Outlook", Hydroforming of Tubes, Extrusions and Sheet Metals, Siegert, K., MAT INFO Werkstoff-Informationsgesellschaft mbH, vol 3, pp. 1-6
- [15] Hwang, Y.M., Altan, T., 2002, "FE simulations of the crushing of circular tubes into triangular cross-sections", Journal of Material Processing Technology, 125-126, pp. 833-838
- [16] J.E., Grey, A.P. Devereaux, W.N. Parker, "Apparatus for making wrought metal T's. US Patent 2,203,868 June 1939
- [17] Kim, S., Kim, T., 2002, "Analytical study for hydroforming", Journal of Materials Processing Technology, 128, pp. 232-239
- [18] Koç, M., Altan, T., 2001, "An overall review of the tube hydroforming (THF) technology, Journal of Materials Processing Technology, 108, pp. 384-393
- [19] Koç, M., Altan, T., 2002, "Prediction of forming limits and parameters in the tube hydroforming process", International Journal of Machine Tools & Manufacture, 42, pp. 123-138

- [20] Marciniak, Z., Duncan, J.L., Hu, S.J., 2002, "Mechanics of Sheet Metal Forming", Butterworth Heinemann, Oxford
- [21] Montepiedra, G., Fedorov, V.V., 1997, "Minimum Bias Designs with Constraints", Journal of Statistical Planning and Inference, 63, pp. 97-111
- [22] Montgomery, D.C., Tunger, G.C., 1994, "Applied Statistics and Probability for Engineers", John Wiley & sons, Inc. New York
- [23] Morphy, G., 2002, "Exploring design flexibility of hydroformed automotive structural parts", www.thefabricator.com
- [24] Morphy, G., 2002, "Hydroforming Journal: Examining tube hydroforming design flexibility - Expansion in the hydroforming die and variable periphery design", www.thefabricator.com
- [25] Morphy, G., 2001, "Pressure-sequence and high-pressure hydroforming, knowing the processes can mean boosting profits", www.thefabricator.com
- [26] Morphy, G., 2003, "Tube hydroforming design flexibility Part IV: Material", www.thefabricator.com
- [27] NIST/SEMATECH e-Handbook of Statistical Methods, <http://www.itl.nist.gov/div898/handbook>, 2004
- [28] Peeters, R., 2001, "3D modelling of the roll forming process, Master Thesis University of Twente, The Netherlands
- [29] Revuelta, A. Larkiola, J., 2004, "Applying Neural Networks in the Final Thickness optimisation of a Thin Hydroformed Part", European Congress on Computational Methods in Applied Sciences and Engineering
- [30] Spörer, J., Delker, M., Zisler, A., Kautz, T., 2003, "Hydroforming at BMW", Hydroforming of Tubes, Extrusions and Sheet Metals, Siegert, K., MAT INFO Werkstoff-Informationsgesellschaft mbH, vol 3, pp. 91-109

Appendices

Appendix A. Design of Experiments

Design Of Experiments (DOE) is the deliberately changing of one or more variables in order to investigate the effect of the changes on one or more response variables. The number of experiments and the spreading of the results in the feasible domain influence the forming of the metamodel. A DOE places the experiments in the feasible domain to obtain a model, which beholds as much information as possible with as low as possible number of experiments. In this section DOEs suited for RSM and used for this project are discussed. A large portion of DOE strategies are not mentioned and for further information is referred to literature [22], [27].

The most common Designs of Experiments are the classical designs. These designs form either a hyper cube or a hyper sphere in the design space. Advanced designs use computer software to place the points in the design space using several criteria, thereby obtaining the ability to fill the feasible domain more efficiently compared to classical design space.

A.1 Levels of a Design

First a quote by Montgomery (1991): *It is our belief that the two-level factorial and fractional factorial designs should be the cornerstone of industrial experimentation for product and process development and improvement.* He went on to say: *There are, however, some situations in which it is necessary to include a factor (or a few factors) that have more than two levels.*

The number of levels determines the maximum function order and the complexity of the design. To reduce the number of experimental runs the number of levels must kept low, while to maximise the obtainable information the number of levels must be high. This contradictive demand of a DOE is the reason for much research in the past to find better designs. As Montgomery stated above the problem considered plays an important roll and two level designs are sufficient for most optimisation problems. Hereafter several designs are explained. To indicating the levels of a design in a DOE, coded variables are used. For a two-level design the higher level is indicated with '+1' and the lower level with '-1'. To obtain a centre run (explained later) '0' is used.

A.2 Full Factorial Design

In a full factorial design the number of runs is equal to all possible combinations of levels from the design variables. In a design with two levels per variable, the number of experimental runs is equal to 2^n , where n is the number of variables. For a design with three levels per variable the number of experimental runs is equal to 3^n . In general, if there are k factors, each at n levels, a full factorial design has n^k runs. The number of experimental runs required for a design depends strongly on the number of variables due to the power of n . The effect is even stronger for a larger number of levels as shown if Table A.1.

Table A.1. Number of experimental runs in a Full Factorial Design

Number of Variables	Two-level Design	Three-level Design
1	2	3
2	4	9
3	8	27
4	16	81
5	32	243

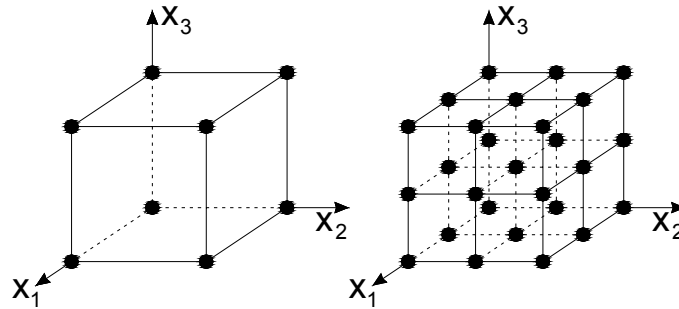


Figure A.1. 2-Level and 3-Level 3-Factor Full Factorial Design

In the figure above both a two and three-level three-factor full factorial design is depicted. The two-level design is capable of predicting the linear effects together with two-factor interaction effects. The response surface adapts to the following form:

$$f(\mathbf{x}) = \alpha_0 + \alpha_i x_i + \alpha_{ij} x_i x_j \quad \text{for } j > i \text{ and } i, j = 1, 2, 3 \quad \text{Eq. A.1}$$

Where x_i is the i^{th} design variable and α_i the corresponding effect. α_{ij} is the effect for the two-factor interaction.

The three-level design is capable of predicting the same effects as the two-level design with addition of the quadratic effects and the three-factor interactions, giving the response surface the following form:

$$f(\mathbf{x}) = \alpha_0 + \alpha_i x_i + \alpha_{ij} x_i x_j + \alpha_{klm} x_k x_l x_m \quad \text{for } i \geq j, m > l > k \quad \text{Eq. A.2}$$

$$\text{and } i, j, k, l, m = 1, 2, 3$$

In which α_{klm} is the effect of the three-factor interaction and α_{ij} is now also the effect of the quadratic term.

In Table A.2 an example is given for a three-factor two-level full factorial design. The design is built by alternating the levels from low to high with steps of 2^{i-1} , where i is the number of the design variable.

Table A.2. Example of a two-level three-factor full factorial design

	X ₁	X ₂	X ₃
1	-1	-1	-1
2	+1	-1	-1
3	-1	+1	-1
4	+1	+1	-1
5	-1	-1	+1
6	+1	-1	+1
7	-1	+1	+1
8	+1	+1	+1

The columns of the design can be considered as vectors, which are orthogonal with respect to each other. This implies that the outcome of the in-product of two arbitrary columns is zero. The orthogonality property of a design is important because it eliminates the correlation of the estimate of the main effects and interactions.

A.3 Fractional Factorial Designs

To decrease the number of experimental runs, a fraction of the factorial design is used to evaluate the optimisation problem. Desired is a design that is both **balanced** and orthogonal. The fraction consists of n^{k-p} runs, where n is the number of levels, k the number of factors and p the fraction. This means that a fraction is a $(\frac{1}{2})^p$ part of the full factorial design.

There are a number of other designs, which are a fraction of a full factorial design, but differ in the number of runs and the combination of levels, like Plackett-Burman, Box-Behnken and John's $\frac{3}{4}$ fractional factorial design. For further information about these designs is referred to literature [22], [27].

For a half fractional factorial design, the full factorial design is split in half. Both halves are a half fractional factorial design and therefore both suited for use as a guide for the experiments. However both designs will likely give a different approximation of the main and interaction effects, which in turn will deflect from the outcome of the full factorial design. Note that the full factorial design is an approximation of the effects itself.

Let us now look how a two-level three-factor fractional factorial design can be composed with preservation of orthogonality. First a full factorial design is built for two factors.

Table A.3. Two factor full factorial design

	X1	X2
1	-1	-1
2	+1	-1
3	-1	+1
4	+1	+1

The third column is generated by multiplying the first and second column, i.e.

$$x_3 = x_1 x_2$$

Table A.4. Three factor fractional factorial design

	X1	X2	X3
1	-1	-1	+1
2	+1	-1	-1
3	-1	+1	-1
4	+1	+1	+1

Instead of using the above stated relation between the columns the right side can be multiplied with '-1', obtaining $x_3 = -x_1x_2$. Combining both designs leads to the full factorial design.

Reducing the number of runs comes with a price, namely the reduction of accuracy of the fitted model. The fractional factorial design of Table A.4 is generated by the multiplication of the first two columns. The ability of obtaining an estimate of the main effect x_3 and the interaction term x_1x_2 is lost. The main effect and interaction term are confounded.

Multiplication (like $x_3 = x_1x_2$) will from now on be written as 3=12. To examine the influence fraction on other terms multiply both sides of the equation with 3:

$$33=123$$

33 is equal to I, a column of all ones. This leads to I=123, which is called a design generator. The term 123 is called a word. Using some algebra the following equations can be formed:

$$I=123 \rightarrow I1=1123 \rightarrow 1=23$$

$$I=123 \rightarrow I2=1223 \rightarrow 2=13$$

Since 11=22=33=I. From this it is seen that all main effects are confounded with interaction terms. The design (number of runs) can therefore only be decreased when the interactions effect is small compared to the main effect.

An indication of the degree of confounding of effect is described by the resolution of a design. This is indicated by a roman numbers, which indicates the length of the smallest word. For instance in a resolution II design the smallest word has a length of two, for instance 12. The design generator is thus I=12, which leads to 1=2. The main effects x_1 and x_2 are confounded with each other. Therefore a resolution II design is not a good design.

A resolution III design has a minimum word length of three, which means that main effects and two-factor interaction terms are confounded. For a resolution IV design the two-factor interaction terms are confounded among themselves and the main effect are confounded with three-factor interactions. For instance the design generator I=1234 lead to:

$$1=234, 2=134, 3=124, 4=123$$

$$12=34, 13=24, 14=23$$

In a resolution V design the main effects are confounded with four-factor interactions and two-factor interactions with three-level interactions. The assumption that third order models are highly unusual for industrial processes, thus the negligible effect of third order terms, lead to the conclusion that a resolution V design or higher will not influence the approximation of the first and second order effects.

A fractional factorial design, n^{k-p} , can be of different resolutions and differ within a resolution. The latter one was shown with the design of Table A.4, where the inverse of a design

generator was used. Also another word with the same length leads to a different design with the same resolution. A 2^{4-1} design can be both a resolution III design and a resolution IV design. In the tables below both designs are shown, with corresponding words.

Table A.5. Resolution III design

	X ₁	X ₂	X ₃	X ₄ (124)
1	-1	-1	-1	1
2	-1	-1	1	1
3	-1	1	-1	-1
4	-1	1	1	-1
5	1	-1	-1	-1
6	1	-1	1	-1
7	1	1	-1	1
8	1	1	1	1

Table A.6. Resolution IV design

	X ₁	X ₂	X ₃	X ₄ (1234)
1	-1	-1	-1	-1
2	-1	-1	1	1
3	-1	1	-1	1
4	-1	1	1	-1
5	1	-1	-1	1
6	1	-1	1	-1
7	1	1	-1	-1
8	1	1	1	1

A.4 Box–Wilson Central Composite Designs

The above-mentioned designs are based on two-level designs. These designs are favourable above three level designs due to the small number of runs. However, quadratic effects, preferable for RSM, cannot be predicted using a two level design. To increase the ability of predicting quadratic effects, Box and Wilson came up with a new design based on two-level designs. These designs, called Central Composite Designs, are capable of predicting quadratic effects, without adding a high number of additional runs.

The design consists out of a two level design added with a centre run and star points. The centre run, located in the exact middle of the design, is suited for better prediction of interaction effects and indicates the presence of quadratic effects. The centre run alone cannot estimate the quadratic effects and therefore the star points are added. The star points, two times the number of design variables, are located at a distance α of the centre of the design. In Figure A.7 the three variants of Central Composite Design for two design variables are depicted. The number of runs of the designs is equal to $2^n + 2n + 1$ (two-level design plus the star points plus the centre run).

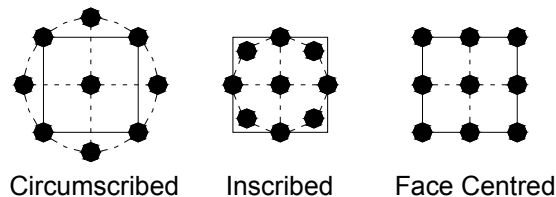


Figure A.7. Central Composite Design

A.4.1 Circumscribed Central Composite Design

The circumscribed design adds star points outside the design space of the two-level design at a distance $|\alpha|$ of the centre of the design space. Therefore each design variable is examined at 5 different levels. This means that the design space is extended. The range of the variables

must be considered when using this design to prevent experimental runs outside the feasible domain.

A.4.2 Inscribed Central Composite Design

If the circumscribed design is not possible, the inscribed design can be used. The base of the design is equal to the circumscribed design, except $|\alpha|$ equals to one and the range of the variables for the two level design is scaled, i.e. the circumscribed design is scaled in such way that all levels are within the original range of the two-level (fractional) factorial design

A.4.3 Face Centred Central Composite Design

The star points for the face centred design are located at $|\alpha| = 1$. This means that in contrast to the two central composite designs mentioned above, the design has three levels per factor. The design is less suited for estimating the quadratic effects due to the number of levels. The advantage however is the better spreading of points in the rectangular design space compared to the inscribed design and the smaller range compared to the circumscribed design. This last argument is important due to potential impossible combinations of levels of the design variables.

A.4.4 Fractional Factorial Central Composite Design

To reduce the number of experimental runs, but still keep the properties of a Central Composite Design, the basis of this design is altered. Instead of using a two-level Full Factorial Design a fraction of this design is chosen. This is normally done when five or more design variables are involved in a design. As shown in Table A.7 the reduction of experimental runs is low for four or less design variables and does not compensate for the confounding of the design.

Table A.7. Number of runs for a Central Composite Design

Design Variables	Central Composite Design with a		
	Full Fraction	½ Fractional	¼ Fraction
2	9	7	6
3	15	11	9
4	25	17	13
5	43	27	19
6	77	45	29
7	143	79	47
8	273	145	81

A.5 Other Designs

The designs described above are a small portion of all existing designs, but probably the most widely used ones. The already mentioned designs, Plackett-Burman, Box-Behnken and John's $\frac{3}{4}$ fractional factorial design, are suited for decreasing the number of runs and still get a reasonable amount of information. The heavily confounded designs, like Plackett-Burman and low-resolution fractional factorial designs are not suited for predicting effects with RSM but convenient tools for screening the design variables. Screening designs are used to determine the design variables with high significance. This is very useful when a large number of design variables are present and the choice cannot be made on forehand. After this step, the remaining design variables are used in a new design for Response Surface Modelling.

Until now only classical designs are mentioned. Another group of designs are the computer-generated designs. These designs use several criteria for placing experimental runs into the design space. A common used criterion is D-optimality, where the minimum distance between two runs is maximized. Other criteria are A-, ASV-, C-, E-, I-, V-optimality and Bayesian. For further information about design of experiments the reader referred to literature ([6], [7], [12], [13] and [21])

With the completed experimental design, the experiments are conducted. The outcome of the experiments is used to fit a metamodel with regression analysis. In the next section the function order of this model is discussed.

Appendix B. Design Variables

The model of figure B.1 is described with seven variables. These variables are used to derive the equations describing the geometry in mathematical form.

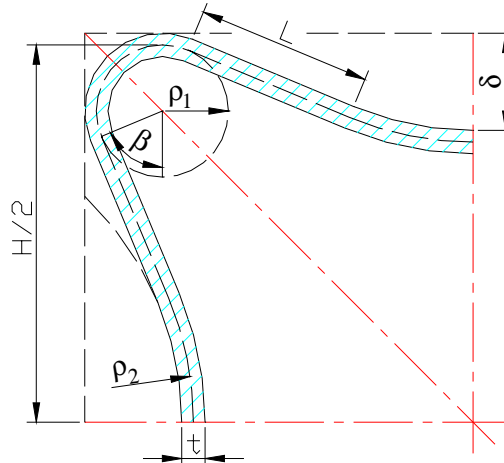


Figure B.1. The model used for optimisation containing two different radii.

Before deriving these equations an indication presented for the values of the variables concerning the radii.

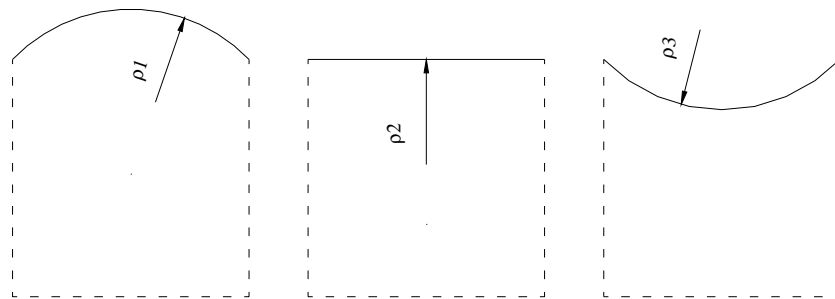


Figure B.2. A concave (left), affine (middle) and convex (right) radius

In figure B.2 three possible situations are presented for the radii. The middle one (affine) is the transition of a concave to a convex radii and visa versa. The signs of the radii are:

$$\begin{aligned}
 \rho_1 > 0 & \quad (\text{concave}) \\
 \rho_2 = \infty \cap \rho_2 = -\infty & \quad (\text{affine}) \\
 \rho_3 < 0 & \quad (\text{convex})
 \end{aligned}
 \tag{Eq. B.1}$$

The transition from concave to convex leads to an infinite radius. This means the formulation of the radius leads to a discontinuous function. To form a continuous function the radius of curvature is introduced. The relation of the radius of curvature and the radius is:

$$\kappa = \frac{1}{\rho}$$

Eq. B.2

This leads to the signs of the radius of curvature according the figure B.2:

$$\begin{aligned} \kappa_1 &> 0 && \text{(concave)} \\ \kappa &= 0 && \text{(affine)} \\ \kappa_3 &< 0 && \text{(convex)} \end{aligned}$$

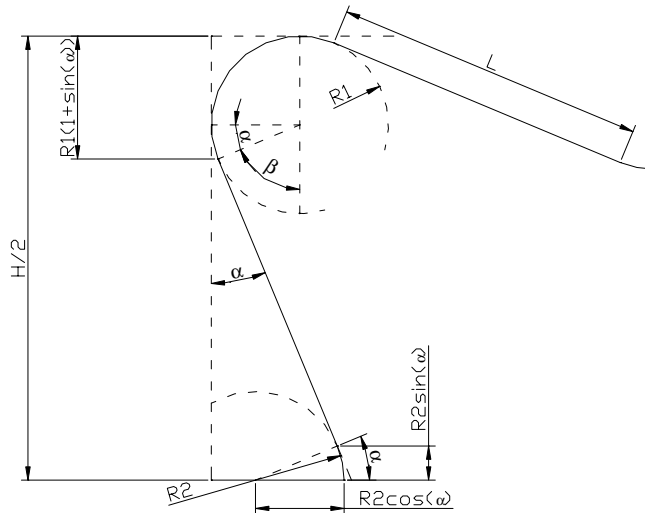
Eq. B.3

The radius of curvature is zero in the transition from concave to convex. With this the radius can be described with a continuous function.

For the derivation of the mathematical description of the tube two cases are considered. The first one is the convex situation and the second one is the concave situation for ρ_2 .

Situation1: convex:

The model is presented in figure B.3



$$\alpha = \frac{\pi}{2} - \beta$$

$$\kappa_1 = \frac{1}{\rho_1}$$

$$\kappa_2 = \frac{1}{\rho_2}$$

$$R_1 = \rho_1$$

$$R_2 = -\rho_2$$

8.2.1... Figure B.3: Convex situation

The height of the tube

$$\begin{aligned} \frac{H}{2} &= R_1(1 + \sin \alpha) + R_2 \sin \alpha + L \cos \alpha \\ &= R_1 + (R_2 + R_1) \sin \alpha + L \cos \alpha \\ &= R_1 + (R_2 + R_1) \cos \beta + L \sin \beta \end{aligned}$$

Eq. B.4

And δ is:

$$\begin{aligned}
\delta &= R_1(1 - \cos \alpha) + R_2(1 - \cos \alpha) + L \sin \alpha \\
&= (R_1 + R_2)(1 - \cos \alpha) + L \sin \alpha \\
&= (R_1 + R_2)(1 - \sin \beta) + L \cos \beta
\end{aligned}
\tag{Eq. B.5}$$

Rewriting both equations to the radius of curvature:

$$\begin{aligned}
\frac{H}{2} &= \rho_1 + (\rho_1 - \rho_2) \cos \beta + L \sin \beta \\
&= \frac{1}{\kappa_1} + \frac{\kappa_2 - \kappa_1}{\kappa_1 \kappa_2} \cos \beta + L \sin \beta
\end{aligned}
\tag{Eq. B.6}$$

$$\begin{aligned}
\delta &= (\rho_1 - \rho_2)(1 - \sin \beta) + L \cos \beta \\
&= \frac{\kappa_2 - \kappa_1}{\kappa_1 \kappa_2} (1 - \sin \beta) + L \cos \beta
\end{aligned}
\tag{Eq. B.7}$$

The perimeter of neural line of the tube is written as:

$$\begin{aligned}
P_{\text{perimeter}} &= 8(R_1(\alpha + \frac{\pi}{4}) + R_2\alpha + L) = 8(R_1(\frac{3\pi}{4} - \beta) - R_2(\beta - \frac{\pi}{2}) + L) \\
&= 8(\rho_1(\frac{3\pi}{4} - \beta) + \rho_2(\beta - \frac{\pi}{2}) + L) = 8\left(\frac{1}{\kappa_1}(\frac{3\pi}{4} - \beta) + \frac{1}{\kappa_2}(\beta - \frac{\pi}{2}) + L\right)
\end{aligned}
\tag{Eq. B.8}$$

Situation 2: Concave situation

The model is presented in figure B.4

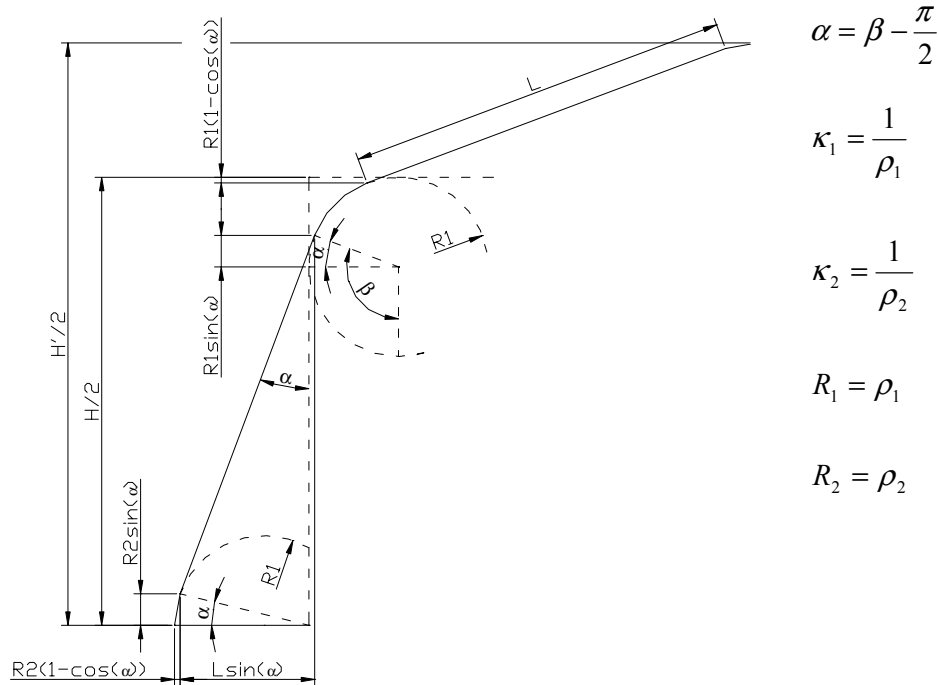


Figure B.4: Convex situation

The height of the tube

$$\begin{aligned}
 H/2 &= R_1(1 - \sin \alpha) + R_2 \sin \alpha + L \cos \alpha \\
 &= R_1 + (R_2 - R_1) \sin \alpha + L \cos \alpha \\
 &= R_1 + (R_1 - R_2) \cos \beta + L \sin \beta
 \end{aligned}
 \tag{Eq. B.4}$$

And δ is:

$$\begin{aligned}
 \delta &= -R_1(1 - \cos \alpha) + R_2(1 - \cos \alpha) + L \sin \alpha \\
 &= (-R_1 + R_2)(1 - \cos \alpha) + L \sin \alpha \\
 &= -(R_1 - R_2)(1 - \sin \beta) - L \cos \beta
 \end{aligned}
 \tag{Eq. B.5}$$

Rewriting both equations to the radius of curvature:

$$\begin{aligned}
 H/2 &= \rho_1 + (\rho_1 - \rho_2) \cos \beta + L \cos \alpha \\
 &= \frac{1}{\kappa_1} + \frac{\kappa_2 - \kappa_1}{\kappa_1 \kappa_2} \cos \beta + L \sin \beta
 \end{aligned}
 \tag{Eq. B.6}$$

$$\begin{aligned}
 \delta &= -(\rho_1 - \rho_2)(1 - \sin \beta) + L \sin \alpha \\
 &= -\frac{\kappa_2 - \kappa_1}{\kappa_1 \kappa_2} (1 - \sin \beta) - L \cos \beta
 \end{aligned}
 \tag{Eq. B.7}$$

The perimeter of neural line of the tube is written as:

$$\begin{aligned}
 P_{perimeter} &= 8(R_1(\frac{\pi}{4} - \alpha) + R_2 \alpha + L) = 8(R_1(\frac{3\pi}{4} - \beta) + R_2(\beta - \frac{\pi}{2}) + L) \\
 &= 8(\rho_1(\frac{3\pi}{4} - \beta) + \rho_2(\beta - \frac{\pi}{2}) + L) = 8\left(\frac{1}{\kappa_1}(\frac{3\pi}{4} - \beta) + \frac{1}{\kappa_2}(\beta - \frac{\pi}{2}) + L\right)
 \end{aligned}
 \tag{Eq. B.8}$$

Considering the wall thickness, the outside perimeter becomes:

$$P_{tube,b} = 8\left(\left(\frac{1}{\kappa_1} + \frac{t}{2}\right)(\frac{3\pi}{4} - \beta) + \left(\frac{1}{\kappa_2} + \frac{t}{2}\right)(\beta - \frac{\pi}{2}) + L\right)
 \tag{Eq. B.9}$$

Summary

$$\text{Situation 1: } \quad H/2 = \frac{1}{\kappa_1} + \frac{\kappa_2 - \kappa_1}{\kappa_1 \kappa_2} \cos \beta + L \sin \beta \quad \delta = \frac{\kappa_2 - \kappa_1}{\kappa_1 \kappa_2} (1 - \sin \beta) + L \cos \beta$$

$$\text{Situation 2: } \quad H/2 = \frac{1}{\kappa_1} + \frac{\kappa_2 - \kappa_1}{\kappa_1 \kappa_2} \cos \beta + L \sin \beta \quad \delta = -\frac{\kappa_2 - \kappa_1}{\kappa_1 \kappa_2} (1 - \sin \beta) - L \cos \beta$$

The height of the tube is described with the same equation, but δ has a different sign. This is due to the missing of an agreement of sign. From now on δ is negative in a convex situation

and positive in a concave situation. This lead to the following equations for the description of the neutral line of the tubes:

$$\frac{H}{2} = \frac{1}{\kappa_1} + \frac{\kappa_2 - \kappa_1}{\kappa_1 \kappa_2} \cos \beta + L \sin \beta$$

$$\delta = -\frac{\kappa_2 - \kappa_1}{\kappa_1 \kappa_2} (1 - \sin \beta) - L \cos \beta$$

Eq. B.10

Appendix C. Necking

Both Koç et al.[19], Marciniak et al. [20] and S. Kim et al. [17] , describe a derivation of the same bursting criterion for the maximal elongation of sheet metal, according to Koç applicable on hydroforming tubes. Below the derivation proposed by Marciniak is represented.

Plain stress deformation is assumed for sheet metal, i.e. the stress in thickness direction is equal to zero ($\sigma_3 = \sigma_r = 0$). Consider a region of a sheet subjected to a uniform deformation. This deformation is described in the following manner:

$$\begin{aligned} \sigma_1; & \quad \varepsilon_1; \\ \sigma_2 = \alpha\sigma_1; & \quad \varepsilon_2 = \beta\varepsilon_1; \\ \sigma_3 = 0; & \quad \varepsilon_3 = -(1 + \beta)\varepsilon_1. \end{aligned} \quad \text{Eq. C.1}$$

Where α and β are the ratio between the first two principal stresses and strains respectively.

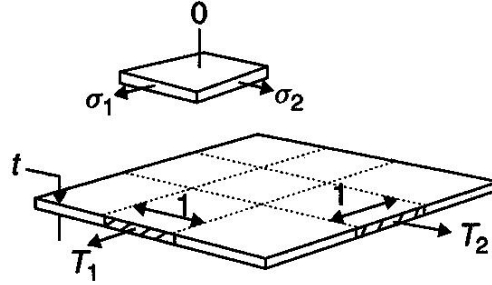


Figure C.1. Uniform deformation of part of a continuous sheet in a plane stress proportional process.

The principal tension in the sheet is presented as:

$$\begin{aligned} T_1 &= \sigma_1 t; \\ T_2 &= \alpha T_1 = \sigma_2 t \end{aligned} \quad \text{Eq. C.2}$$

Differentiating equation Eq. C.2:

$$\frac{dT_1}{T_1} = \frac{d\sigma_1}{\sigma_1} + \frac{dt}{t} = \frac{d\sigma_1}{\sigma_1} + d\varepsilon_3 = \frac{d\sigma_1}{\sigma_1} - (1 + \beta)d\varepsilon_1 \quad \text{Eq. C.3}$$

Which is only valid for $\beta > -1$. If $\beta < -1$, then the material flow towards the region is bigger then from the region, thereby thickening the sheet. Thus, a work-hardening material will never reach its maximum tension.

When the tensions reach a maximum, equation Eq .3 becomes zero, which results in:

$$\frac{1}{\sigma_1} \frac{d\sigma_1}{d\varepsilon_1} = 1 + \beta \quad \text{Eq. C.4}$$

The relation between the stress and strain is described with the work hardening relation of Hollomon Eq. C.5. The relation is proportional during deformation for which α and β are constant, thus the relation can be written for a single direction:

$$\begin{aligned} \bar{\sigma} &= C\bar{\varepsilon}^n \\ \sigma_1 &= C'\varepsilon_1^n \end{aligned} \quad \text{Eq. C.5}$$

Differentiation and substitution into equation Eq. C.4 results in:

$$\frac{1}{\sigma_1} \frac{d\sigma_1}{d\varepsilon_1} = \frac{n}{\varepsilon_1} \quad \text{Eq. C.6}$$

$$\varepsilon_1 = \frac{n}{1+\beta} \varepsilon_2 = \frac{\beta n}{1+\beta} \quad \text{Eq. C.7}$$

$$\varepsilon_1 + \varepsilon_2 = n \quad \text{Eq. C.8}$$

The strain at which necking occurs is shown in Eq. C.8 and is the summation of the two principal strains in the sheet. In Figure C.2 (a) the criterion for bursting is shown as function of the two principal strains and in Figure C.2 (b) the experimental determination boundary.

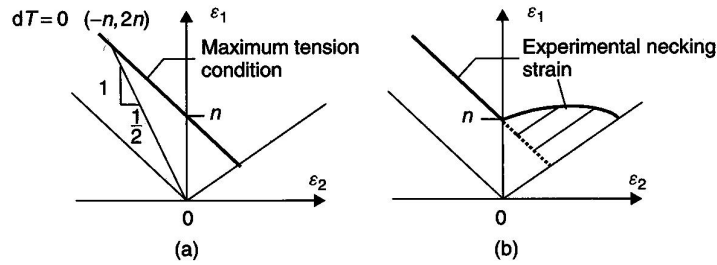
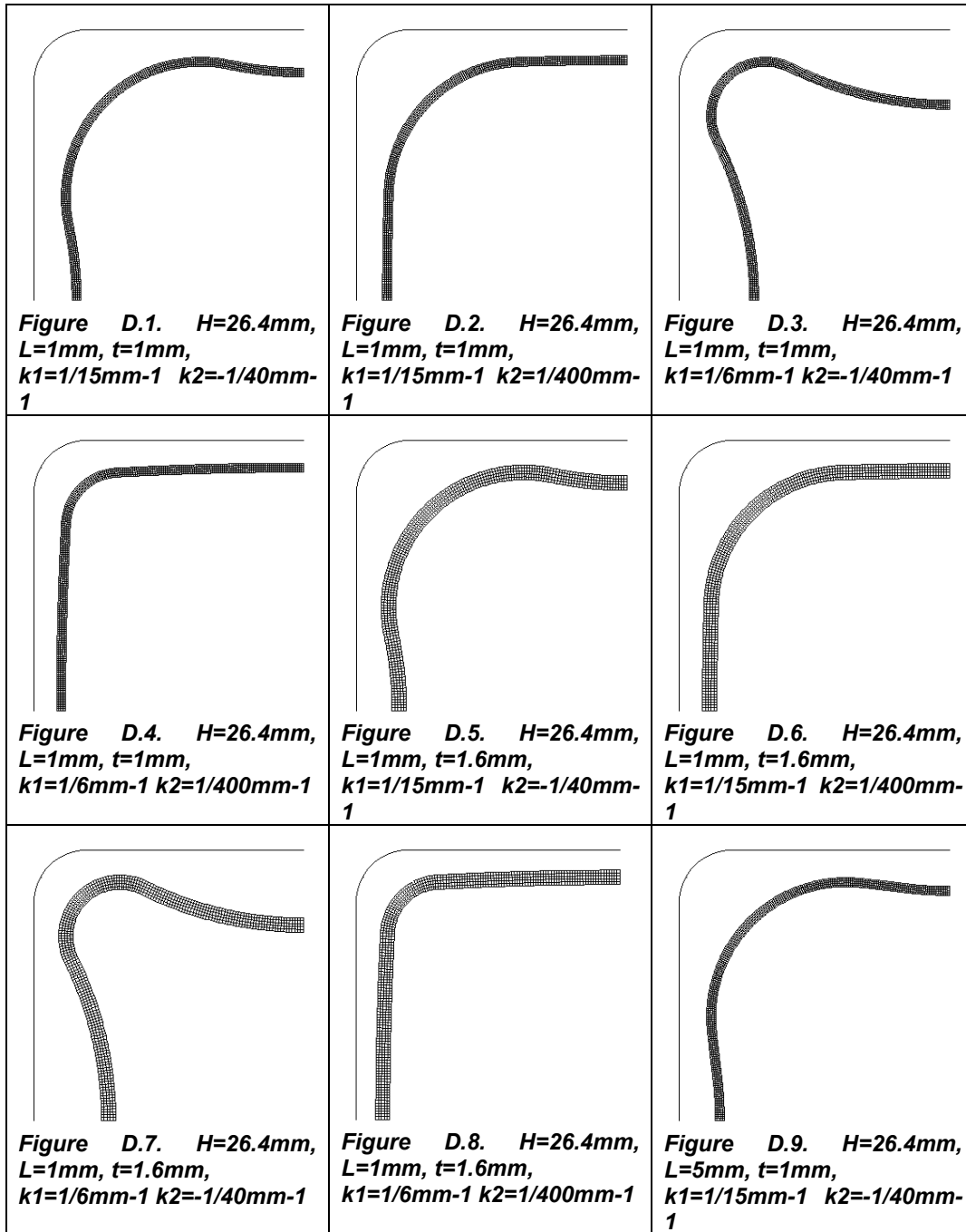
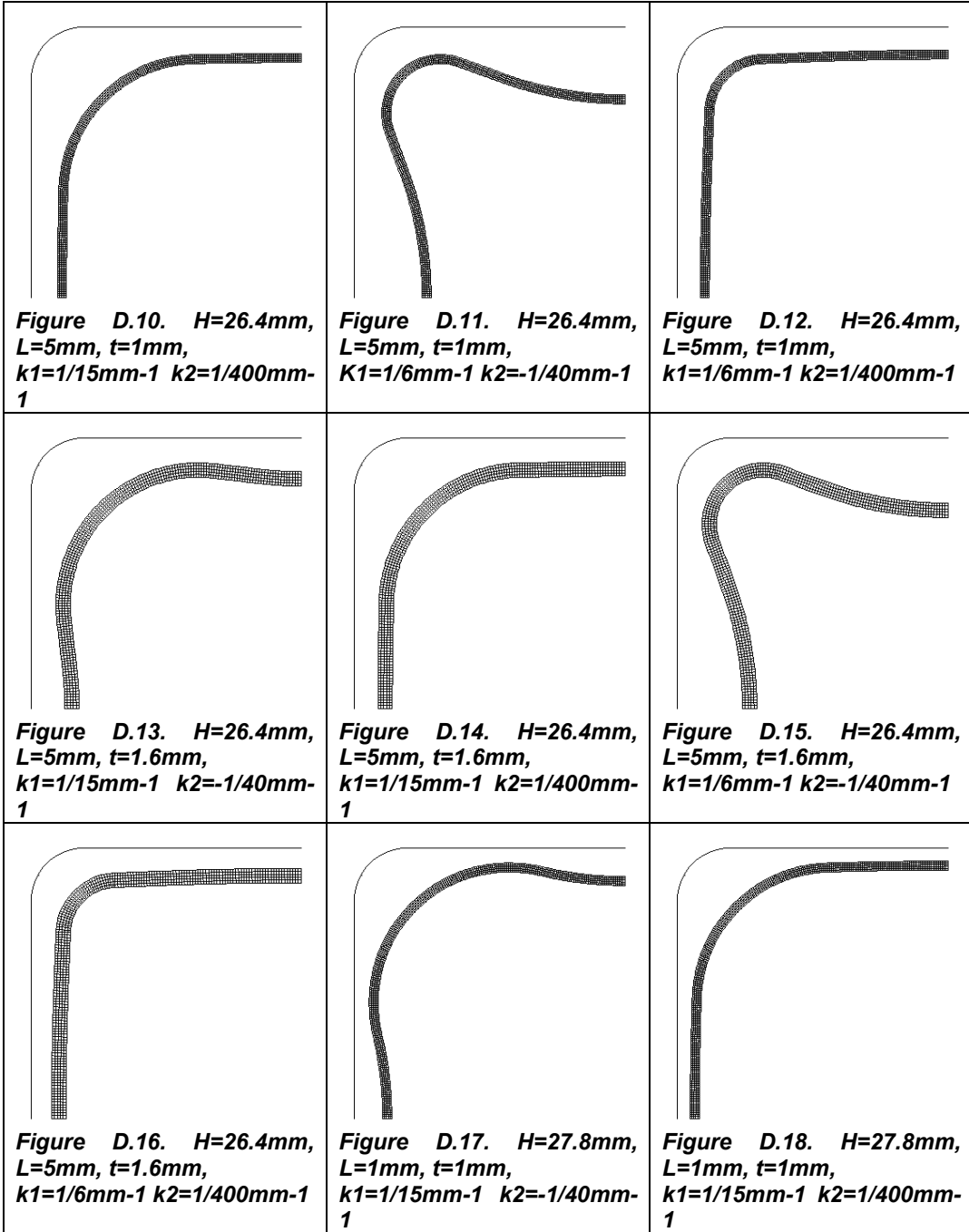


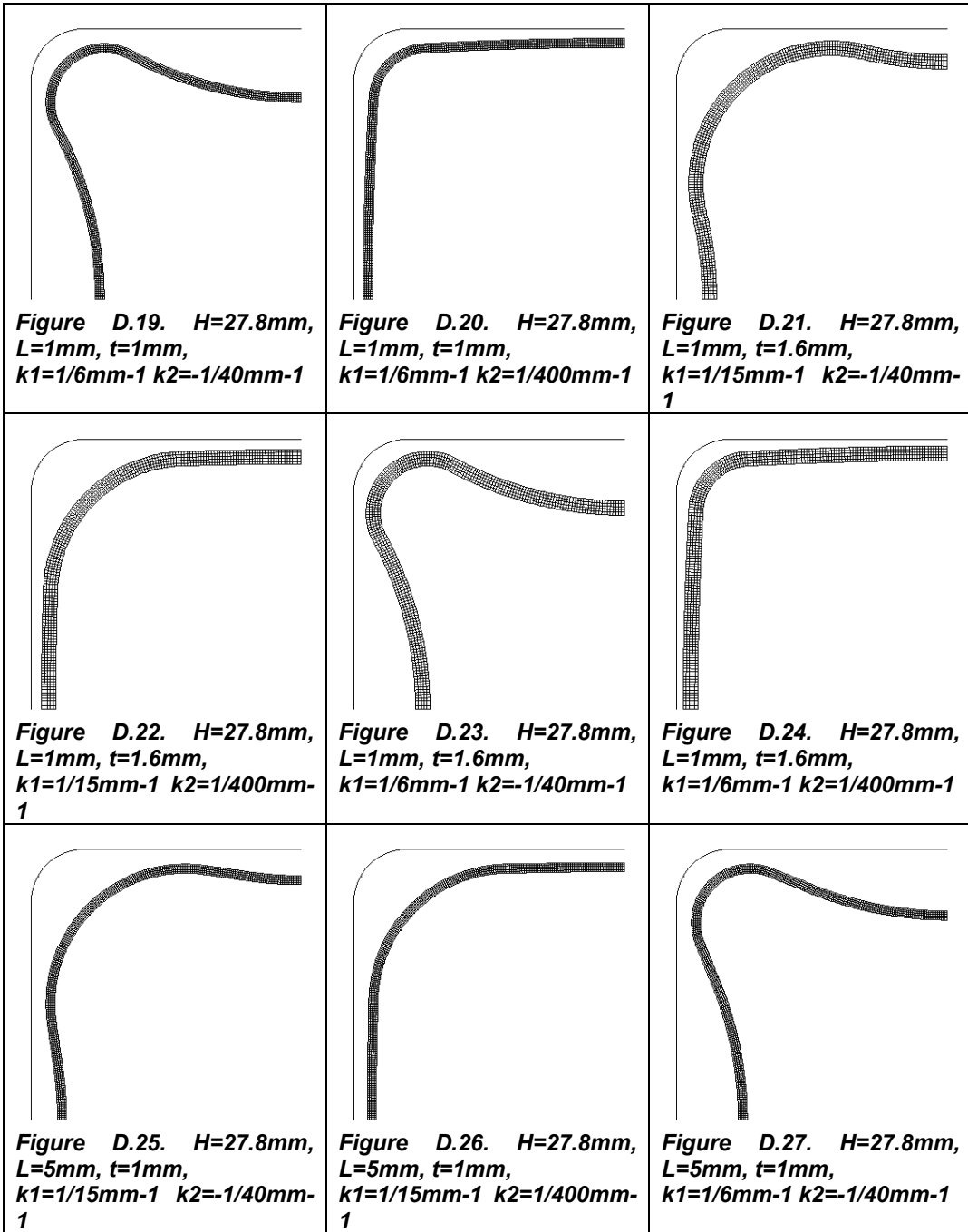
Figure C.2. (a) Strains at the maximum tension in a continuous sheet, (b) Experimentally observed necking strains in sheet

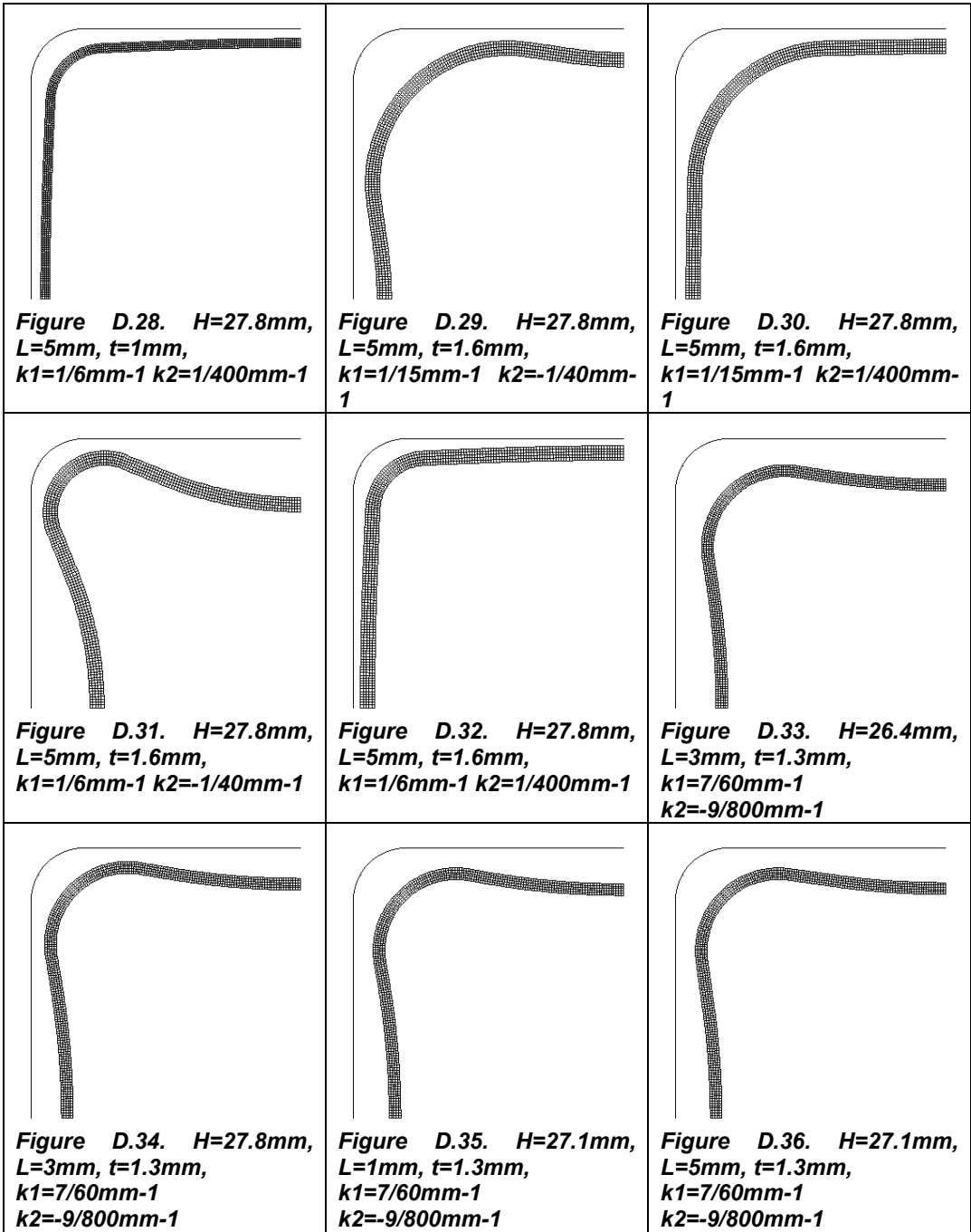
Appendix D. Finite Element Models for the Two-Dimensional Simulations

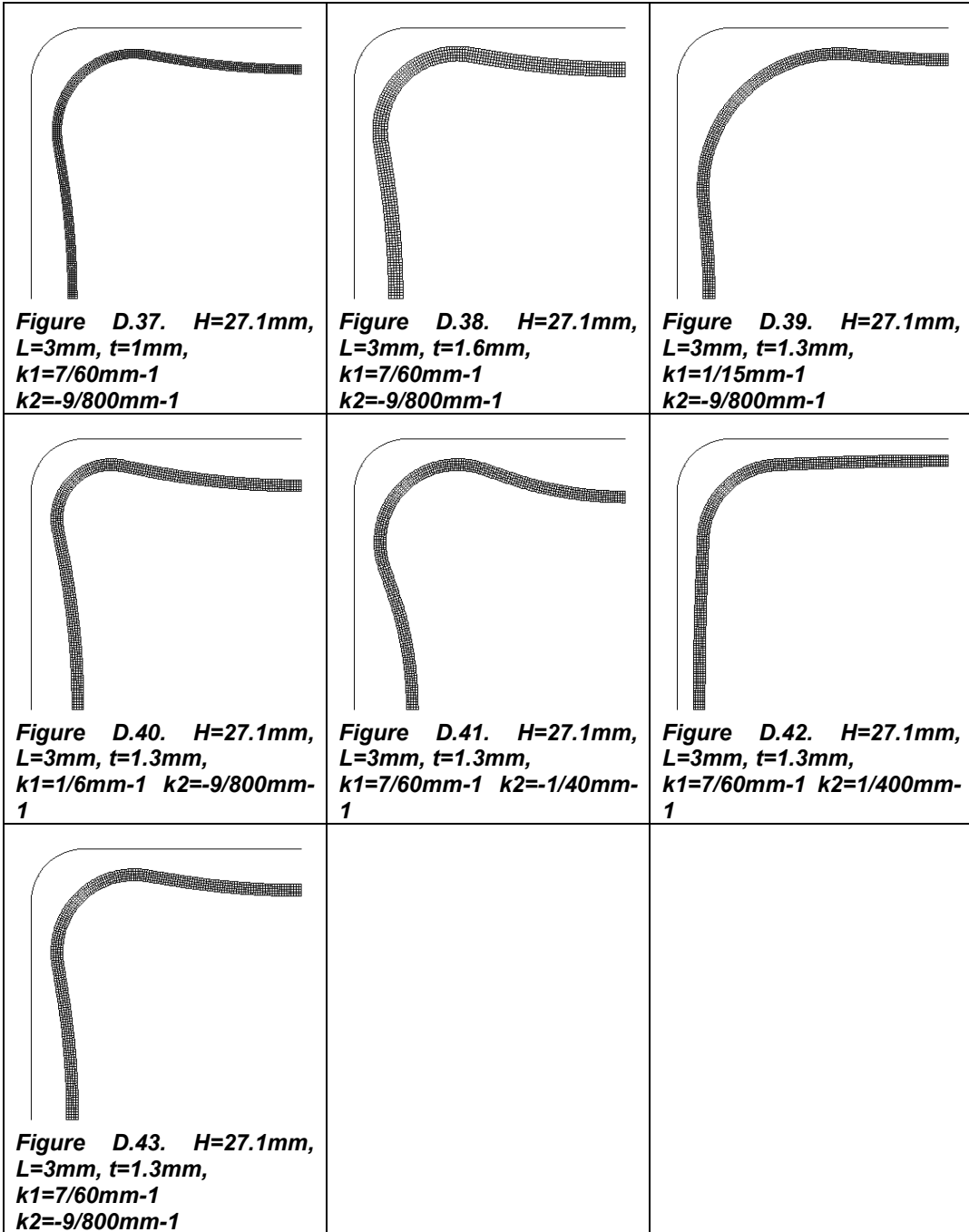
Below the 2D finite element models are depicted used for the optimisation of chapter 5. The figure numbers correspond to the experimental run number of table 4.2.



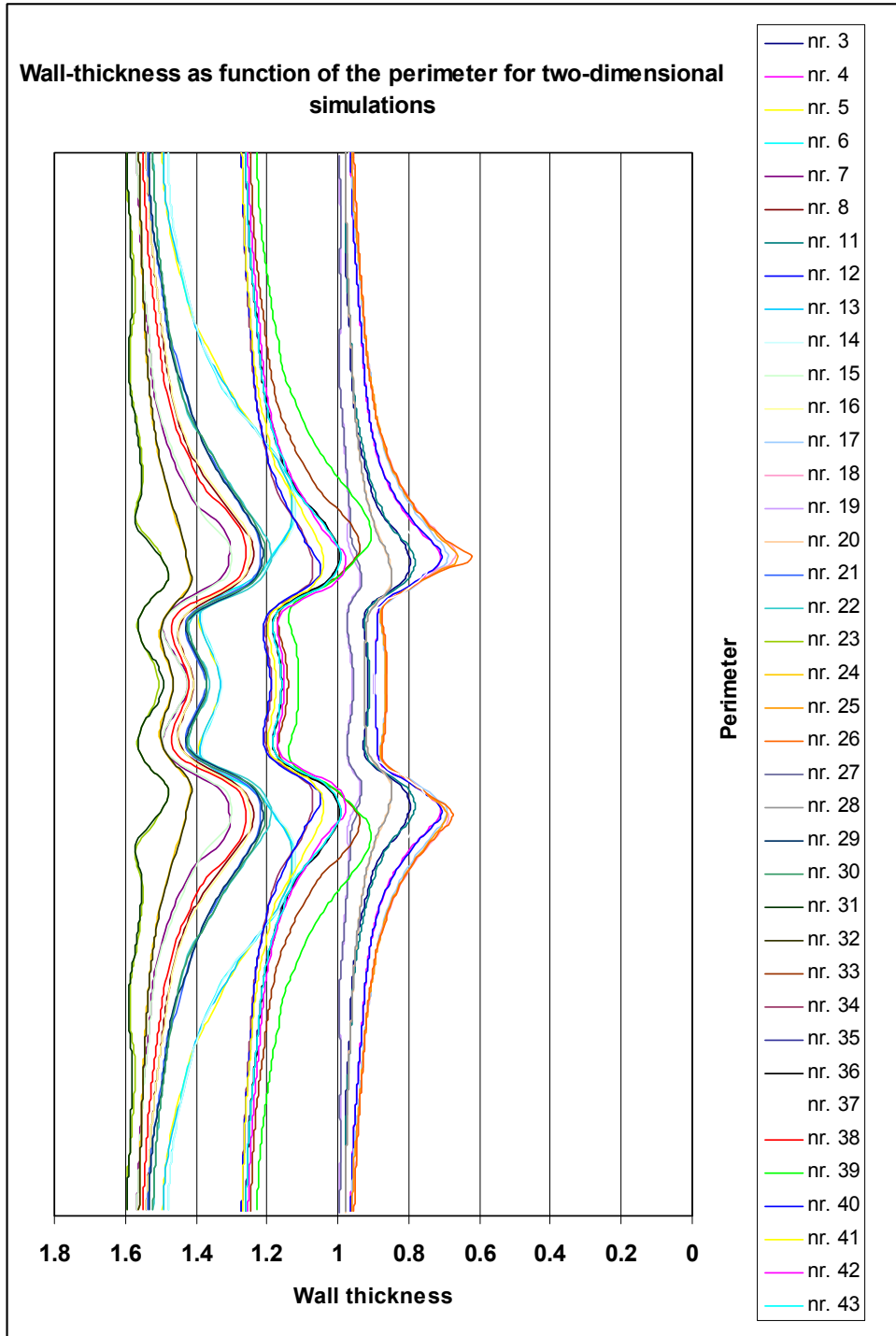




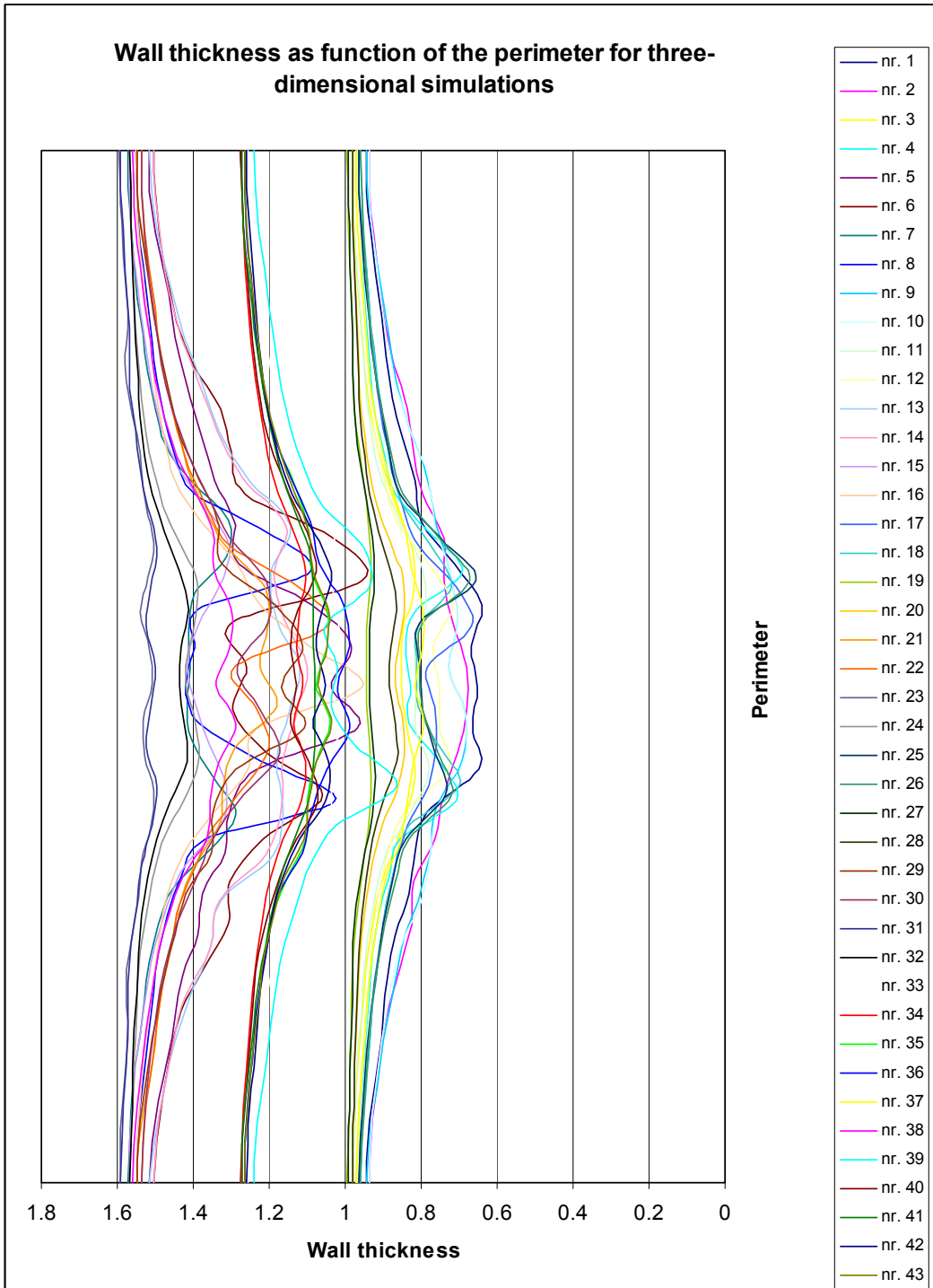




Appendix E. Wall Thickness as Function of the Perimeter



Wall thickness as function of the perimeter for three-dimensional simulations



Appendix F. Confidence Intervals of the Metamodel

Table F.1. Effects of the linear metamodel for two-dimensional simulations

	f_5	f_6	f_7
β_0	0.0773	0.1099	0.0668
$\beta_1 H$	-0.0167	-0.0353	-0.0143
$\beta_2 L$	0.0002	0.0002	0.0003
$\beta_3 t$	0.0095	0.0249	-0.0054
$\beta_4 \kappa_1$	-0.0239	-0.0531	-0.0220
$\beta_5 \kappa_2$	0.0046	0.0074	0.0046

Table F.2. 95% Confidence intervals for the effects of the linear metamodel for two-dimensional simulations

	f_5		f_6		f_7	
β_0	0.0750	0.0795	0.1051	0.1146	0.0646	0.0689
$\beta_1 H$	-0.0192	-0.0141	-0.0407	-0.0299	-0.0167	-0.0118
$\beta_2 L$	-0.0022	0.0027	-0.0050	0.0054	-0.0021	0.0027
$\beta_3 t$	0.0070	0.0121	0.0195	0.0303	-0.0079	-0.0030
$\beta_4 \kappa_1$	-0.0264	-0.0213	-0.0585	-0.0477	-0.0245	-0.0196
$\beta_5 \kappa_2$	0.0021	0.0070	0.0021	0.0126	0.0023	0.0070

Table F.3. Effects of the linear metamodel with interactions for two-dimensional simulations

	f_5	f_6	f_7
β_0	0.0751	0.1040	0.0665
$\beta_1 H$	-0.0139	-0.0279	-0.0139
$\beta_2 L$	0.0002	0.0002	0.0003
$\beta_3 t$	0.0122	0.0323	-0.0051
$\beta_4 \kappa_1$	-0.0212	-0.0456	-0.0217
$\beta_5 \kappa_2$	0.0041	0.0067	0.0044
$\beta_{12} HL$	0.0001	0.0000	0.0001
$\beta_{13} Ht$	-0.0029	-0.0112	0.0008
$\beta_{14} H\kappa_1$	-0.0067	-0.0089	-0.0044
$\beta_{15} H\kappa_2$	0.0009	-0.0003	0.0003
$\beta_{23} Lt$	-0.0004	-0.0006	-0.0004
$\beta_{24} L\kappa_1$	0.0001	0.0002	0.0000
$\beta_{25} L\kappa_2$	-0.0002	-0.0003	-0.0002
$\beta_{34} t\kappa_1$	-0.0033	-0.0151	0.0021
$\beta_{25} t\kappa_2$	-0.0007	-0.0003	-0.0018
$\beta_{45} \kappa_1 \kappa_2$	0.0036	0.0058	0.0033

Table F.4. 95% Confidence intervals for the effects of the linear metamodel with interactions for two-dimensional simulations

	f_5		f_6		f_7	
β_0	0.0740	0.0762	0.1019	0.1061	0.0655	0.0675
$\beta_1 H$	-0.0152	-0.0126	-0.0303	-0.0254	-0.0151	-0.0128
$\beta_2 L$	-0.0009	0.0014	-0.0019	0.0024	-0.0007	0.0013
$\beta_3 t$	0.0109	0.0136	0.0299	0.0348	-0.0063	-0.0039
$\beta_4 \kappa_1$	-0.0225	-0.0198	-0.0481	-0.0432	-0.0229	-0.0205
$\beta_5 \kappa_2$	0.0029	0.0052	0.0045	0.0088	0.0034	0.0054
$\beta_{12} HL$	-0.0011	0.0013	-0.0022	0.0022	-0.0010	0.0011
$\beta_{13} Ht$	-0.0042	-0.0015	-0.0137	-0.0086	-0.0004	0.0020
$\beta_{14} H\kappa_1$	-0.0081	-0.0054	-0.0114	-0.0063	-0.0056	-0.0032
$\beta_{15} H\kappa_2$	-0.0003	0.0021	-0.0025	0.0019	-0.0007	0.0014
$\beta_{23} Lt$	-0.0015	0.0008	-0.0028	0.0016	-0.0015	0.0006
$\beta_{24} L\kappa_1$	-0.0011	0.0013	-0.0020	0.0024	-0.0010	0.0010
$\beta_7 L\kappa_2$	-0.0013	0.0009	-0.0024	0.0018	-0.0012	0.0008
$\beta_{34} t\kappa_1$	-0.0047	-0.0019	-0.0176	-0.0125	0.0009	0.0033
$\beta_{25} t\kappa_2$	-0.0019	0.0005	-0.0025	0.0019	-0.0028	-0.0007
$\beta_{45} \kappa_1 \kappa_2$	0.0025	0.0048	0.0036	0.0080	0.0023	0.0043

Table F.5. Effects of the quadratic metamodel for two-dimensional simulations

	f_5	f_6	f_7
β_0	0.0773	0.1011	0.0658
$\beta_1 H$	-0.0167	-0.0358	-0.0143
$\beta_2 L$	0.0002	0.0002	0.0003
$\beta_3 t$	0.0095	0.0244	-0.0055
$\beta_4 \kappa_1$	-0.0239	-0.0536	-0.0221
$\beta_5 \kappa_2$	0.0046	0.0074	0.0046
$\beta_{11} H^2$	-0.0013	-0.0002	-0.0010
$\beta_{22} L^2$	0.0016	0.0043	0.0012
$\beta_{33} t^2$	-0.0009	0.0004	-0.0003
$\beta_{44} \kappa_1^2$	0.0033	0.0124	0.0043
$\beta_{55} \kappa_2^2$	-0.0028	-0.0053	-0.0028

Table F.6. 95% Confidence intervals for the effects of the linear metamodel for two-dimensional simulations

	f_5		f_6		f_7	
β_0	0.0719	0.0827	0.0905	0.1117	0.0607	0.0710
$\beta_1 H$	-0.0194	-0.0139	-0.0413	-0.0304	-0.0169	-0.0117
$\beta_2 L$	-0.0024	0.0029	-0.0050	0.0054	-0.0022	0.0028
$\beta_3 t$	0.0067	0.0123	0.0189	0.0298	-0.0081	-0.0028
$\beta_4 \kappa_1$	-0.0267	-0.0211	-0.0590	-0.0481	-0.0247	-0.0194
$\beta_5 \kappa_2$	0.0019	0.0072	0.0021	0.0126	0.0021	0.0072
$\beta_{11} H^2$	-0.0106	0.0079	-0.0185	0.0180	-0.0099	0.0078
$\beta_{22} L^2$	-0.0076	0.0109	-0.0140	0.0226	-0.0077	0.0100
$\beta_{33} t^2$	-0.0101	0.0084	-0.0179	0.0187	-0.0092	0.0086
$\beta_{44} \kappa_1^2$	-0.0060	0.0125	-0.0059	0.0307	-0.0046	0.0131
$\beta_{55} \kappa_2^2$	-0.0120	0.0065	-0.0235	0.0130	-0.0117	0.0060

Table F.7. Effects of the quadratic metamodel with interactions for two-dimensional simulations

	f_5	f_6	f_7
β_0	0.0781	0.1029	0.0659
$\beta_1 H$	-0.0133	-0.0281	-0.0141
$\beta_2 L$	0.0002	0.0002	0.0003
$\beta_3 t$	0.0128	0.0321	-0.0052
$\beta_4 \kappa_1$	-0.0206	-0.0458	-0.0218
$\beta_5 \kappa_2$	0.0041	0.0067	0.0044
$\beta_{12} HL$	0.0001	0.0000	0.0001
$\beta_{13} Ht$	-0.0035	-0.0109	0.0009
$\beta_{14} H\kappa_1$	-0.0074	-0.0086	-0.0042
$\beta_{15} H\kappa_2$	0.0009	-0.0003	0.0003
$\beta_{23} Lt$	-0.0004	-0.0006	-0.0004
$\beta_{24} L\kappa_1$	0.0001	0.0002	0.0000
$\beta_2 L\kappa_2$	-0.0002	-0.0003	-0.0002
$\beta_{34} t\kappa_1$	-0.0040	-0.0148	0.0023
$\beta_{25} t\kappa_2$	-0.0007	-0.0003	-0.0018
$\beta_{45} \kappa_1 \kappa_2$	0.0036	0.0058	0.0033
$\beta_{11} H^2$	-0.0022	-0.0022	-0.0011
$\beta_{22} L^2$	0.0008	0.0023	0.0011
$\beta_{33} t^2$	-0.0017	-0.0016	-0.0004
$\beta_{44} \kappa_1^2$	0.0024	0.0104	0.0042
$\beta_{55} \kappa_2^2$	-0.0036	-0.0073	-0.0029

Table F.8. 95% Confidence intervals for the effects of the quadratic metamodel with interactions for two-dimensional simulations

	f_5		f_6		f_7	
β_0	0.0767	0.0795	0.0996	0.1061	0.0642	0.0676
$\beta_1 H$	-0.0142	-0.0125	-0.0301	-0.0261	-0.0151	-0.0130
$\beta_2 L$	-0.0005	0.0009	-0.0014	0.0019	-0.0005	0.0012
$\beta_3 t$	0.0120	0.0137	0.0301	0.0341	-0.0063	-0.0042
$\beta_4 \kappa_1$	-0.0214	-0.0197	-0.0478	-0.0438	-0.0229	-0.0208
$\beta_5 \kappa_2$	0.0034	0.0048	0.0050	0.0083	0.0035	0.0053
$\beta_{12} HL$	-0.0006	0.0008	-0.0017	0.0018	-0.0008	0.0010
$\beta_{13} Ht$	-0.0044	-0.0026	-0.0130	-0.0088	-0.0002	0.0020
$\beta_{14} H\kappa_1$	-0.0083	-0.0065	-0.0107	-0.0066	-0.0053	-0.0031
$\beta_{15} H\kappa_2$	0.0002	0.0016	-0.0020	0.0014	-0.0006	0.0012
$\beta_{23} Lt$	-0.0011	0.0004	-0.0023	0.0011	-0.0013	0.0005
$\beta_{24} L\kappa_1$	-0.0006	0.0008	-0.0015	0.0019	-0.0009	0.0009
$\beta_2 L\kappa_2$	-0.0009	0.0005	-0.0019	0.0014	-0.0011	0.0007
$\beta_{34} t\kappa_1$	-0.0048	-0.0031	-0.0169	-0.0127	0.0011	0.0034
$\beta_{25} t\kappa_2$	-0.0014	0.0000	-0.0020	0.0015	-0.0027	-0.0009
$\beta_{45} \kappa_1 \kappa_2$	0.0029	0.0044	0.0041	0.0076	0.0024	0.0042
$\beta_{11} H^2$	-0.0045	0.0002	-0.0078	0.0033	-0.0041	0.0019
$\beta_{22} L^2$	-0.0016	0.0031	-0.0033	0.0078	-0.0019	0.0041
$\beta_{33} t^2$	-0.0041	0.0006	-0.0071	0.0040	-0.0033	0.0026
$\beta_{44} \kappa_1^2$	0.0000	0.0047	0.0049	0.0160	0.0013	0.0072
$\beta_{55} \kappa_2^2$	-0.0060	-0.0013	-0.0128	-0.0017	-0.0059	0.0001

Appendix G. Bending of Sheet

This section describes a simple way for determining the stresses and strains induced by a bending process, which is a good indication for the stress and strain situation in a tube produced according to the tubular blank process.

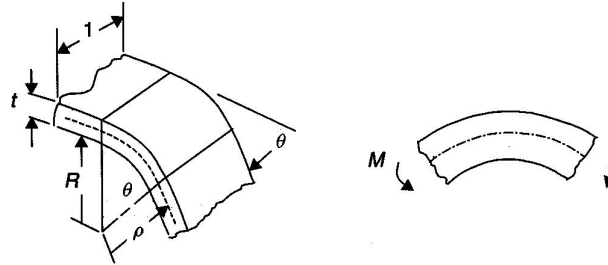


Figure G.1. A unit length of a continuous strip bent along a line.

In Figure G.1 a sheet subjected to a bending moment is displayed. The basic assumption is sheet metal in a plane stress situation. Furthermore, the strains across the width of the sheet is assumed zero, i.e. the sides in Figure G.1 stay at an equal distance to each other.

The stress and strain situation is described as follows:

$$\varepsilon_1; \quad \varepsilon_2 = 0; \quad \varepsilon_3 = -\varepsilon_1 \quad \text{Eq. G.1}$$

$$\sigma_1; \quad \sigma_2 = \frac{1}{2} \sigma_1; \quad \sigma_3 = 0 \quad \text{Eq. G.2}$$

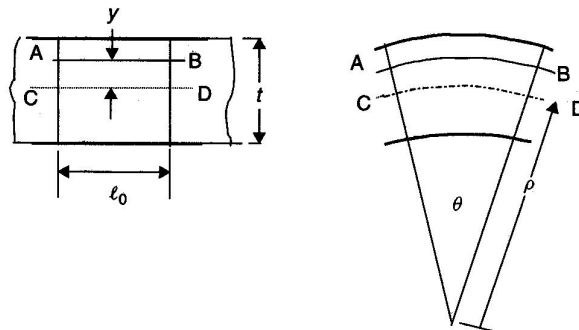


Figure G.2. Deformation of longitudinal fibres in bending condition.

In Figure G.2 a part of the sheet is represented in the starting and deformed condition. The fibre CD corresponds to the neutral line and remains of the same length during bending, when no normal stress is applied. The fibre AB undergoes a positive elongation for $y > 0$ and a negative elongation for $y < 0$. The following applies for fibre AB:

$$\varepsilon_1 = \ln\left(\frac{\rho_{AB}}{\rho_0}\right) = \ln\left(\frac{\rho_0 + y}{\rho_0}\right) = \ln\left(1 + \frac{y}{\rho_0}\right) \quad \text{Eq. G.3}$$

with ρ_{AB} the radius of fibre AB, ρ_0 the radius of the neutral line (fibre CD) and y the distance from the neutral line to fibre AB.

If $\rho \gg t$ then the elongation can be approached by:

$$\varepsilon_1 = \ln\left(1 + \frac{y}{\rho_0}\right) \approx \frac{y}{\rho_0} \quad \text{Eq. G.4}$$

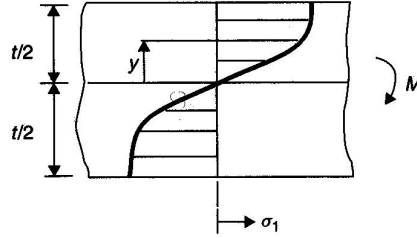


Figure G.3. Stress distribution for a power-law-hardening sheet bent without tension.

A model describing the work hardening relation between the stresses and strains can be written as $\bar{\sigma} = C\bar{\varepsilon}^n$ (Hollomon). Using the relations for $\bar{\sigma}$ en $\bar{\varepsilon}$, stated in Eq. G.5 and Eq. G.6 the relation can be rewritten for the hoop direction:

$$\bar{\sigma} = \sqrt{\frac{1}{2}\{(\sigma_1 - \sigma_2)^2 + (\sigma_2 - \sigma_3)^2 + (\sigma_3 - \sigma_1)^2\}} \quad \text{Eq. G.5}$$

$$\bar{\varepsilon} = \sqrt{\frac{2}{3}(\varepsilon_1^2 + \varepsilon_2^2 + \varepsilon_3^2)} \quad \text{Eq. G.6}$$

$$\sigma_1 = C'\varepsilon_1^n \quad \text{Eq. G.7}$$

Substitution of Eq. G.4 into Eq. G.7 leads to a relation between the stress and the radius of the bend.

$$\sigma_1 = C'\left(\frac{y}{\rho_0}\right)^n \quad \text{Eq. G.8}$$

Summarised; the stresses and strains in the bent sheet can be described as follows, schematic represented in Figure G.4:

$$\varepsilon_1 \approx \frac{y}{\rho_0}; \quad \varepsilon_2 = 0; \quad \varepsilon_3 \approx -\frac{y}{\rho_0} \quad \text{Eq. G.9}$$

$$\sigma_1 = C'\left(\frac{y}{\rho_0}\right)^n; \quad \sigma_2 = \frac{C'}{2}\left(\frac{y}{\rho_0}\right)^n; \quad \sigma_3 = 0 \quad \text{Eq. G.10}$$

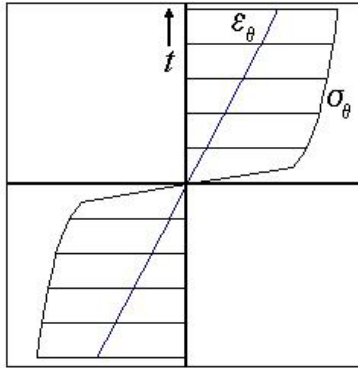


Figure G.4. The variation of stress and strain in the hoop direction of the bend sheet

In the finite element package DiekA the work hardening of the material is calculated using the equivalent strain. For a von Mises material model the equivalent strain is:

$$\bar{\epsilon} = \sqrt{\frac{2}{3}(\epsilon_1^2 + \epsilon_2^2 + \epsilon_3^2)} \quad \text{Eq. G.11}$$

Using Eq. G.10 this leads to:

$$\bar{\epsilon} = \left| \frac{2y}{\sqrt{3}\rho_0} \right| \quad \text{Eq. G.12}$$

Appendix H. Screening Designs

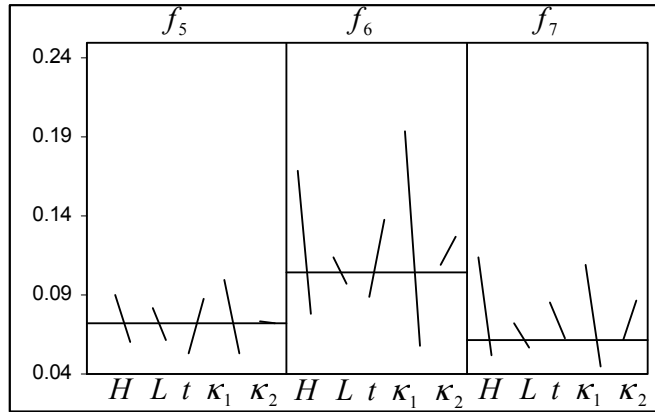
In this appendix the screening designs used in section 7.1 are described. These designs are five-factor two-level fractional factorial designs of resolution III and are formed from a three-factor two-level full factorial design. The remaining columns are formed by multiplication of two or more columns. These multiplications are showed above the table with x_i the variable corresponding to the i^{th} column.

(a) Multiplications:

$$x_4 = x_1x_2$$

$$x_5 = x_1x_3$$

	H	L	t	k1	k2
1	-1	-1	-1	+1	+1
2	+1	-1	-1	-1	-1
3	-1	+1	-1	-1	+1
4	+1	+1	-1	+1	-1
5	-1	-1	+1	+1	-1
6	+1	-1	+1	-1	+1
7	-1	+1	+1	-1	-1
8	+1	+1	+1	+1	+1

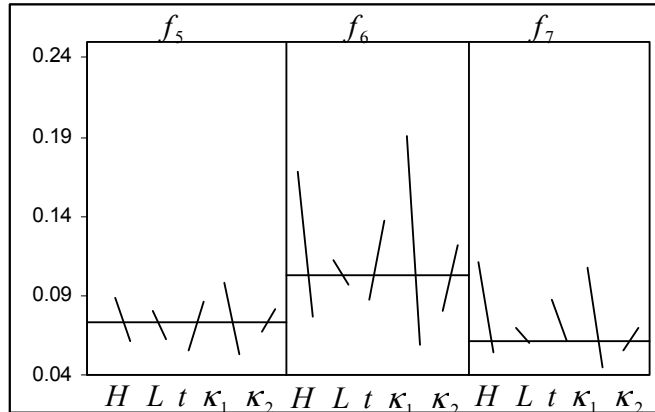


(b) Multiplications:

$$x_4 = x_1x_2$$

$$x_5 = -x_1x_3$$

	H	L	t	k1	k2
1	-1	-1	-1	+1	-1
2	+1	-1	-1	-1	+1
3	-1	+1	-1	-1	-1
4	+1	+1	-1	+1	+1
5	-1	-1	+1	+1	+1
6	+1	-1	+1	-1	-1
7	-1	+1	+1	-1	+1
8	+1	+1	+1	+1	-1

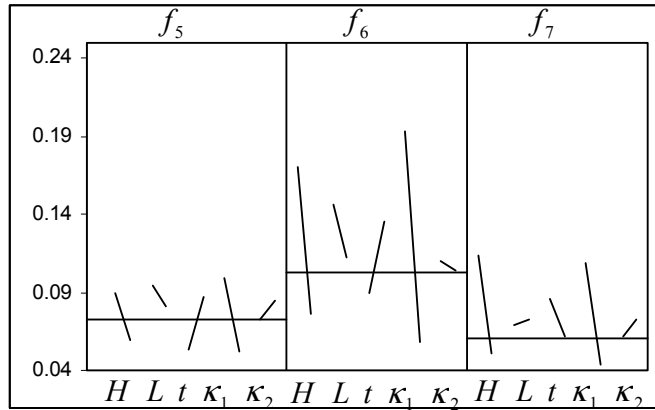


(c) Multiplications:

$$x_4 = -x_1x_2$$

$$x_5 = x_1x_3$$

	H	L	t	k1	k2
1	-1	-1	-1	-1	+1
2	+1	-1	-1	+1	-1
3	-1	+1	-1	+1	+1
4	+1	+1	-1	-1	-1
5	-1	-1	+1	-1	-1
6	+1	-1	+1	+1	+1
7	-1	+1	+1	+1	-1
8	+1	+1	+1	-1	+1

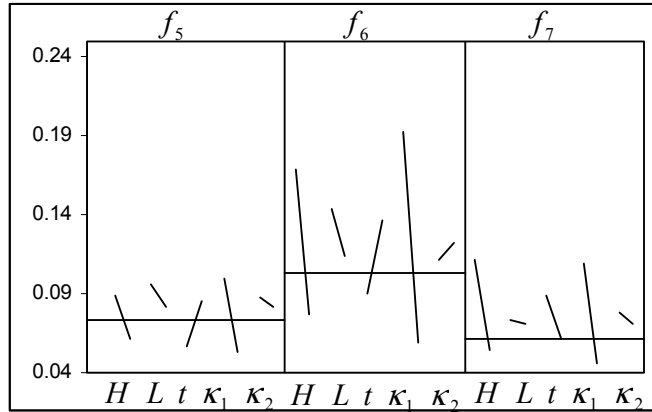


(d) Multiplications:

$$x_4 = -x_1 x_2$$

$$x_5 = -x_1 x_3$$

	H	L	t	k1	k2
1	-1	-1	-1	-1	-1
2	+1	-1	-1	+1	+1
3	-1	+1	-1	+1	-1
4	+1	+1	-1	-1	+1
5	-1	-1	+1	-1	+1
6	+1	-1	+1	+1	-1
7	-1	+1	+1	+1	+1
8	+1	+1	+1	-1	-1

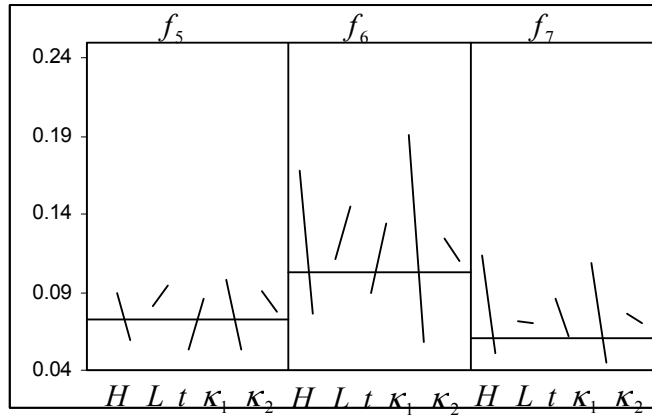


(e) Multiplications:

$$x_4 = x_1 x_2$$

$$x_5 = x_2 x_3$$

	H	L	t	k1	k2
1	-1	-1	-1	+1	+1
2	+1	-1	-1	-1	+1
3	-1	+1	-1	-1	-1
4	+1	+1	-1	+1	-1
5	-1	-1	+1	+1	-1
6	+1	-1	+1	-1	-1
7	-1	+1	+1	-1	+1
8	+1	+1	+1	+1	+1

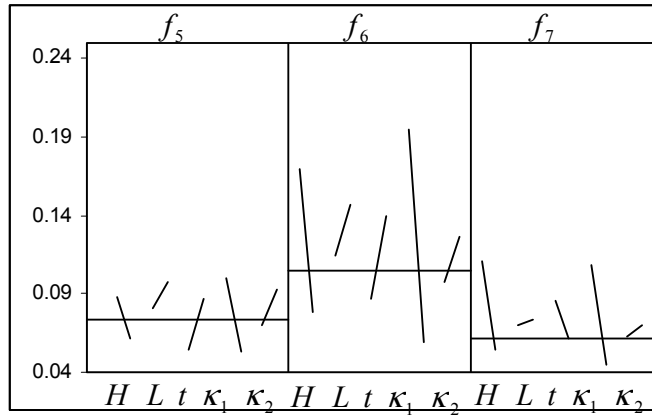


(f) Multiplications:

$$x_4 = x_1 x_2$$

$$x_5 = -x_2 x_3$$

	H	L	t	k1	k2
1	-1	-1	-1	+1	-1
2	+1	-1	-1	-1	-1
3	-1	+1	-1	-1	+1
4	+1	+1	-1	+1	+1
5	-1	-1	+1	+1	+1
6	+1	-1	+1	-1	+1
7	-1	+1	+1	-1	-1
8	+1	+1	+1	+1	-1

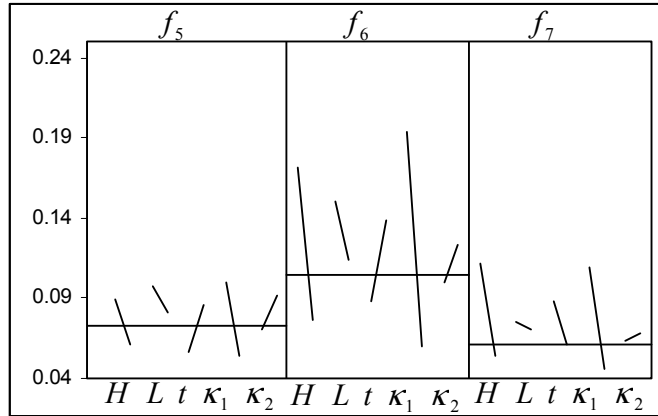


(g) Multiplications:

$$x_4 = -x_1 x_2$$

$$x_5 = x_2 x_3$$

	H	L	t	k1	k2
1	-1	-1	-1	-1	+1
2	+1	-1	-1	+1	+1
3	-1	+1	-1	+1	-1
4	+1	+1	-1	-1	-1
5	-1	-1	+1	-1	-1
6	+1	-1	+1	+1	-1
7	-1	+1	+1	+1	+1
8	+1	+1	+1	-1	+1

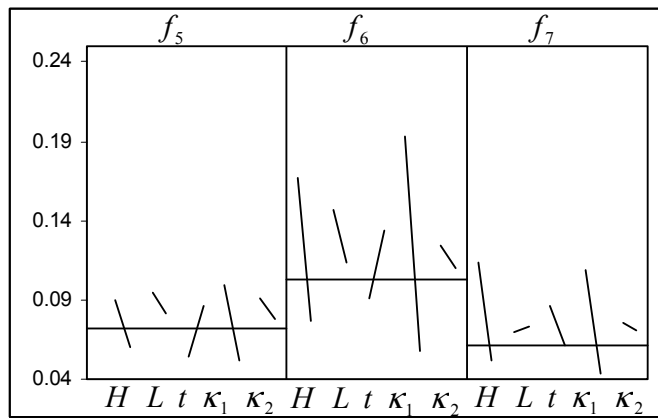


(h) Multiplications:

$$x_4 = -x_1 x_2$$

$$x_5 = -x_2 x_3$$

	H	L	t	k1	k2
1	-1	-1	-1	-1	-1
2	+1	-1	-1	+1	-1
3	-1	+1	-1	+1	+1
4	+1	+1	-1	-1	+1
5	-1	-1	+1	-1	+1
6	+1	-1	+1	+1	+1
7	-1	+1	+1	+1	-1
8	+1	+1	+1	-1	-1

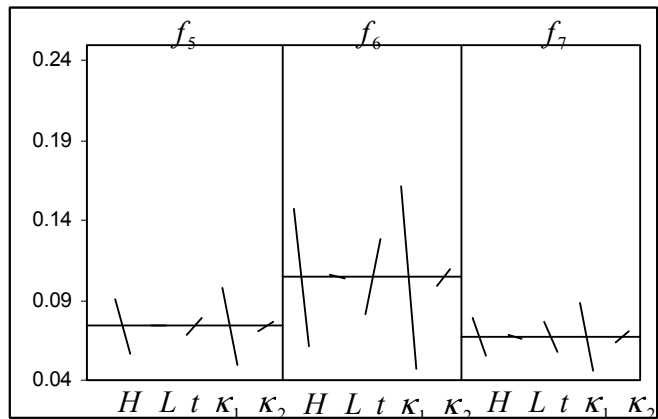


(i) Multiplications:

$$x_4 = x_1 x_3$$

$$x_5 = x_2 x_3$$

	H	L	t	k1	k2
1	-1	-1	-1	+1	+1
2	+1	-1	-1	-1	+1
3	-1	+1	-1	+1	-1
4	+1	+1	-1	-1	-1
5	-1	-1	+1	-1	-1
6	+1	-1	+1	+1	-1
7	-1	+1	+1	-1	+1
8	+1	+1	+1	+1	+1

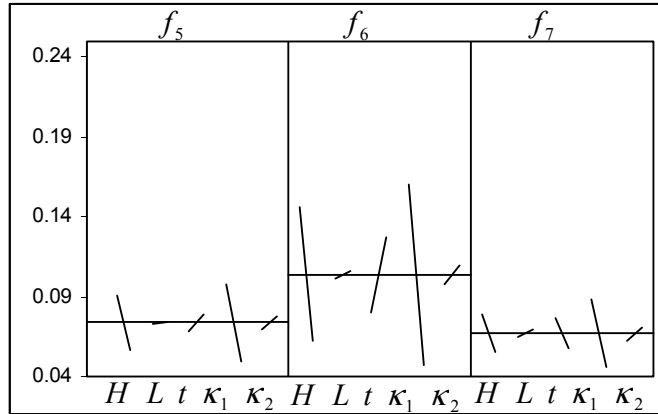


(j) Multiplications:

$$x_4 = x_1 x_3$$

$$x_5 = -x_2 x_3$$

	H	L	t	k1	k2
1	-1	-1	-1	+1	-1
2	+1	-1	-1	-1	-1
3	-1	+1	-1	+1	+1
4	+1	+1	-1	-1	+1
5	-1	-1	+1	-1	+1
6	+1	-1	+1	+1	+1
7	-1	+1	+1	-1	-1
8	+1	+1	+1	+1	-1

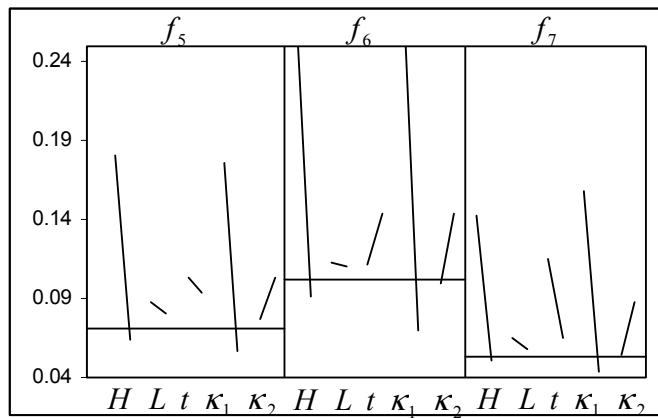


(k) Multiplications:

$$x_4 = -x_1 x_3$$

$$x_5 = x_2 x_3$$

	H	L	t	k1	k2
1	-1	-1	-1	-1	+1
2	+1	-1	-1	+1	+1
3	-1	+1	-1	-1	-1
4	+1	+1	-1	+1	-1
5	-1	-1	+1	+1	-1
6	+1	-1	+1	-1	-1
7	-1	+1	+1	+1	+1
8	+1	+1	+1	-1	+1



(l) Multiplications:

$$x_4 = -x_1 x_3$$

$$x_5 = -x_2 x_3$$

	H	L	t	k1	k2
1	-1	-1	-1	-1	-1
2	+1	-1	-1	+1	-1
3	-1	+1	-1	-1	+1
4	+1	+1	-1	+1	+1
5	-1	-1	+1	+1	+1
6	+1	-1	+1	-1	-1
7	-1	+1	+1	+1	-1
8	+1	+1	+1	-1	-1

